**République Algérienne Démocratique Et Populaire**
**Ministère De L'enseignement Supérieur Et De La Recherche Scientifique**
**Université 20 Août 1955 Skikda**


**Faculté De Technologie**
**Département De Génie Des Procédés**

**Réf : D012126014D**

**Laboratoire de domiciliation : Laboratoire de Physico-Chimie des Surfaces et des Interfaces (LRPCSI)**

# THÈSE

## EN VUE DE L'OBTENTION DU DIPLOME DE

## DOCTORAT EN 3ème CYCLE_LMD

**Domaine :** Science et technologie **Filière :** Génie des procédés

**Spécialité :** Génie des polymères

Présentée par

**BOUDAGHA Seif El Islam**

*Intitulée*

# Elaboration de nouveaux nanomatériaux et leurs applications

Soutenu le : 06/05/2026 Devant le jury composé de :

| *Nom et Prénom* | *Grade* | *Etablissement* | *Qualité* |
|---|---|---|---|
| **Mme ZOUAOUI Emna** | Professeur | Université de Skikda | Présidente |
| **Mme SOBHI Chafia** | Professeur | Université de Skikda | Promotrice |
| **M. KRAIM Khairedine** | MCA | ENSET Skikda | Examinateur |
| **Mme DAIRI Badrina** | MCA | Université de Skikda | Examinateur |
| **Mme DALI Mounira** | MCB | Université de Annaba | Invitée |

***Année universitaire :*** *2025-2026*

**People's Democratic Republic of Algeria**
**Ministry of Higher Education and Scientific Research**
**University 20 August 1955 Skikda**


**Faculty of Technology**
**Process Engineering Department**

**Ref : D012126014D**

**Home laboratory: Laboratoire de Physico-Chimie des Surfaces et des Interfaces (LRPCSI)**

# THESIS

## Thesis submitted in partial fulfillment of the requirements for the degree 3rd CYCLE_LMD Doctorat

**Domain:** Science and technology **Field:** Process engineering

**Spécialty:** Polymer engineering

Presented by

**BOUDAGHA Seif El Islam**

*Entitled*

# Elaboration of new nanomaterials and their applications

Organized in: May 6, 2026 In front of a jury composed of :

| *First & last name* | *Grade* | *Etablissement* | *Quality* |
|---|---|---|---|
| **Mme ZOUAOUI Emna** | Professeur | University of Skikda | President |
| **Mme SOBHI Chafia** | Professeur | University of Skikda | Thesis Director |
| **Mr KRAIM Khairedine** | MCA | ENSET Skikda | Examiner |
| **Mme DAIRI Badrina** | MCA | University of Skikda | Examiner |
| **Mme DALI Mounira** | MCB | University of Annaba | Invited |

***Academic year :*** *2025-2026*

## Acknowledgements

In the name of God, and no name is higher than the name of God. Praise and thanks be to God, the Merciful God, who has made everything subservient to us. I thank God, the Highest, who granted us the strength and patience to complete this humble work... Praise be to God.

Beginning to write this page is the most difficult and complex part of the research, due to the importance and number of individuals who contributed in any way to the success and completion of this work. Upon completion, I wish to express my profound gratitude and sincere respect to my thesis supervisor, **Pr. Sobhi Chafia**, for her invaluable support, guidance, kind spirit, and insightful advice throughout this work. I am deeply appreciative of her generosity, dedication, and the encouragement she has provided over the years.

I wish to extend my sincere appreciation to all members of the examination jury for their consideration and evaluation of my thesis. I am especially grateful to **Pr. Zouaoui Emna** of the University of Skikda for the honor of presiding over the jury. I also express my thanks to **Dr. Khairedine Kraim** from the Higher Normal School of Technological Education ENSET, Skikda and **Dr. Dairi Badrina** of the University of Skikda for their thoughtful review and their contribution to the assessment of this work.

This research was carried out across the various pedagogical laboratories of the Process Engineering and Petrochemicals Departments within the Faculty of Technology. I extend my sincere gratitude to all laboratory engineers for their technical assistance, with special appreciation to Engineer **Slama Hamida** for her continuous support throughout both my Master's and doctoral studies.

I am also deeply grateful to the Laboratory for Growth and Characterization of New Semiconductors at the University of Sétif. I express my profound thanks to the head of the laboratory, **Pr. Ahmed Zouaoui**, for granting me access to the facilities over the past years and for providing the resources and equipment necessary to conduct this work. **Pr. A Zouaoui** has been not only a distinguished researcher, but also an exceptional teacher, mentor, and guide. I also extend my sincere thanks to all the laboratory engineers for their technical support: **Dr. Yacine, Mr. Kamal, Mr. Foudil, and Mr. Imad.**

I extend my heartfelt thanks to the teams of the Biotechnology Technical and Scientific Analysis Program (PTAPC) in Laghouat, Bejaia, and Biskra. I am particularly grateful to **Dr. Othmane Djermoune** and **Mr. Younsaoui** from Bejaia, as well as **Dr. Nebbar** from Biskra, whose invaluable assistance enabled me to complete all the necessary characterizations for this research. I also wish to convey my gratitude to the laboratory of the Biotechnology Research Center of Constantine (CRBT), under the supervision of **Dr. Bensouici Chawki**, for the warm welcome and support they provided throughout the course of my work. Finally, I extend my

**Acknowledgements**

sincere thanks to the Polytechnic School of Constantine for their valuable contribution to the various characterization analyses.

I would like to express my sincere gratitude to the Faculty of Pharmacy at Ege University, where I had the opportunity to complete my advanced training. I am especially thankful to **Pr. Emel Öykü Çetin Uyanıkgil** Head of the Biopharmaceutics and Pharmacokinetics Laboratory, for her warm welcome, guidance, and for providing all the resources necessary to carry out the practical experiments. I also extend my appreciation to **Dr. Mustafa Ökeer**, Mr. **Yalçın çelik Aydın**, and all the laboratory engineers for their invaluable assistance throughout my stay.

I extend my deepest gratitude and sincere appreciation to **Dr. Dali Mounira** from the University of Annaba for all the assistance, generous support and guidance she has provided me. I also extend my thanks to **Pr. Abdelghani Djahoudi** from the same institution and **Pr. Malika Foudia** and **Pr. Embarek Bentouhami** from University of Setif 1 for kindly welcoming me into their laboratories and allowing me to conduct the practical experiments. I would also like to express my gratitude to **Pr. Hacene Bendjeffal** and **Dr. Boudjedir Atidel** of ENSET, Skikda for their valuable advice.

I would like to express my gratitude to the engineers in the laboratories of Technology Hall, all with their names, especially **Noura Abdennouri**.

In difficult times, they were a source of support. I extend my deepest gratitude to my dear friends **PhD. lyes Othmane, Dr. Abdennouri Amjed, Dr. Bouzenad Nawal, PhD. djamel Dini, Dr. Nada Hamrouche, PhD. Hana Bouchetta, and Dr. Mourad Latoui**. We shared wonderful moments and many challenges together. I cannot adequately express my gratitude for your constant help, unwavering encouragement, and advice. No words can truly capture the sincere feelings you have shown me, nor the profound memories that will stay with me. Every moment we shared, every challenge we faced, and every project we undertook will remain etched in my heart. Thank you for our years of camaraderie and the research path we embarked upon together and will continue to follow. In moments of need, when all doors seemed closed, your hands were always there to lift me up.

I also want to thank all the names I may have inadvertently omitted professors, engineers, colleagues, and friends for their support, guidance, and advice. Thank you to everyone who has planted a positive seed in my life.

## *Dedication*

*I extend my hand to those who brought me into this life, I extend my hand to those who were the light, the radiance, and the great embrace. I extend my hands overflowing with my love and tears of gratitude. I dedicate this humble work to the sun of my life and the moon of my nights, to you, my parents,* ***Abdelkader*** *and* ***Atika****.*

*To my unwavering support, to those who brought smiles to my life. My siblings:* ***Yacin, Samra, Djoudi, Daoud, Hafid, Imane, Badis, and Khawla****.*

*To the dearest in my heart, to the flowers of my life: my nephews and nieces.*

*To my friends who have accompanied me on this journey, sharing with me the challenges, setbacks, and successes.*

*With my sincere love and gratitude to all, I dedicate this work to you.*

# Abstract

The utilization of renewable plant-based nanotechnology in the production of nanomaterials is becoming increasingly important; it is a low-cost approach that allows for the development of nanostructures with distinctive functional properties. This thesis examines the application of an aqueous *Cynoglossum creticum* leaf extract (Ccl-extract) in the synthesis of silver nanoparticles (Ccl-AgNPs) and silver/polyaniline nanocomposites (Ag/PANI NCs) for biopharmaceutical and analytical purposes. The first section of the study evaluates the effects of extraction conditions and synthesis parameters on nanoparticle formation and characterizes the resulting Ccl-AgNPs using spectroscopic and microscopic techniques. Furthermore, the biological properties of the green Ccl-AgNPs were investigated, revealing promising antioxidant activities and a good inhibitory effect on bacterial growth, particularly against *Pseudomonas aeruginosa*. Analytically, Ccl-AgNPs demonstrated SPR-based colorimetric sensing capabilities for the selective detection of neomycin sulfate in complex matrices. The second part focuses on the green synthesis of polyaniline nanotubes (PANI-NT) via a soft-template self-assembly process and the subsequent deposition of silver nanoparticles onto these nanotubes using Ccl-extract as reducing and stabilizing agents. The producing Ag/PANI nanocomposites (containing different masses of PANI ranging from 50 to 250 mg) were characterized and assessed for biological performance. Incorporation of silver nanoparticles enhanced the antioxidant and antibacterial activities of PANI-NT, attributed to synergistic interactions and improved surface area.



**Keywords:** *Cynoglossum creticum*, Silver nanoparticles, polyaniline nanotubes, nanocomposites, biological activities, Colorimetric sensing.

# Résumé

L'utilisation de la nanotechnologie végétale renouvelable pour la production de nanomatériaux revêt une importance croissante ; cette approche économique permet le développement de nanostructures aux propriétés fonctionnelles distinctives. Cette thèse examine l'application d'un extrait aqueux de feuilles de *Cynoglossum creticum* (Ccl-extract) à la synthèse de nanoparticules d'argent (Ccl-AgNPs) et de nanocomposites argent/polyaniline (Ag/PANI NCs) à des fins biopharmaceutiques et analytiques. La première partie de l'étude évalue l'influence des conditions d'extraction et des paramètres de synthèse sur la formation des nanoparticules et caractérise les Ccl-AgNPs obtenues par des techniques spectroscopiques et microscopiques. De plus, les propriétés biologiques des Ccl-AgNPs ont été étudiées, révélant des activités antioxydantes prometteuses et un bon effet inhibiteur sur la croissance bactérienne, notamment contre *Pseudomonas aeruginosa*. Sur le plan analytique, les Ccl-AgNPs ont démontré des capacités de détection colorimétrique par résonance plasmonique de surface (SPR) pour la détection sélective du sulfate de néomycine dans des matrices complexes. La seconde partie porte sur la synthèse verte de nanotubes de polyaniline (PANI-NT) par un procédé d'auto-assemblage sur matrice souple et le dépôt subséquent de nanoparticules d'argent sur ces nanotubes, en utilisant un extrait de Ccl-extract comme agent réducteur et stabilisant. Les nanocomposites Ag/PANI obtenus (contenant différentes masses de PANI, de 50 à 250 mg) ont été caractérisés et leurs performances biologiques évaluées. L'incorporation de nanoparticules d'argent a amélioré les activités antioxydantes et antibactériennes des PANI-NT, ce qui est attribué à des interactions synergiques et à une surface spécifique accrue.

**Mots-clés :** *Cynoglossum creticum*, nanoparticules d'argent, nanotubes de polyaniline, nanocomposites, activités biologiques, détection colorimétrique.

# ملخص

تتزايد أهمية استخدام تقنية النانو النباتية المتجددة في إنتاج المواد النانوية؛ فهي نهج منخفض التكلفة يسمح بتطوير بنى نانوية ذات خصائص وظيفية مميزة. تبحث هذه الرسالة في استخدام مستخلص مائي من أوراق نبات السينوجلوسوم كريتيكوم (*Cynoglossum creticum* ;مستخلص Ccl) في تخليق جسيمات نانوية فضية (Ccl-AgNPs) ومركبات نانوية فضية/بولي أنيلين (Ag/PANI NCs) لأغراض صيدلانية حيوية وتحليلية. يُقيّم القسم الأول من الدراسة آثار ظروف الاستخلاص ومعايير التخليق على تكوين الجسيمات النانوية، ويُحدد خصائص جسيمات Ccl-AgNPs الناتجة باستخدام تقنيات طيفية ومجهرية. علاوة على ذلك، تم دراسة الخصائص البيولوجية لجسيمات Ccl-AgNPs الخضراء، كاشفةً عن أنشطة مضادة للأكسدة واعدة وتأثير مثبط جيد لنمو البكتيريا، وخاصةً ضد الزائفة الزنجارية ( *Pseudomonas aeruginosa*). تحليليًا، أظهرت جسيمات النانو الفضية Ccl-AgNPs قدرات استشعار لونية قائمة على SPR للكشف الانتقائي عن كبريتات النيومايسين في مصفوفات معقدة. يركز الجزء الثاني على التخليق الأخضر لأنابيب نانوية بولي أنيلين (PANI-NT) عبر عملية تجميع ذاتي باستخدام قالب ناعم، وترسيب جسيمات نانوية فضية لاحقًا على هذه الأنابيب باستخدام مستخلص Ccl كعامل اختزال وتثبيت. تم توصيف وتقييم أداء مركبات النانو الفضية/PANI المنتجة (التي تحتوي على كتل مختلفة من PANI تتراوح بين 50 و250 ملغ) من حيث الأداء البيولوجي. عزز دمج جسيمات النانو الفضية الأنشطة المضادة للأكسدة والبكتيريا لـ PANI-NT، ويعزى ذلك إلى التفاعلات التآزرية وتحسين مساحة السطح.



**الكلمات المفتاحية**: *Cynoglossum creticum*، جسيمات نانوية فضية، أنابيب نانوية بولي أنيلين، مركبات نانوية، أنشطة بيولوجية، الاستشعار اللوني.

**Table of contents**

Table of contents

List of figures

## Chapter I

**List of tables**

## List of abbreviations

- **ABTS** : Ethylbenzothiazoline-6-sulfonic acid
- **AgNPs :** Silver Nanoparticles
- **Ag/PANI-NCs :** Silver/Polyaniline nanocomposites
- **AuNPs :** Gold nanoparticles
- **ATCC** : American Type Culture Collection
- **APS :** Ammonium persulfate
- **BET:** Brunauer-Emmett-Teller
- **BHA :** Butylated hydroxyanisole
- **BHT :** Butylated hydroxytoluene
- **BJH:** Barrett-Joiner-Hallender
- **CA :** citric acid
- **Ccl-AgNPs:** Cynoglossum creticum-mediated silver nanoparticles
- **Ccl-extract :** Cynoglossum creticum leaves extract
- **CMAR**: carcinogenic, mutagenic, asthmagenic, or reproductive toxicants
- **DSC :** Differential scanning calorimetry
- **DPPH:** 2,2-diphenyl-1-picrylhydrazyl
- **EDS:** X-ray spectroscopy coupled with energy dispersive
- **EB:** Emeraldine base
- **ES :** Emeraldine salt
- **ESEM:** environmental scanning electron microscope (ESEM)
- **FCC:** Face-centered cubic
- **FTIR :** Fourier transform infrared
- **$IC_{50}$:** Half-maximal inhibitory concentration
- **LEB:** Leucoemeraldine base
- **LSPR:** Localized surface plasmon resonance
- **LOD:** Limit of detection
- **NMs:** Nanomaterials
- **NPs:** Nanoparticles
- **MIC :** Minimum inhibition concentration
- **NEO:** Neomycin sulfate
- **NEO–Ccl-AgNPs :** Neomycin sulfate – silver nanoparticles complex
- **OVAT:** one-variable-at-a-time
- **PAB:** Pernigraniline base
- **PANI :** Polyaniline
- **PANI-NS:** Polyaniline nanostructure
- **PANI-NT:** Polyaniline nanotubes
- **PAs** : Pyrrolizidine alkaloids
- **PL:** Photoluminescence
- **ROS** : Reactive oxidative stress
- **SPR:** surface plasmon resonance
- **TFC:** Total flavonoid content
- **TGA:** Thermogravimetric analysis
- **TPC:** Total polyphenol content
- **UV-Vis :** Ultraviolet-visible spectroscopy
- **XRD :** X-ray diffraction analysis

# *General Introduction*

With the onset of the third millennium, the rapid evolution of advanced technologies has profoundly transformed traditional scientific paradigms, fostering unprecedented breakthroughs that have reshaped numerous industrial sectors and, more broadly, the dynamics of human life[1–3]. Among these transformative developments, nanotechnology has emerged as one of the most interdisciplinary and revolutionary scientific domains. It encompasses the study, manipulation, and engineering of systems and matter at the nanometer scale[4]. The unique properties and phenomena at this level, such as quantum effects and tunable electronic behavior, have spurred the creation of innovative fabrication techniques and next-generation materials, collectively known as nanomaterials, capable of enhancing performance and addressing pressing global challenges in energy, health, and environmental sustainability[5,6]. From a diverse range of nanomaterials, silver nanoparticles (AgNPs) and polyaniline nanostructured (PANI-NS) have emerged as highly promising candidates. These materials, representing inorganic and organic nanomaterials respectively, combine superior biological and physicochemical properties that have increasingly attracted the attention of the scientific community as potential substances for research projects aimed at developing high-performance and sustainable technologies for the 21st century[7,8].

Like noble nanomaterials, AgNPs are characterized by high ionization potential, excellent charge and surface area, strong light absorption, and surface plasmon resonance (SPR) effects, as well as potent antimicrobial and anticancer properties. These features account for their extensive use in biosensing, gene delivery, diagnostics, drug therapy, photo and chemical catalysis, and energy harvesting[9–11]. Global production, estimated at around 550 metric tons annually, primarily relies on chemical and physical synthesis strategies[12]. However, these methods often involve health and ecological risks such as environmental toxicity, cytotoxicity, genotoxicity, and carcinogenesis, as well as high cost limitations in terms of specialized equipment, energy, and time. Therefore, new research aims to develop reliable, more economical, less toxic, and more environmentally friendly methods for producing AgNPs. Green nanobiotechnology, which integrates biotechnology, nanotechnology, and green chemistry, and utilizes natural biological resources, offers a sustainable alternative[13,14]. Biotechnology concerns the manipulation, modification, and exploitation of biological agents and living organisms to create useful products; nanotechnology explores materials at the nanoscale[15]; and green chemistry, or sustainable chemistry, represents a philosophical and methodological shift toward minimizing the environmental risks of chemical production.

Guided by the Twelve Principles developed by Paul Anastas and John Warner, this approach encourages the design, manufacture, and management of chemical processes that minimize waste, toxicity, and energy consumption[16]. By integrating these disciplines, bio-nanotechnology seeks to establish a comprehensive and ethically responsible model for the synthesis of nanomaterials.

Plant biomass and its extracts represent the most significant natural resource for bionanotechnology-based synthesis, offering a cost-effective, efficient, and environmentally compliant approach that aligns with all twelve principles of green chemistry[17]. Extracts provide bioactive phytochemicals like polyphenols, flavonoids, tannins, alkaloids, polysaccharides, and glycosides, which function as reducing, stabilizing and coating agents during AgNP formation, enabling controlled particle size, diverse morphologies, dispersibility, and high colloidal stability[18]. Beyond their role in nanoparticle synthesis, these phytochemicals possess intrinsic therapeutic activities. Consequently, plant-derived AgNPs often exhibit enhanced biocompatibility, reduced bioavailability, and superior biological performance compared with chemically synthesized counterparts. This improvement is largely attributed to the synergistic interaction between silver and bioactive constituents[19].

Among the common herbaceous species of the Mediterranean basin, particularly northeastern Algeria, *Cynoglossum creticum* (blue dog tongue) is notable. This biennial species, to the Boraginaceae family, thrives mainly along open habitats, field and forest edges, and roadsides. Although *C. creticum* is considered a poisonous herb for grazing animals due to its high concentrations of hepatotoxic pyrrolizidine alkaloids (PAs), it has long held a place in traditional Mediterranean medicine[20,21]. Reports have confirmed its therapeutic potential stemming from its rich phytochemical composition of active secondary metabolites, particularly in its aerial parts, specifically the leaves[22,23]. Despite its abundant phytochemical profile and documented biomedicinally potential, *C. creticum* has not yet been thoroughly investigated or exploited in green nanobiotechnology, leaving its ability to mediate nanomaterials synthesis a promising avenue for research.

Neomycin sulfate (NEO) is an important aminoglycoside antibiotic in veterinary medicine and serves as a key therapeutic agent for controlling a broad spectrum of bacterial infections in cattle and other livestock[24]. In addition to its clinical applications, NEO is commonly incorporated into feed formulations and milk replacers as a growth promoter additive and prophylactic agent[25]. However, improper dosing, excessive feed supplementation, and inadequate disposal practices can result in drug contamination. NEO can leach into nearby

water systems and animal products as drug residues. Ecosystems exposure to neomycin promotes genomic mutations and increases the development of antibiotic-resistant bacteria[26]. Neomycin can also pose a risk of ingestion and accumulation in the human body through animal-derived food products, causing serious side effects such as nephrotoxicity, neurotoxicity, cardiotoxicity, and irreversible ototoxicity[27,28].

In addition to these environmental and public health concerns, analytical detection of NEO is also challenging due to the absence of inherent chromophores or fluorophores in its structure. Standard methods such as high-performance liquid chromatography and mass spectrometry (HPLC-MS) therefore require labor-intensive and costly derivatization steps using chromogenic reagents, limiting their suitability for routine or in-situ analysis[29,30]. The creation of precise analytical methods for qualitative and quantitative sensing in complex systems is of substantial practical importance. Advances in nanotechnology provide promising alternatives, especially for detecting trace NEO contaminants in heterogeneous environmental and biological systems[31,32]. In particular, colorimetric sensing platforms based on the surface plasmon resonance (SPR) properties of silver nanoparticles offer a rapid, low-cost, and user-friendly method with high accuracy for analytes detection[33,34].

Recently, polyaniline nanostructures (PANI-NS), the second significant intrinsically conducting polymer (ICP), have emerged as innovative organic conjugate nanomaterials, characterized by exceptional electronic conductivity, high pseudocapacitance, and remarkable thermal, chemical, and environmental stability[35,36]. In addition, PANI exhibits intelligent chromogenic behavior, making it valuable for applications in smart sensors platforms and energy storage and transmission devices. Nanostructured forms of PANI such as nanofibers and nanotubes have also overcome the poor processability of bulk PANI, thereby expanding opportunities for biopharmaceutical and biomedical applications. However, these structural improvements have not consistently translated into enhanced biological performance; although antibacterial and antioxidant activities have increased, intensified cellular interactions have raised concerns regarding uptake, bioaccumulation, potential toxicity, and long-term biological safety[37]. Integrating silver nanoparticles with PANI nanostructures has yielded hybrid organic-inorganic composites with synergistic enhanced functional performance of both components. Ag/PANI nanohybrid demonstrate improved biological properties, including stronger antibacterial activity and more robust redox behavior, making them attractive for environmental monitoring, antimicrobial coatings, and biomedical applications[38–40]. Nevertheless, to date green bionanotechnology strategies using plant extracts have yet to be applied to integrate

AgNPs into the PANI-NS, despite their promise for improving biocompatibility, enhancing antimicrobial and antioxidant efficacy, and reducing associated toxic concerns.

This work primarily aims to value and utilize the plant matter of a toxic herbaceous species, which poses a threat to livestock and is widespread in northern Algeria in nanotechnology applications. This was achieved by employing an aqueous extract of *Cynoglossum creticum* leaves to synthesize green silver nanoparticles (Ccl-AgNPs) and develop silver/polyaniline nanocomposites (Ag/PANI NCs). The study further examines the potential applications of the synthesized Ccl-AgNPs, with particular emphasis on biopharmaceutical and analytical fields. This was done through antioxidant and antimicrobial tests and colorimetric sensing of neomycin sulfate. Within this framework, the effects of AgNPs bio-incorporation and deposition on green polyaniline nanotube (PANI-NT) were also explored, focusing on enhancing the biological performance of Ag/PANI NCs. The thesis is structured and organized into four main chapters encompassing the theoretical foundations, experimental approach and results, and discussion pertinent to these research objectives.

- Chapter I presents a comprehensive theoretical framework for nanotechnology, covering classification of nanomaterials, silver nanoparticles, polyaniline nanostructures, and key strategies for synthesizing silver-polyaniline nanocomposites.
- Chapter II explores the potential of *C. criticum* leaves as a green platform for the synthesis of AgNPs. It emphasizes on optimizing hydro-extraction and nanoparticle synthesis processes discusses a comprehensive physicochemical characterization of the resulting Ccl-AgNPs.
- Chapter III examines the pharmaceutical potential of Ccl-AgNPs by evaluating their antioxidant and antimicrobial activities, as well as their performance as a colorimetric sensor for detecting neomycin sulfate in real environmental, biological, and veterinary samples.
- Chapter IV addresses the synthesis and characterization of green PANI nanotubes and Ag/PANI nanocomposites, and investigates their potential biological functionalities.

The thesis concludes by summarizing the principal research findings and emphasizing the potential of purposing unwanted plant biomass for applications in nanotechnology.

## References


1. Ansari I, Barati M, Sadeghi Moghadam MR, Ghobakhloo M. An Industry 4.0 readiness model for new technology exploitation. *IJQRM*. 2023;40(10):2519-2538. doi:10.1108/IJQRM-11-2022-0331

2. Jamwal A, Agrawal R, Sharma M, Giallanza A. Industry 4.0 Technologies for Manufacturing Sustainability: A Systematic Review and Future Research Directions. *Applied Sciences*. 2021;11(12):5725. doi:10.3390/app11125725

3. Vicente KJ. *The Human Factor: Revolutionizing the Way People Live with Technology*. 1st ed. Routledge; 2013. doi:10.4324/9780203944479

4. Khatoon UT, Velidandi A. An Overview on the Role of Government Initiatives in Nanotechnology Innovation for Sustainable Economic Development and Research Progress. *Sustainability*. 2025;17(3):1250. doi:10.3390/su17031250

5. Malik S, Muhammad K, Waheed Y. Nanotechnology: A Revolution in Modern Industry. *Molecules*. 2023;28(2):661. doi:10.3390/molecules28020661

6. Chaikittisilp W, Yamauchi Y, Ariga K. Material Evolution with Nanotechnology, Nanoarchitectonics, and Materials Informatics: What will be the Next Paradigm Shift in Nanoporous Materials? *Advanced Materials*. 2022;34(7):2107212. doi:10.1002/adma.202107212

7. Mishra PK, Sharma HK, Gupta R, Manglik M, Brajpuriya R. A critical review on recent progress on nanostructured polyaniline (PANI) based sensors for various toxic gases: Challenges, applications, and future prospects. *Microchemical Journal*. 2025;208:112369. doi:10.1016/j.microc.2024.112369

8. Dawadi S, Katuwal S, Gupta A, Lamichhane U, Thapa R, Jaisi S, Lamichhane G, Bhattarai DP, Parajuli N. Current Research on Silver Nanoparticles: Synthesis, Characterization, and Applications. Karimi-Maleh H, ed. *Journal of Nanomaterials*. 2021;2021:1-23. doi:10.1155/2021/6687290

9. Ahmed B, Bilal Tahir M, Sagir M, Hassan M. Bio-inspired sustainable synthesis of silver nanoparticles as next generation of nanoproduct in antimicrobial and catalytic applications. *Materials Science and Engineering: B*. 2024;301:117165. doi:10.1016/j.mseb.2023.117165

10. Eker F, Duman H, Akdaşçi E, Witkowska AM, Bechelany M, Karav S. Silver Nanoparticles in Therapeutics and Beyond: A Review of Mechanism Insights and Applications. *Nanomaterials*. 2024;14(20):1618. doi:10.3390/nano14201618

11. Sharma D, Raveena, Ngasainao MR, Kumari P. Development of enzyme-based biosensor for residual detection of organophosphate pesticides using functionalized nanocellulose-modified silver nanoparticles. *Microchemical Journal*. 2024;207:111856. doi:10.1016/j.microc.2024.111856

12. Shen L, Li QQ, Kang YH, Xiang QQ, Luo X, Chen LQ. Metabolomics reveals size-dependent persistence and reversibility of silver nanoparticles toxicity in freshwater algae. *Aquatic Toxicology*. 2023;258:106471. doi:10.1016/j.aquatox.2023.106471

13. Patra JK, Baek KH. Green Nanobiotechnology: Factors Affecting Synthesis and Characterization Techniques. Chen W, ed. *Journal of Nanomaterials*. 2014;2014(1):417305. doi:10.1155/2014/417305

14. Sivakami A, Sarankumar R, Vinodha S. Introduction to Nanobiotechnology: Novel and Smart Applications. In: Pal K, ed. *Bio-Manufactured Nanomaterials*. Springer International Publishing; 2021:1-22. doi:10.1007/978-3-030-67223-2_1

15. Chen C, Hu Y, Ikeuchi M, Jiao Y, Prasad K, Su YH, Xiao J, Xu L, Yang W, Zhao Z, Zhou W, Zhou Y, Gao J, Wang JW. Plant regeneration in the new era: from molecular mechanisms to biotechnology applications. *Sci China Life Sci*. 2024;67(7):1338-1367. doi:10.1007/s11427-024-2581-2

16. Anastas P, Eghbali N. Green Chemistry: Principles and Practice. *Chem Soc Rev*. 2010;39(1):301-312. doi:10.1039/B918763B

17. Eker F, Akdaşçi E, Duman H, Bechelany M, Karav S. Green Synthesis of Silver Nanoparticles Using Plant Extracts: A Comprehensive Review of Physicochemical Properties and Multifunctional Applications. *IJMS*. 2025;26(13):6222. doi:10.3390/ijms26136222

18. Shahzadi S, Fatima S, Ul Ain Q, Shafiq Z, Janjua MRSA. A review on green synthesis of silver nanoparticles (SNPs) using plant extracts: a multifaceted approach in photocatalysis, environmental remediation, and biomedicine. *RSC Adv*. 2025;15(5):3858-3903. doi:10.1039/D4RA07519F

19. Manzoor SI, Jabeen F, Patel R, Alam Rizvi MM, Imtiyaz K, Malik MA, Dar TA. Green synthesis of biocompatible silver nanoparticles using *Trillium govanianum* rhizome extract: comprehensive biological evaluation and *in silico* analysis. *Mater Adv*. 2025;6(2):682-702. doi:10.1039/D4MA00959B

20. Dresler S, Szymczak G, Wójcik M. Comparison of some secondary metabolite content in the seventeen species of the Boraginaceae family. *Pharmaceutical Biology*. 2017;55(1):691-695. doi:10.1080/13880209.2016.1265986

21. Selvi F, Sutorý K. A synopsis of the genus *Cynoglossum* (Boraginaceae-Cynoglosseae) in Italy. *Plant Biosystems - An International Journal Dealing with all Aspects of Plant Biology*. 2012;146(2):461-479. doi:10.1080/11263504.2012.667842

22. Arroussi J, Ouerfelli M, Smaoui A, Ahmed HB, Kaâb SB, Kaâb LBB. Antioxidant activity of seven plant extracts collected from Tunisia and their allelopathic potential on Lactuca sativa L. and Phalaris minor L. *South African Journal of Botany*. 2022;148:135-143. doi:10.1016/j.sajb.2022.04.029

23. Menghini L, Ferrante C, Zengin G, Mahomoodally MF, Leporini L, Locatelli M, Cacciagrano F, Recinella L, Chiavaroli A, Leone S, Brunetti L, Orlando G. Multiple pharmacological approaches on hydroalcoholic extracts from different parts of *Cynoglossum creticum* Mill. (Boraginaceae). *Plant Biosystems - An International Journal Dealing with all Aspects of Plant Biology*. 2019;153(5):633-639. doi:10.1080/11263504.2018.1527790

24. Blanchard C, Brooks L, Beckley A, Colquhoun J, Dewhurst S, Dunman PM. Neomycin Sulfate Improves the Antimicrobial Activity of Mupirocin-Based Antibacterial Ointments. *Antimicrob Agents Chemother*. 2016;60(2):862-872. doi:10.1128/AAC.02083-15

25. Buss LN, Yohe TT, Cangiano LR, Renaud DL, Keunen AJ, Guan LL, Steele MA. The effect of neomycin inclusion in milk replacer on the health, growth, and performance of male Holstein calves during preweaning. *Journal of Dairy Science*. 2021;104(7):8188-8201. doi:10.3168/jds.2020-19827

26. Lee S, Kim C, Liu X, Lee S, Kho Y, Kim WK, Kim P, Choi K. Ecological Risk Assessment of Amoxicillin, Enrofloxacin, and Neomycin: Are Their Current Levels in the Freshwater Environment Safe? *Toxics*. 2021;9(8):196. doi:10.3390/toxics9080196

27. Wu Y, Meng W, Guan M, Zhao X, Zhang C, Fang Q, Zhang Y, Sun Z, Cai M, Huang D, Yang X, Yu Y, Cui Y, He S, Chai R. Pitavastatin protects against neomycin-induced ototoxicity through inhibition of endoplasmic reticulum stress. *Front Mol Neurosci*. 2022;15:963083. doi:10.3389/fnmol.2022.963083

28. Lin Y, Zhang Q, Chen L, Liu Y, Lin X, Peng X, Cao H, Lei Y, Wang X. Neomycin affects cardiovascular and hematopoietic system via the PI3K/Akt pathway in zebrafish larvae. *Ecotoxicology and Environmental Safety*. 2025;296:118203. doi:10.1016/j.ecoenv.2025.118203

29. Jie M, Zhu A, Zhu B, Guo R, Lan S, He J, Lang X, Bai Y. A ratiometric fluorescent probe based on Lu-Eu-DPA nanoparticles for sensitive and visual detection of gentamicin sulfate, neomycin, and erythromycin in food. *Food Measure*. 2025;19(7):4657-4668. doi:10.1007/s11694-025-03279-6

30. Dessai S, Mannur VS, Koli R, Dhond M, Badiger P. Quality by design-engineered reversed-phase high-performance liquid chromatography method development and validation for simultaneous estimation of neomycin sulfate and beclomethasone dipropionate in bulk and pharmaceutical dosage form. *Separation Science Plus*. 2024;7(6):2400001. doi:10.1002/sscp.202400001

31. El-Didamoony MA, Elkady EF, Sayed RM, Batakoushy HA, Mostafa EA. Highly Sensitive Spectrofluorimetric and Colorimetric Quantitation of Neomycin Using Nanosilver-Fluorescein Hybrid: A Comprehensive Assessment of Greenness and Blueness. *Luminescence*. 2025;40(1):e70094. doi:10.1002/bio.70094

32. Cheubong S, Teepoo S, Wechakorn K, Cheubong C. Highly sensitive determination of neomycin residues in milk samples using a fast, simple competitive carbon dot-linked immunosorbent assay (CDs-LISA). *Journal of Food Composition and Analysis*. 2025;142:107502. doi:10.1016/j.jfca.2025.107502

33. Khan S, Ali I, Ali A, Toloza CAT, Ahmad N, Shah MR. Vanillin-nicotinic hydrazine schiff base triazole-thiazole functionalized silver nanoparticles: A novel and portable sensing platform for neomycin. *Optical Materials*. 2025;164:117088. doi:10.1016/j.optmat.2025.117088

34. Ali I, Raja DA, Ahmed F, Fazal M, Hameed A, Shah MR, Malik MI. Triazole thiazole 4-Nitrobenzohydrazide Schiff base-stabilized silver nanoparticles for selective and efficient

detection of neomycin. *Journal of Molecular Structure*. 2024;1315:138971. doi:10.1016/j.molstruc.2024.138971

35. Wang J, Zhang D. One-Dimensional Nanostructured Polyaniline: Syntheses, Morphology Controlling, Formation Mechanisms, New Features, and Applications. *Adv Polym Technol*. 2013;32(S1). doi:10.1002/adv.21283

36. Kheilnezhad B, Firoozabady AS, Aidun A. An Overview of Polyaniline in Tissue Engineering.

37. Li YS, Chen BF, Li XJ, Zhang WK, Tang HB. Cytotoxicity of Polyaniline Nanomaterial on Rat Celiac Macrophages In Vitro. Lee MH, ed. *PLoS ONE*. 2014;9(9):e107361. doi:10.1371/journal.pone.0107361

38. Jia Q, Shan S, Jiang L, Wang Y, Li D. Synergistic antimicrobial effects of polyaniline combined with silver nanoparticles. *J of Applied Polymer Sci*. 2012;125(5):3560-3566. doi:10.1002/app.36257

39. Shaban M, Rabia M, Fathallah W, El-Mawgoud NA, Mahmoud A, Hussien H, Said O. Preparation and Characterization of Polyaniline and Ag/ Polyaniline Composite Nanoporous Particles and Their Antimicrobial Activities. *J Polym Environ*. 2018;26(2):434-442. doi:10.1007/s10924-017-0937-1

40. Guimarães ML, Da Silva FAG, Da Costa MM, De Oliveira HP. Coating of conducting polymer-silver nanoparticles for antibacterial protection of Nile tilapia skin xenografts. *Synthetic Metals*. 2022;287:117055. doi:10.1016/j.synthmet.2022.117055

# *Chapter I*

## *Theoretical art about nanotechnology, silver nanoparticles, and polyaniline nanostructure*

## I.1.Introduction

A quarter century into the twenty-first millennium, it is possible to affirm B. Clinton's vision of a century defined by science, supported by knowledge, and shaped by technology with bolder exploratory ideas[1]. Today, cognitive advancements are driving global awareness and societies toward a new cultural paradigm that prioritizes sustainable development and the protection of natural resources through cleaner, safer, and cost-effective production technologies. Nanotechnology meets these expectations transformatively, enabling the reduction of industrial costs, reducing reliance on heavy machinery and fossil fuels, and improving functional efficiency and product longevity[2,3]. Nanotechnology defines modern innovation and radical exploration, integrating the dynamics of many different fields and disciplines. Its transformative impact is particularly evident in the development and application of nanomaterials, which serve as the foundational elements of this technology. These materials have demonstrated significant potential in various sectors, particularly in healthcare and environmental science.

This chapter will offer a comprehensive theoretical overview of nanotechnology, nanomaterials, silver nanoparticles, polyaniline nanostructures, and their nanocomposites. It begins by outlining the current status of nanotechnology within the global market, then traces the historical evidence that proves the chronological development of the concept of nanotechnology. A systematic classification of nanomaterials will be presented, based on critical parameters such as size, morphology, chemical composition, origin, toxicity, and other distinctive features. Special attention will be paid to silver nanoparticles and nanopolyaniline, including the role of their physicochemical and biological properties on their functions and application performance, and the various approaches to synthesizing these materials. Furthermore, the chapter will explore the key strategies reported in the literature for the design, integration, and functionalization of silver polyaniline nanocomposites. The chapter will conclude by synthesizing the main insights presented, establishing a foundation for the subsequent discussion of experimental methodologies.

## I.2. Nanotechnology

Nanotechnology has recently achieved rapid expansion with tremendous leaps in technical and applied processes, contributing to stimulating economic growth, improving the quality of life, and changing modern social dynamics [4,5] . Nanotechnology is a major focus of science and technology research; it is an innovative and multidisciplinary field that deals specifically with phenomena, systems, and materials at the nanometer scale, where at least one dimension is in this range. This field focuses on the characterization, design, synthesis, and manufacturing of nanostructured materials with distinct shapes and sizes for purposes and applications in various sectors, such as the food, medical, pharmaceutical, renewable energy, and electronics industries, and even to reduce environmental problems and challenges.

Nanotechnology is gradually dominating various industrial and service sectors across the globe, as the worldwide market value of nanotechnology jumped from roughly $16 billion in 2010 to $27 billion in 2015 and reached approximately $76 billion in 2020 [6]. It is also anticipated that its global market value will reach $170 billion and $288 billion by 2026 and 2030, respectively[7]. The growing global market for nanotechnology-based products and services is due to several factors, such as the need to miniaturize devices resulting from technological advances as well as government and private sector expenditures and investments in nanotechnology, especially in developed countries such as the United States, China, and the European Union. An estimated $250 billion has been invested in nanotechnology worldwide, and in 2016, several national nanotechnology initiatives were started in over 60 nations[8,9].

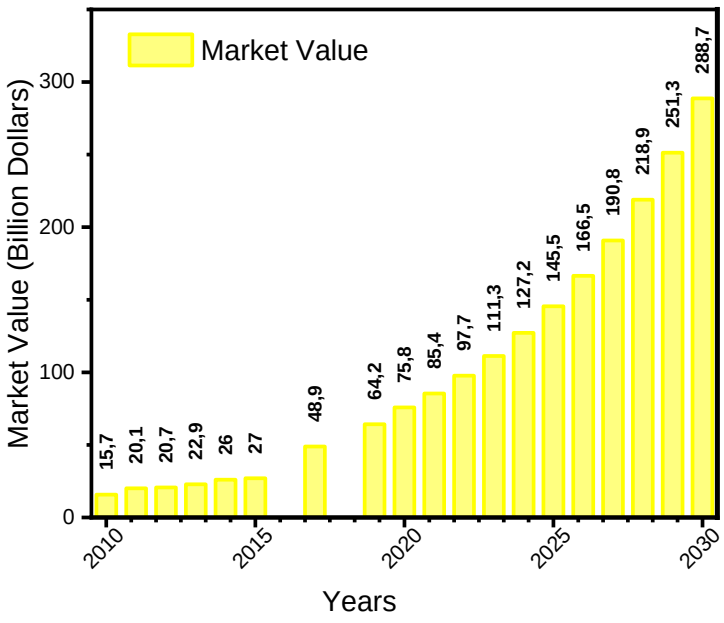


**FIGURE.I.1.** Projected changes in the global nanotechnology market value over the last two decades [7,10].

### I.2.1. Historical development of nanotechnology

In truth, although nanotechnology is considered the groundbreaking discovery of the second half of the 20th century, as well as one of the fastest-developing fields in recent decades, affecting all aspects of life[11]. However, there were early ideas and uses of nanotechnology; numerous historical evidences, such as the unique colors of Chinese silk, Egyptian cosmetics, and colored bottles, indicate the exploitation of materials at the nanoscale by ancient artists and craftsmen despite their lack of awareness of nano concepts and technologies[12,13].

The use of natural asbestos nanofibers in strengthening ceramic matrices since before 2500 BC is one of the oldest discovered examples that proves the antiquity of human exploitation of nanotechnology[14]. The ancient Egyptians also used many lead-based cosmetic formulations more than 4000 years ago, and the Greeks and Romans followed them in developing black hair dyes based on paste of calcium hydroxide and lead oxide that were applied to gray hair (Figure.I.2.(a)). Sulfur from the keratin proteins in hair interacts with the paste blend, forming layers of lead sulfide nanocrystals (PbSNPs)[13,15]. Additionally, Egyptian blue ($CaCuSi_4O_{10}$), one of the first synthetic dyes, was created by the Egyptians by forming a complex sintered mixture of nanosized glass and quartz in the early third millennium BC (Figure. I.2(b)). Archaeological excavations indicate that Egyptian blue was used in jewelry,

glass, and pictorial effects[16,17]. Celtic red enamels made between 400 and 100 BC have been reported to contain nanoparticles of copper and cuprous oxide[18] (Figure. I .2(c)).

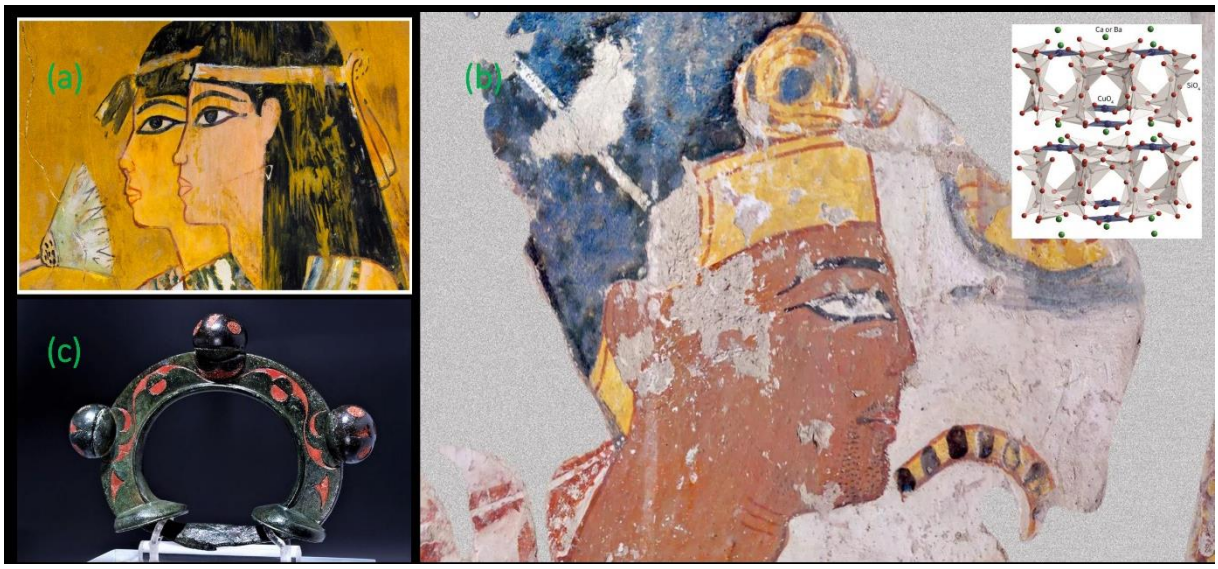


**FIGURE.I.2.**Archaeological evidence of nanomaterials used in ancient civilizations: a) a mural of Qenamun, 1550–1292 BC (Egyptian Museum of Barcelona); b) a stela of Ramesses II, circa 1100 BC (Tomb of Nakhtemune, Egypt); c) a rein Guide artifact painted in champleve enamel, circa 1st century BC (Museum of Wales).

The Middle Ages also witnessed various exploitations and applications of nanotechnology without scientific understanding, which are evident in glassware, cathedrals, Arab swords, and even in medical prescriptions[19,20]. The Roman Lycurgus Cup, made in the 4th century and now housed at the British Museum in London, is one of the most famous historical instances of nanotechnology[21]. This glass piece is characterized by a change in its color when exposed to different light wavelengths (dichroic glass), which is mostly owing to nanoparticles with a diameter of 50-100 nm in the glass matrix. X-ray diffraction analysis (XRD) of the Lycurgus Cup revealed that it contains nanoparticles of both silver-gold alloy (Ag-Au NPs) with a ratio of Ag:Au ~7:3 and copper (CuNPs) with a ratio of 10%[22,23] . Later in the Medieval Ages, stained glass was produced to embellish numerous churches throughout Europe[24] . This glass is distinguished by its bright yellow and deep red colors, which are mainly due to colloidal silver and gold nanoparticles formed as a result of the addition of gold chloride and silver nitrate as coloring agents during the processing of molten glass, which is mainly composed of pure sand (SiO2)[25,26].

Nanotechnology also contributed to Islamic war industries during the Middle Ages, as evidenced by the unique Damascus sword made using alloys of wootz steel imported from Sri Lanka and India. Physicochemical analyses of the sword produced by the blacksmith Assad

Ullah showed that it mainly contains carbon nanotubes with exceptional elasticity and tensile strength[27] . Figure. I.3.(a-c) shows surface patterns of Damascus swords and high-resolution transmission electron microscope images of a specimen, demonstrating the presence of carbon nanotubes and nanowires with high chemical stability, even in acid. Also of interest are the early applications of nanotechnology in the field of medicine, particularly in Indian culture[28]. The Ayurvedic Bhasma, developed in the 7th century to treat many chronic illnesses, is a unique innovation in medical history. Ayurvedic Bhasma is a mineral-based medicinal ash mixed with herbal extracts manufactured by Putapaka and Kupipakwa procedures[29,30]. The Putapaka method is based on the principle of heating minerals at high temperatures and quenching them with herbal juices repeatedly, which ensures detoxification of minerals and formation of bioactive nanomaterials[15,31]. While the Kupipakwa method is based on complex processes that begin with Shodhana, which is the treatment of specific minerals with different medicines to purify them from physical and chemical impurities. followed by preparation of Kajjali, a fine black paste made by mixing and grinding the Shodhana product with purified mercury and sulfur. The Kajjali is stored in a Kachakupi, which is a glass covered with seven layers of cloth and mud and placed in a sand bath known as Valukayantra. Finally, the medicinal product is collected in the form of a finely ground powder of nano-dimensions[32].

Despite the pioneering usage of nanotechnology in the Middle Ages, this technology was not addressed or explored from a scientific point of view until the modern era, specifically in the 1850s by researcher Michael Faraday. In 1857, he first reported the synthesis of colloidal gold nanoparticles (AuNPs) by reducing gold salts with a solution of white phosphorus, where he discovered the effects of quantum size on the optical properties of gold in its colloidal and bulk form[33]. Gustav Mie later in 1908 provided a theoretical framework explaining the specific colors of mineral colloids[34]. The 1940s marked a shift to industrial applications, as rubber was reinforced with nano-silicon dioxide as an alternative to carbon black[35] .

The invention of the transmission electron microscope (TEM) in 1931 by Max Knoll and Ernst Ruska (Figure.I.3.(d,e)) at the University of Berlin also revolutionized science in the modern era[36]. This microscope shoots a beam of electrons through the material, enabling the capture of highly detailed images at resolutions of less than 1 nanometer. Manfred von Ardenne developed the first scanning electron microscope (SEM) in 1938, as illustrated in Figure.I.3(f). However, its commercialization was delayed until 1965 due to the complexity of the required technology[37]. The SEM operates on the principle of scanning the surface of a sample with a focused beam of electrons, which allows for the creation of highly detailed images with a

resolution of a few nanometers that reveal the morphology and structures of the material's surface[38].

Nonetheless, it is historically likely that the actual launch of nanotechnology as a scientific concept was in the famous speech "There's Plenty of Room at the Bottom" delivered by the American physicist Richard Feynman on December 29, 1959, at the California Institute of Technology (Caltech), on the sidelines of the American Physical Society meeting[39]. Although Richard Feynman did not coin the term "nanotechnology," he referred to the idea of developing technological capabilities to engineer individual atoms to create small machines at the molecular level by proposing his hypothesis of encoding the volumes of the Encyclopedia Britannica on the head of a pin. The first formal introduced of the term nanotechnology was mentioned in a research paper by the Japanese Prof. Norio Taniguchi published in 1974[40]. Taniguchi provided a precise definition of nanotechnology, framing it within the context of advancements in nanoscale semiconductor technologies and emphasizing precision manufacturing processes at the nanometer scale[41].

Academic Eric Drexler also contributed to the popularization and expansion of nanotechnology in the 1980s, drawing on Feynman's insights into his ideas known as "molecular nanotechnology"[42] . His well-known book, "Motions of Creation: The Coming Age of Nanotechnology" (1986), highlights contemporary applied nanotechnology research and traces the conceptual development of this technology[43]. This book played a pivotal role in shaping contemporary nanotechnology research and advancing its recognition as a multidisciplinary scientific field.

The invention of the scanning tunneling microscope (STM) by Gerd Binnig and Heinrich Rohrer in 1981 (Figure.I.3.(h)), followed by the development of the atomic force microscope (AFM) by Gerd Binnig, Calvin Quate, and Christoph Gerber in 1986, marked transformative milestones in nanosurface science and technology[44,45]. These tools allowed for the imaging and manipulation of material surfaces and their topology at atomic resolution, enabling unprecedented explorations of nanoscale phenomena and the birth of the science of clustering with the discovery in 1985 of fullerenes[46]. They are uckyball-shaped objects consisting of 60 carbon molecules with distinct molecular properties that bridged the gap between atomic clusters and bulk materials and inspired research into related nanomaterials[47]. This was followed in 1991 by the discovery of carbon nanotubes by Sumio Iijima et al., which exhibited extraordinary surface area, electrical, and thermo-mechanical features that reshaped the academic community's view of nanomaterials technology[48].

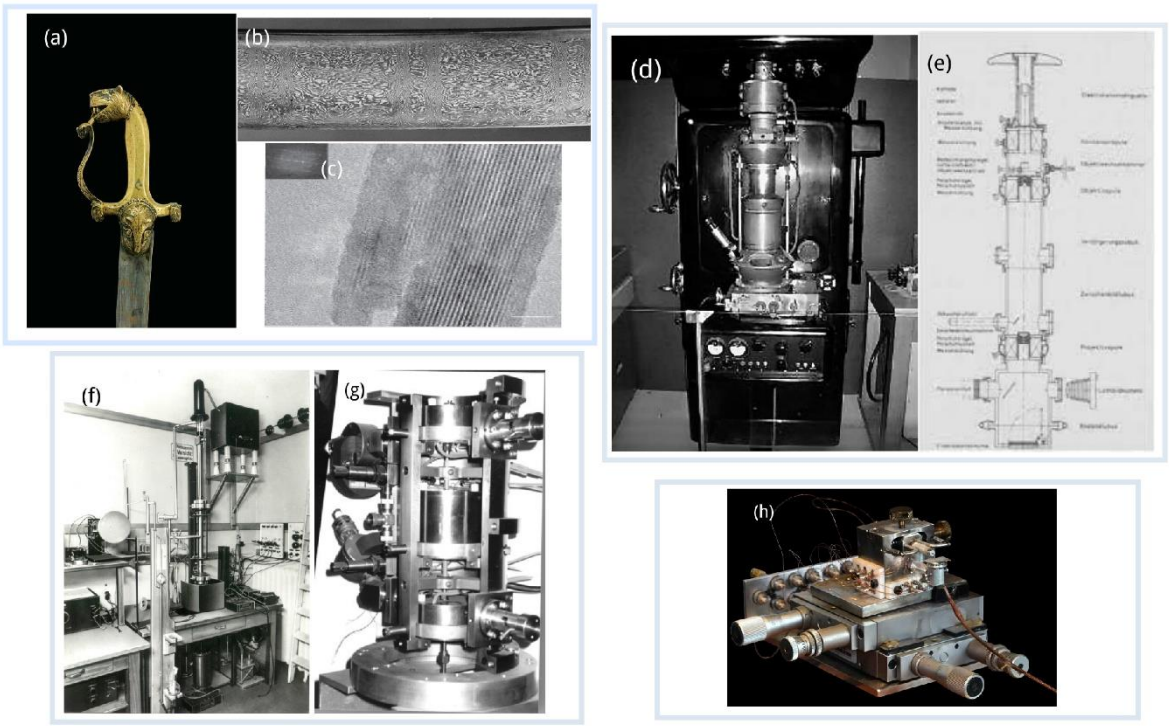


**FIGURE.I. 3.** a) Tipu Sultan's sword made of Damascus steel (Ex-Wigington Collection); b) blade surface of the Mohammad ladder Shamshir sword[27]; c) HRTEM images of carbon nanotubes in a Damascus sword showing Multiwalled carbon nanotubes[49]; d) the first electron microscope was made by Ruska and Knoll and produced by Siemens in 1939 (Deutsches Museum, Munich); e) cross-section of the first two-stage electron microscope, designed by Ruska in 1934[36]; f) image taken from the first scanning transmission electron microscope with an electron beam diameter of on the target approximately 10 nm, developed in 1938 (Siemens Historical Institute, Munich); g) sextupole corrector of STEM microscope with a field-emission electron source and a single lens, designed by Crowe et al[50]; and h) Scanning tunneling microscope, made in 1986 (Museum of the History of Science, Geneva).

Recognizing the future potential of nanotechnology as a leading field for driving the pace of development, the United States established the National Science Foundation Nanotechnology Program in 1991 and a program called the National Nanotechnology Initiative (NNI) in 2001, fostering interdisciplinary research and innovation. These efforts have accelerated the development of nanotechnology as a multidisciplinary field capable of contributing to significant advances in wide range of industrial activities such as medical, pharmaceutical, transformational, energy, and electronics, which drive economic and technological growth[51,52].

## I.3. Nanomaterials (NMS)

Nowadays, it is possible to observe the rapid development of technology based on nanomaterials compared to its counterpart that uses bulk materials. In reality, nanomaterials are the backbone of nanotechnology due to their unique features and dimensions that enable nanotechnology applications to be the most potential solutions to address many contemporary challenges and problems. The continuous development of nanomaterials is expected to play a pivotal role in driving technological innovation and improving human life in the future[53,54]. Epidemics have historically posed significant threats to humanity, causing widespread mortality of population groups and deadly famines[55]. Nanomaterials have been used to diagnose and treat many epidemic illnesses and limit their spread, such as monkeypox, which has recently increased suddenly, and the Covid-19 pandemic, which led to a global health and economic crisis between 2019 and 2022[56,57]. Additionally, green technological research based on nanomaterials works to mitigate environmental risks such as pollution, climate change, and global warming. Nanomaterials can be described as the last solution to save environmental life.

Materials with at least one dimension in the range between 1 and 100 nm are called nanomaterials. At this scale, the dimensions are so small that they fall well below the threshold of visibility to the naked eye, as the smallest objects discernible under ideal conditions are approximately 10 μm[58]. For comparison, the thickness of a human hair is 50 μm, which is 50,000 times larger than 1 nm. Actually, there is no universally standardized definition or legislation for nanomaterials, but most regulations agree on key criteria: materials with one dimension in the nano range are nanomaterials, as well as materials with a size fewer than 100 nm, and those exhibiting phenomena that depend on this dimension, i.e., they have different properties than their counterparts with larger dimensions[59,60]. At nanoscale dimensions, physical, chemical, thermal, optical, and magnetic properties are enhanced, enabling unique and versatile applications across numerous sectors.

### I.3.1. Sources and Classifications of Nanomaterials

The diversity of sources, structural composition, shape, and other biochemical and physical properties of nanomaterials necessitate the classification and definition of nanomaterials into a set of categories in order to gain a deeper understanding of their properties to suit advanced applications. Several methods are used to classify nanomaterials, based on the adopted philosophy, characteristics, and targeted applications. In general, nanomaterials may

be organized using six primary criteria: origin, size and dimensions, composition, porosity, and toxicity.

### *1. Classification by Origin of NMs*

Our cosmic system and terrestrial life are filled with an enormous variety of nanostructures, which may be divided into four groups based on their origin: natural, bio-inspired, incidental, and manufactured nanomaterials.

#### *1.1. Natural nanomaterials*

Natural nanomaterials encompass all nanoscale forms that are formed naturally, either through natural mechanical, chemical, or biological processes, without the intervention of any anthropogenic activities[14]. Natural NMs constitute an important component of the terrestrial ecosystem, as they can be found in all the Earth's spheres. In the hydrosphere, NMs exhibit unique compositions and functionalities. For instance, magnetite nanoparticles ($Fe_3O_4$-NPs) are prevalent in both marine and freshwater systems and help magnetotactic bacteria (MTB) navigate to preferred environments using the Earth's magnetic field[61]. Additionally, siliceous ooze, one of the most important bio-pelagic ocean sediments, originates from silica nanoparticles ($SiO_2$) produced by marine microorganisms like diatoms algae[62].

The atmosphere, particularly the troposphere, also contains various nanomaterials that influence cloud formation and atmospheric chemistry. Notably, nano-graphene and fullerenes contribute to aerosol dynamics and light scattering[63]. A wide range of mineral-based nanomaterials are found in the lithosphere, including silica nanoparticles ($SiO_2$), titanium dioxide nanoparticles ($TiO_2$), and aluminum oxide nanoparticles ($Al_2O_3$), which contribute to the structure and acidity of the soil, geochemical cycles, and the availability of nutrients. Furthermore, nanoclays such as montmorillonite and kaolinite exhibit significant adsorption capacities for organic pollutants and heavy metals[64].

The biosphere also witnesses a remarkable nanodiversity, which is created through various biological processes. Several microorganisms exist in nanoform, including foraminifera, viruses, bacteria (nanobes), and actinomycetes[65,66] . Additionally, plants and fungi absorb mineral ions from water and soil, subsequently accumulating them into nanoparticles, such as sulfide quantum dots and metal-based nanoparticles (e.g., silver and gold NPs)[67] . There are also organic nanostructures like cellulose nanofibers in plants, enzymes and protein molecules, as well as biocolloidal systems such as blood and milk.

In the insect world, highly organized nanostructures have naturally developed on wing surfaces, providing protective functions against environmental pollutants and moisture. The phenomenon of iridescence in insects arises from the interaction of light with microscopic nanostructures in their exoskeletons, demonstrating an advanced example of biologically mediated structural coloration[68,69] . Figure.I.4 highlights the structural and morphological color features of some iridescent insects. Furthermore, calcium carbonate ($CaCO_3$) nanoparticles, formed through biomineralization, are essential components of seashells, coral reefs, and the human bone matrix.

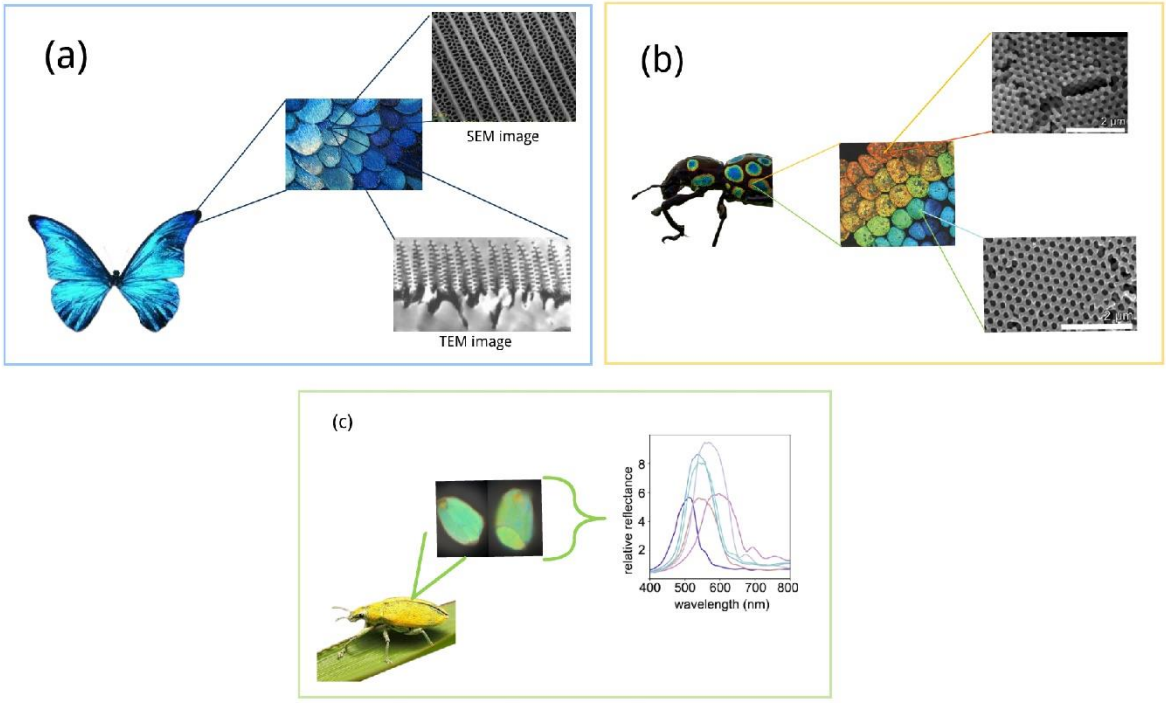


**FIGURE.I. 4.** Structural Basis of Iridescence Insects. a) Morpho rhetenor butterfly: photograph, magnified wing section, and corresponding TEM and SEM images revealing nanostructured scales[70,71]; b) SEM images of Pachyrrhynchus congestus pavonius (weevil) wing scales displaying annular spots with iridescent colors ranging from blue-green to orange-red[72]; c) Epi-reflectance microscopy images and reflectance spectra of scale sections from the golden dust weevil Hypomeces squamosus[73].

### *1.2. Engineered nanomaterials*

Engineered nanomaterials are designed materials that are intentionally produced by different physicochemical, biological, and hybrid techniques with specific properties to meet their intended purposes[59]. Unlike natural nanomaterials, which exhibit various regular and irregular morphological structures, synthetic nanomaterials are typically designed with uniform and specific shapes and high surface area. Historical records indicate that the commercial production of engineered nanomaterials began in the 1940s with the aerosol-based synthesis of

fumed silica, and in the 1960s, aqueous solutions were used to manufacture silica nanospheres. This was followed by rapid advancement in the production of different types of nanomaterials to meet industrial demands, particularly the manufacturing of metal oxides and polymer-based nanocomposites[14].

Predicting the future trajectory of engineered nanomaterials remains challenging due to their vast diversity and widespread applications, particularly in the pharmaceutical and medical sectors. By 2019, engineering nanoproducts exceeded 22% of the pharmaceutical market, and the size of the medical nanomarket is projected to surpass $350.8 billion by the end of 2025[74]. However, concerns are growing about the behavior of manufactured nanomaterials towards environmental systems, as current scientific understanding remains insufficient for accurate predictions. Reports have confirmed the release of manufactured nanomaterials into the environment as industrial waste or with consumer product degradation. Notably, nano-titanium dioxide and nanosilver are being detected in urban environments due to their emission from exterior building paints[75,76].

### *1.3. Biomimetic and bioinspired nanomaterials*

Biomimetic and bioinspired nanomaterials represent the materials that derive their design principles from the structures, mechanisms, or characteristics of naturally occurring biological nanomaterials. However, a critical distinction exists between the concepts of biomimetic and bioinspired approaches[77]. The term biomimetics refers to artificial mimics of the architecture and functions of natural nanomaterials, as well as biological approaches and strategies, with the objective of manufacturing similar products. This approach seeks to replicate nano-nature designs to achieve comparable functionalities[78]. Conversely, the term bioinspired encompasses a broader and more adaptable paradigm, which refers to direct or indirect mimicry of methods and techniques related to materials and phenomena at the nanoscale. Bioinspired methodologies extract key design elements and translate them into innovative nanomaterial systems[79].

Researchers have drawn inspiration from nature to create many materials for pharmaceutical and biomedical purposes and applications. A notable example includes the mimic protein synthesis for designing unique nanostructures in the shapes of cubes, anemone-like, and two- and three-dimensional nanomaterials[80]. Additionally, targeted therapies biomimetic nanoparticles have exhibited exceptional biocompatibility. Biocompartmentalization can be mimicked by encapsulating and functionalizing nanoparticles with cellular membranes derived from platelets, red blood cells, or cancer cells. This a strategy

facilitates the loading and entrapment of therapeutic molecules for targeted treatment of inflammatory diseases[81], as schematically depicted in Figure.I.5(a). Beyond biomedical applications, biomimetic and bioinspired approaches have also influenced advancements in material science. The adhesion properties of gecko feet have inspired the development of superior adhesive products, while the self-cleaning superhydrophobic characteristics of lotus leaves which attributed to their unique combination of microstructure bumps and valleys decorated with a nano-waxy particles on their surface (Figure.I.5(b)), have driven the development of a new generation self-cleaning coatings[82].

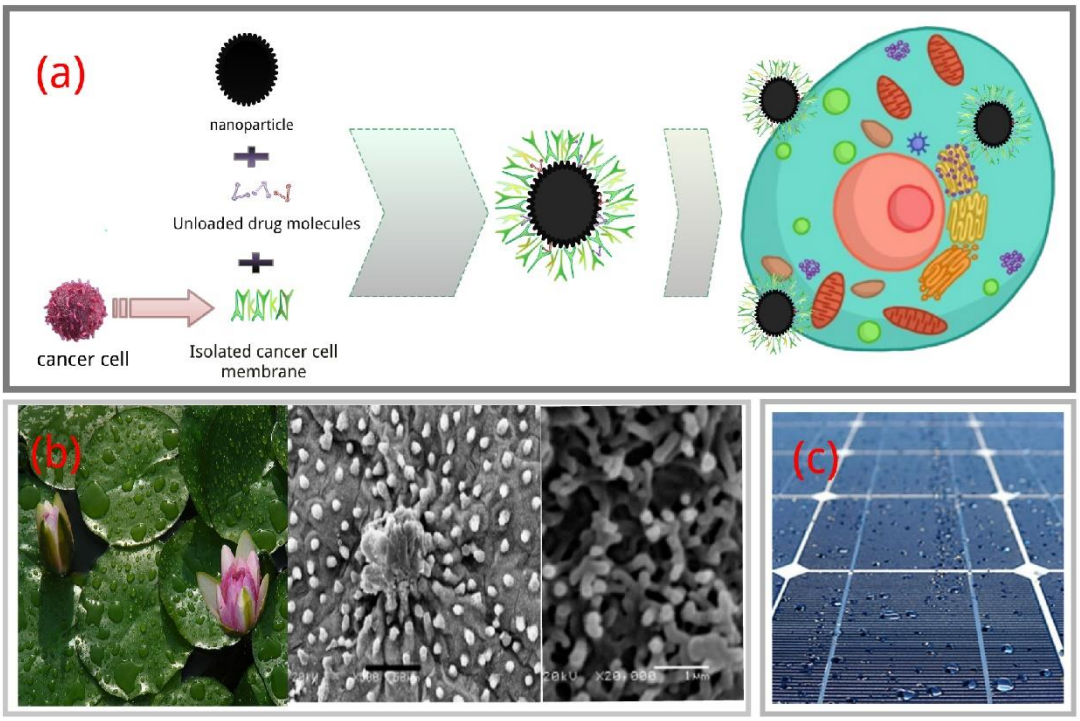


**FIGURE.I. 5.**a) Schematic of drug-loaded nanoparticles encapsulated by an isolated cancer cell membrane; b) Photographs of lotus leaves soaked in water and SEM images of their surface at different magnifications[83]; and c) A model of a floor coated with a transparent, self-cleaning nano-silicon-based coating developed by Nanoshell Company (Layton, Utah, USA).

### *1.4 Incidental nanomaterials*

Incidental nanomaterials are unintentional by-products generated during anthropogenic processes or natural events resulting from human intervention. The production and atmospheric release of incidental nanomaterials in urban environments are escalating in response to increasing human activities, including exhaust gases of transportation, combustion-based waste treatment, energy production, mineral extraction and processing, and food manufacturing. Routine human exposure to hazardous carbon nanotubes has been documented as a

consequence of petroleum combustion[84,85]. Additionally, forest fires also contribute to the formation of diverse adventitious nanomaterials, such as cement particles and fumed silica.

***2. Classification by Dimensionality***

H. Gleiter in 2000 was the first to systematically classify nanomaterials in light of studying the solid-state properties[86]. His classification framework considered the size of material across three spatial dimensions, along with its atomic structure and chemical composition, ultimately leading to the categorization of nanomaterials into three groups according to their microstructure. Subsequently, V.V. Pokropivny and V.V. Skorokhod[87], proposed a more refined classification based on spatial dimensionality and electronic movement in each dimension. Based on this approach, nanomaterials were divided into four distinct types: zero-dimensional (0D), one-dimensional (1D), two-dimensional (2D), and three-dimensional (3D).

***2.1. Zero-dimensional nanomaterials***

Zero-dimensional nanomaterials (0D-NMs) represent the most common type, characterized by their confinement in all three spatial dimensions within the nanoscale, i.e., their size does not exceed 100 nm. The 0D-NMs are the simplest structures in mass, resembling dots, and have different morphologies such as spherical, hollow-spherical, cubic, and core-shell. They are commonly referred to as nanoclusters, nanoparticles, or nanocrystals. Fullerenes, magnetic nanoparticles, noble metal nanoparticles, as well as graphene, carbon, and inorganic quantum dots are among the notable explored examples of 0D-NMs. A key feature of these materials is their exceptionally high surface-to-volume ratio, which enhances the number of active edge sites per unit mass. Furthermore, quantum confinement effects contribute to their distinctive physicochemical properties, such as high photoluminescence efficiency, surface plasmon resonance, and chemical stability, making them highly relevant for various advanced technological applications[88,89].

***2.2. One-dimensional nanomaterials***

Nanostructures that are confined to two dimensions on the nanometer scale, with a third dimension beyond the nanoscale range, are classified as one-dimensional nanomaterials. Compared to their zero-dimensional counterparts, these materials are characterized by nanoscale diameters and lengths relatively extend 100 nm, and thus include nanostructures in the form of wires, tubes, fibers, rods and ribbons. Recently, 1D-NMs like carbon nanotubes (CNTs), metallic nanowires (such as silver, gold, and metal oxides), and conductive polymeric nanomaterials such as poly(styrene sulfonate) (PEDOT:PSS) and nanopolyaniline have become

the focus of intensive research[90,91]. This is largely due to their outstanding properties, which stem from their high-aspect-ratio structure, granting them extreme thinness, lightweight, high stretchability, high transparency, elevated porosity, and better permeability, which enables their exploitation and application in the construction of percolation networks for wearable electronic skins, absorption and filtration membranes, wound dressings, and scaffolds for tissue engineering[92,93].

### *2.3. Two-dimensional nanomaterials*

Two-dimensional nanomaterials are structures with one dimension at the nanoscale and two dimensions outside the scale. They are characterized by their atomic thickness, typically comprising one to several atomic layers, while their lateral dimensions can reach the limits of micrometers[94]. This unique structural configuration endows them with distinctive shape-dependent properties, including high optical transparency, exceptional mechanical flexibility, a large specific surface area, and unique surface charge[95] . 2D-NMs exist in various forms, with lamellar architectures being among the most well-known, such as graphite, graphene oxide, reduced graphene oxide, montmorillonite clay, black phosphorus, and layered double hydroxides. Additionally, other morphological variants include nanoplates (e.g., bismuth selenide ($Bi_2Se_3$)), nanowalls such as silicon-based nanomaterials and manganese (II,III) oxide ($Mn_3O_4$), and nanodisks like copper sulfide ($Cu_2S$).

### *2.4.Three-dimensional nanomaterials*

Three-dimensional nanomaterials are bulk nanomaterials whose dimensions are not confined to the nanoscale, i.e., exceeding 100 nanometers. Bulk nanomaterials are typically composed of individual nanoscale components (0D, 1D, and 2D) that are clustered or distributed in larger random media with anisotropic orientations, forming distinctive morphologies such as nanoflowers, polyhedra, hollow nanocages, nanocones, and nanocoils. Compared to bulk conventional materials, 3D-NMs exhibit superior properties due to the quantum size effect, which allows for a large specific surface area, macro- & mesoporous channels (high porosity), and improved mechanical and electrical performance. These properties offer many desirable advantages for catalytic, sensing, drug delivery, and energy storage applications, such as biocompatibility, potential for surface chemistry functionalization, and a high percentage of exposed atoms[96,97].

### *3. Classification based on chemical and elemental composition*

Structurally, nanomaterials can consist of a single chemical element or complex multi-element configurations. Based on their chemical composition, nanomaterials can be systematically categorized into four primary classes: inorganic, organic, carbon, and composite.

#### *3.1. Inorganic nanomaterials*

Inorganic nanomaterials encompass a broad range of compounds derived from all elements except carbon, including metals, metal oxides, silicon, and ceramics. Inorganic NMs exhibit several distinctive properties, most notably their high stability compared to other counterparts, hydrophilicity, and relatively low cytotoxicity. Among inorganic nanomaterials, metal-based NMs have garnered significant research interest, especially in the field of bioengineering. Metallic nanomaterials can be obtained via two primary approaches: metal-destructive methods or synthetic processes utilizing monovalent, divalent, or trivalent metal ions. Although metal-based NMs can be derived from a wide range of metallic elements, noble and transition metals such as gold, silver, copper, aluminum, cobalt, nickel, and iron are predominantly exploited and utilized[77,98]. This preference is attributed to their exceptional surface characteristics, including surface-to-volume ratios, substantial surface charge, and good porosity, as well as optical properties such as broad absorption across the solar electromagnetic spectrum and confined surface plasmon resonance (Figure.I.6(a)).

Another significant subclass category of metallic nanomaterials exists in the oxidized state, known as metal oxide NMs. These materials consist of positively charged metal ions and negatively charged oxygen ions, exemplified by compounds such as titanium dioxide ($TiO_2$), iron (III) oxide ($Fe_2O_3$), and silicon dioxide ($SiO_2$). The abundance of oxygen in the atmosphere (21%) has facilitated the natural formation of a diverse array of bulk metal oxides and mixed metal oxides in the Earth's crust[20]. When these bulk structures are destructed to the nanoscale, they exhibit novel quantum mechanical properties that are highly relevant for heterogeneous catalysis and energy harvesting technologies.

Another important category of inorganic nanomaterials is nanoceramics, which are solid, semi-metallic materials composed of metallic and non-metallic elements. These typically include oxides, nitrides, carbonates, phosphates, and carbides, with representative examples such as clay minerals, hydroxyapatite (HAp), zirconia ($ZrO_2$), silicon nitride ($Si_3N_4$), and calcium carbonate ($CaCO_3$). Nanoceramics are obtained through sequential processes involving high-temperature heating followed by rapid cooling. These materials are characterized by high mechanical strength and stiffness, thermal and electrical insulation, and remarkable corrosion

resistance in aggressive chemical environments. Their structural resemblance to the tooth composition and their high biocompatibility have enabled their application in medical fields (Figure.I.6(b)), such as antimicrobial agents against cariogenic microbes, drug delivery systems for targeting tumors and glaucoma, and tissue regeneration[99,100].

### *3.2. Organic nanomaterials*

Organic nanomaterials encompass a diverse class of nanoscale structures derived from organic molecules. Nanostructures are formed through the self-assembly of simple molecular precursors, such as monomers and polar lipids, via weak non-covalent intermolecular interactions. The interaction (e.g., hydrogen bonding and hydrophobic effects) drives the organization of molecules into well-defined structures, including particles, spheres, fibers, tubes, and films ranging in size from 10 to 1000 nm. The chemical bonding of the carbon backbone with heteroatoms, imparts organic nanostructures functional properties, reactivity, biodegradability, and non-toxicity.

One prominent subclass of organic nanomaterials is polymers in nanoscale form, referred to as polymer nanoparticles (PNPs), which consist of a solid-mass matrix network of particles. PNPs are widely utilized in the pharmaceutical and therapeutic sectors because of enhanced bioavailability. A notable instance is polyethylene glycol (PEG) nanoparticles, which possess highly hydrated, flexible chains that confer non-immunogenicity, extend drug circulation half-life, and minimize plasma protein adsorption[101]. There are also polymer micelles, which are self-assembled amphiphilic copolymers containing a hydrophobic tail and a hydrophilic head in a specific solvent. Another important category is polymeric micelles, which are amphiphilic copolymers that self-assemble in solution to form core-shell structures with a hydrophobic tail and a hydrophilic head; this formation mechanism is demonstrated in Figure.I.6(c). Polymeric micelles can be used in pharmaceutical formulations for the encapsulation of both hydrophobic and hydrophilic drugs[102,103]. Their core-shell architecture provides advantages such as micellar association, selective targeting, and protection of encapsulated drugs from oxidative degradation in vivo and ex vivo. Beyond pharmaceuticals, polymeric micelles have broad uses in the food industry, such as extracting enzymes and proteins from animal and plant products and complexation of DNA[104].

Lipid-based nanomaterials represent another major class of organic nanostructures, with significant bio-applications. Lipid bilayers, which are natural self-assembled structures composed of polar lipids, serve as the fundamental matrix of cell membranes and are also found in certain viruses and bacteria. Bioinspired lipid nanomaterials, including Langmuir-Blodgett

films, nano-lipid carriers (NLCs), and solid lipid nanoparticles (SLNs), have been extensively developed for targeted drug delivery[105]. These systems are particularly effective in transporting hydrophilic and hydrophobic molecules, especially cytotoxic drugs, with high precision. Lipid nanomaterials have also emerged as a key technology for RNA delivery in the treatment of cancer and viral infections, including COVID-19[57,106]. Their capability to facilitate site-specific drug release enhances therapeutic efficacy while minimizing systemic side effects.

### *3.3. Carbon nanomaterials*

Carbon-based nanomaterials represent a distinctive and interesting class of materials primarily composed of carbon, the third most abundant element in our Earth's system. These materials can be found in multiple allotropic forms and phases, each with unique physicochemical properties. This structural diversity arises from variations in carbon-carbon bonding configurations at the structural level. For instance, $sp^3$-hybridized covalent bonds confer high rigidity, whereas $sp^2$-hybridized bonds impart relatively softer mechanical and conductive structures characteristics[107]. This class includes amorphous nanodiamonds, fullerenes, graphene (derived from the exfoliation of three-dimensional layered graphite), and single- and multi-walled carbon nanotubes (CNTs), as illustrated in Figure.I.6(d).

Carbon nanomaterials are particularly valued for their exceptional properties, including high specific surface area, thermal stability, electrical conductivity, mechanical strength, electron affinity, structural versatility, and chemical resistance to acidic environments[20,27]. These properties make them integral to various commercial applications and multidisciplinary research fields. Specifically, they are utilized as electrode materials in nanoelectronics, energy storage systems such as lithium-ion batteries, supercapacitors, and hydrogen storage technologies. Bulk graphite serves as a neutron moderator and reflector in nuclear reactors[108]. Furthermore, carbon nanomaterials also play an important role in environmental applications, functioning as highly efficient gaseous adsorbents for pollutants like hydrogen sulfide ($H_2S$), carbon monoxide (CO), and nitric oxide (NO), as well as for the removal of organic dyes, pharmaceuticals, and heavy metal contaminants from aqueous systems.

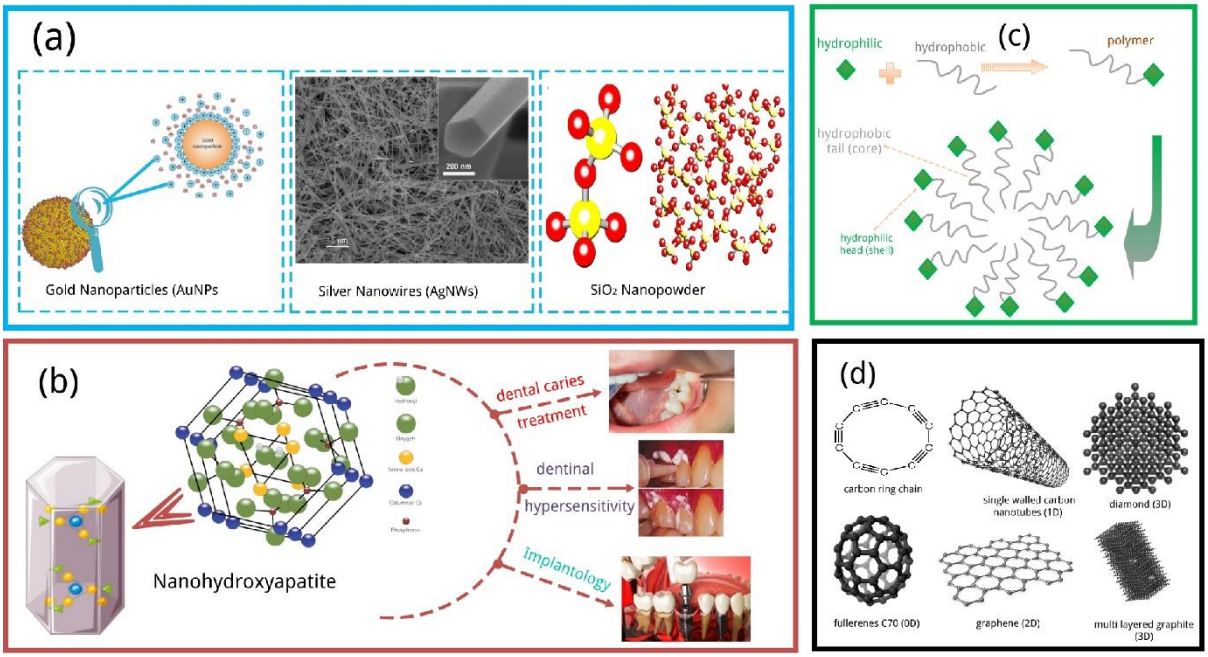


**FIGURE.I. 6**.a) schematic representation of a gold nanoparticle, SEM image highlighting cross-section of silver nanowires[109], and atomic structure of amorphous silica nanopowder; b) crystal structure of nanohydroxyapatite and its various applications in dental science; c) diagram illustrating the self-assembly mechanism of a spherical polymeric micelle; and d) structure schematics of carbon nanomaterials with different dimensions.

### *3.4. Nanocomposites*

Nanocomposites represent a suitable alternative to overcome the limitations of conventional bulk materials and homogeneous NMs. They are characterized by complex multiphase structures, where at least one of their phases is at the nanoscale or exhibits nanometric phase separation. The broad definition of nanocomposite encompasses various configurations, including NMs of different chemical compositions and dimensions combined together, nanomaterials integrated with larger-scale materials, and nanomaterials incorporated within bulk matrices. Nanocomposites manifest in many forms, such as colloids, hydrogel, and porous media, though hybrid nanocomposites comprising a bulk matrix (metallic, polymeric, or ceramic) reinforced with nanoscale phases are the most common and widely investigated[58,110]. The nanophasing process is designed to enhance or introduce new properties to the bulk material, leveraging synergistic interactions between components. The incorporation of bentonite fillers in polyolefin polymers improves thermal stability, flame retardancy, and biodegradability, while the integration of fibers into ceramic matrices markedly strengthens mechanical properties and dimensional stability.

***4. Classification according to dispersion and stability of NMs***

Nanomaterials are categorized according to their dispersibility into dispersed and aggregated states. The dispersion characteristic of NMs in different media, like solvents and matrices, is a key factor influencing their synthesis, stability, and functional applications. Optimal dispersion is defined by the absence of clustering, agglomeration, or aggregation, ensuring that particles remain uniformly and separately distributed from each other. The specific surface area of NMs is inversely proportional to the agglomeration; any degree of particle agglomeration adversely affects their physicochemical and biological properties. Several intrinsic factors influence the formation of agglomerates and aggregates, such as surface charge, particle size and concentration, as well as pH and ionic strength of the media[111,112]. Current knowledge about the dispersion state of nanomaterials is insufficient for its precise quantification. However, there are various analytical characterization techniques that allow for an estimation of dispersion quality by assessing particle size, distribution, surface charge, and stability. These include dynamic light scattering (DLS), electrophoretic light scattering (ELS), ultraviolet-visible (UV-vis) spectroscopy, and zeta potential (ZP) analysis.

DLS provides the hydrodynamic diameter of particles (Z-average) and the polydispersity index (PDI), where PDI values range from 0 to 1 (from monodisperse to polydisperse). The degree of dispersion can be inferred from the PDI value: a range of 0.1–0.3 indicates excellent dispersion, 0.3–0.5 suggests moderate dispersion, and values above 0.5 signify aggregation[14,113]. Furthermore, the zeta potential (ζ-potential) of NMs serves also as an important indicator of the dispersion stability of particles. Defined as the electrical potential at the shear or sliding plane, which is related to the surface charge and electrostatic interactions between particles (attractive and repulsive forces)[114]. Nanomaterials with zeta potential values between -25 mV and +25 mV exhibit poor dispersion stability and a strong tendency to aggregate, while stability improves further from this range. Similarly, the stability of nanodispersions can be monitored by measuring the characteristic absorption ($\lambda_{max}$) of nanomaterials in the UV-vis spectrum.

***5. Classification based on nanomaterials porosity***

Nanomaterials possess voids and channels at the structural level, technically referred to as pores. The size and distribution of pores determine the surface properties of nanomaterials, their diffusion behavior, and interactions with ions and molecules. Porosity allows nanomaterials to exhibit superior adsorption, absorption, permeability, and fluid transport properties. According to the International Union of Pure and Applied Chemistry (IUPAC), NMs

are classified into three main groups based on their pore length and size: macroporous, mesoporous, and microporous nanostructures[115]. The first group, "macroporous," includes NMs characterized by pore diameters larger than 50 nm, such as porous gels, calcium carbonate, and biomass-derived carbon nanomaterials. The large pore volume and resulting high surface area allow them to be adapted for therapeutic applications, where they facilitate the controlled transport of therapeutic molecules such as chemotherapeutic agents (e.g., peptide NuBCP-9 (N9)), and loading complex biomolecules like oligonucleotides, enzymes, and proteins[116,117].

Mesoporous nanomaterials, also referred to as super-nanoporous materials, possess pore diameters less than 50 nm and greater than 2 nm. They are characterized by a large specific surface area and tunable pore geometry, which provide ample storage capacity for guest molecules. Mesoporous NMs have outstanding applications in environmental and catalysis fields. For instance, activated carbon is widely employed in water treatment for the adsorption of organic pollutants and metal ions. The molecules form a thin layer within the pore channels and on the surface of the carbon matrix, facilitating efficient separation from aqueous media[118]. Mesoporous silica serves as a robust support for heterogeneous catalysts in various reactions, like the hydrogenation of p-nitrophenol, the oxidation of glycerol to glyceric acid, and polymerization processes.

Nanomaterials with narrow pores (less than 2 nm) are classified as microporous materials. Metal-organic frameworks, hydroxyapatite, nanoclays, and zeolites are examples of microporous materials with pioneering applications in industrial chemistry and sustainable processes, including selective catalysis, gas separation, sensing technologies, and membrane filters. Microporous nanomaterials are further categorized into two subgroups: super-micropore NMs, which have pore diameters between 0.7 and 2 nm, and ultra-microporous nanomaterials (pores smaller than 0.7 nm)[119].

***6. Classified according to potential toxicity***

The tremendous leap in nanotechnology, particularly the development and manufacture of nanomaterials, has been accompanied by a dangerous increase in human exposure. Due to their ultra-small size, nanomaterials can enter the body through multiple routes, including ingestion, inhalation, injection, and skin penetration, enabling direct cellular interactions[120,121]. Despite this, most research focuses on the synthesis of new nanomaterials without addressing or assessing their biological effects. A comprehensive understanding of their environmental impact, toxicological properties, and long-term consequences is essential before integrating

them into industrial applications. Nanotoxicology, a new scientific branch, seeks to investigate and understand the mechanisms of nanomaterial uptake, exposure pathways, and physicochemical interactions[122]. This discipline also aims to establish standardized protocols for assessing nanomaterial toxicity in both human health and environmental contexts. Based on their toxicity potential, nanomaterials can be categorized into two distinct groups.

The first group of nanomaterials consists of biopersistent, low-toxic particles, referred to as granular biodurable particles (GBP). Also known as low-toxicity dust or poorly soluble low-toxicity (PSLT) nanomaterials, similar to silicon carbide and titanium dioxide[123]. GBPs are highly persistent in living and biological systems but exhibit minimal toxicity due to their inert surface properties and lack of harmful substance release. Studies have confirmed that the systemic availability of GBP nanomaterials resulting from inhalation, dermal, and oral exposures is relatively low, and they pose no significant systemic risks[121,124]. Furthermore, compared to their bulk counterparts, GBP-NMs do not have a novel toxicity associated with their nanoscale size.

The second group encompasses nanomaterials that are carcinogenic, mutagenic, asthmagenic, or reproductive toxicants (CMAR). As outlined by the British Standards Institution, nanoforms of bulk materials designated as CMARs retain the same hazardous properties[125]. The toxicity of this type of nanomaterial is primarily attributed to the release of toxic ions and the generation of reactive oxygen species (ROS) on their surfaces. On the other hand, CMAR nanomaterials internalize into cells, where they interact with genetic material (DNA and RNA), nuclear proteins, and cytoplasmic components. These interactions cause structural damage to cellular organelles and induce genotoxicity by disrupting biochemical pathways, DNA replication, transcription, and repair mechanisms[85,126]. Carbon nanoparticles have been reported to bind to single-stranded nucleotides during DNA replication, while fullerenes $C_{60}$ have been linked to mutagenic effects in liver microsomes[127,128].

In addition to genotoxicity, reproductive toxicity is another significant concern, as NMs translocate via systemic circulation to reproductive organs such as the testis, epididymis, and prostate, where they accumulate. NMs can penetrate the blood-testis barrier (BTB) and nuclear membranes of sperm cells, leading to morphological mutations and reduced sperm viability. In vivo studies[129,130], demonstrate that zinc oxide nanoparticles (ZnO NPs) can disrupt the cell membrane and outer mitochondrial membrane in Sertoli cells within the BTB, while cerium oxide nanoparticles ($CeO_2$ NPs) cause degeneration of the seminiferous tubules in mice.

## I.4. Silver nanoparticles

For over 5,000 years, human have recognized the utility of silver, and many peoples have incorporated it for various applications, including nourishment item storage, tableware, water purification, and medicinal treatments. Eighteenth-century medical texts documented confirm the use of silver in treating burn wounds due to their antiseptic and antimicrobial properties[131,132]. Furthermore, silver is one of the seven ancient metals that have played a pivotal role in the advancement of civilization. Its use in coinage facilitated trade between societies, and its luster and malleability contributed to the creation of jewelry and artifacts that have endured through time.

Silver (Ag) is a naturally occurring element with an atomic number of 47. It is one of the rarest elements in the Earth's crust, ranking 67th in abundance, with a concentration of approximately 75 parts per billion (ppb), or about 1 mmol/kg. Silver is commonly found in soil and rocks in its metallic form and is often associated with copper, lead, and gold ores. Among noble metals, Ag exhibits the lowest density (10.5 g/cm$^3$) and is characterized by its high ductility, excellent electrical and thermal conductivity (63 × 10$^6$ S/m and 429 W/m·K, respectively), low chemical reactivity, and remarkable stability.

The extraction of silver is primarily conducted through mining operations, with the largest producers being South American countries such as Peru, Mexico, and Chile, alongside China and Australia. Global silver production exceeds 28,000 metric tons annually (~1.029 million troy ounces), with an estimated market value of US$20 billion[133]. The superior biological and physicochemical properties of silver have contributed to its growing applications in advanced sectors[134]. Figure I.7 presents the relative global distribution of silver applications by 2024, with the industrial sector accounting for 50.6% of the total global silver market, consuming approximately 680.5 million ounces (Moz). Of which over 110 Moz are used for photovoltaic (PV) installations and US$3.1 billion for catalysts, underscoring the role of Ag in sustainable and green manufacturing[135]. More than 27% of global demand is related to investment and coin markets (183.3 and 190.9 million ounces, respectively); the remaining demand is distributed among traditional applications, jewelry (208.7 Moz), tableware (54.2 Moz), and photography (25.5 Moz)[136].

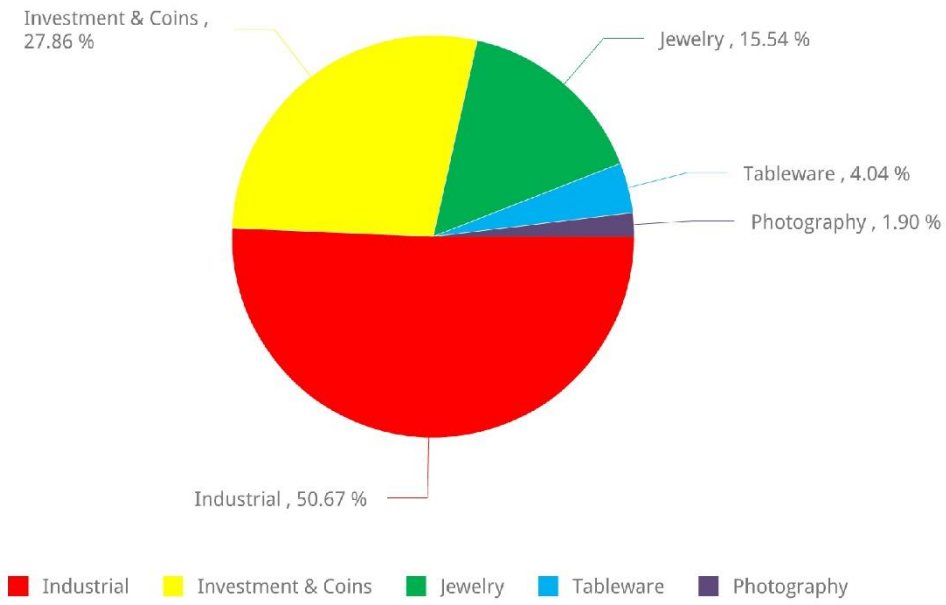


**FIGURE.I. 7.**Global distribution of silver demand across sectors for 2024, as % (from the World Silver Survey 2025, The Silver Institute)[136].

Over the past three decades, with the emergence of nanotechnology as a prominent research field, nanosilver has been extensively proposed as a novel form of silver with enhanced and distinct characteristics. These improvements compared to bulk silver stem from unique nanoscale phenomena, such as the quantum size effect, atomic-surface interactions, quantum tunneling, and an increased surface-to-volume ratio[137,138]. Among the various nanoforms of silver, nanoparticles are the most commonly explored owing to their exceptional optical, electromagnetic, chemical, and biological properties. Silver nanoparticles hold vast application potential across diverse fields, including photocatalysis, sensing, energy harvesting, solar cell technology, and food packaging. In the biomedical area, they are being actively studied for their therapeutic capabilities in wound healing, tissue regeneration, drug delivery, bioimaging, hyperthermia, anticancer and antidiabetic treatments, and bone cement formulations.

### I.4.1. Silver Nanoparticles Properties

The potential applications of silver nanoparticles are intrinsically linked to their unique physicochemical properties, including particle distribution and morphology, agglomeration state, surface chemistry and coverage, and surface area, as well as their solubility and reactivity within various media. Among their most distinctive characteristics are their optical properties, which arise from the interaction of AgNPs with light. The interaction induces collective

oscillation of the free conduction band electrons on the AgNPs surface, known as the localized surface plasmon resonance (LSPR) phenomenon. These oscillations lead to radioactive decay and strong absorption and scattering in visible and near-infrared light, accompanied by conversion of photon emission energy into heat[138,139]. The LSPR property renders AgNPs highly sensitive to environmental changes, making them particularly valuable for advanced applications such as biodiagnostics, laser treatments, radiotherapy, photothermal therapy, chemical and biological sensing, bioimaging, photocatalysis, and solar cell technologies[140,141] .

Pure silver is renowned for its superior electrical conductivity compared to other metals due to the presence of free electrons in the atomic structure (single valence electron). When an electric field is applied, the free electrons travel easily through the silver metal lattice, forming a conductive path. Similarly, AgNPs also exhibit electrical conductivity; however, their behavior differs from bulk silver due to quantum effects and modifications in their electronic structure. Factors such as quantum confinement, discrete energy levels, and altered band structures between the valence and conduction bands influence their electronic transitions[60]. Thanks to their excellent conductivity and low surface roughness, AgNPs have emerged as promising materials for applications in microelectronics, antennas, and electronically conductive adhesives[142]. Moreover, AgNPs possess a higher ionization potential compared to bulk silver, further affecting their conductivity. Another notable characteristic of AgNPs that enhances their potential in sensing and optoelectronic applications is their electroreflectance (ER) effect, where the absorption spectrum of the particles alters with the change of stored electronic charge, which can be observed with the withnaked eye[143].

The surface charge of AgNPs represents a critical property that influences their colloidal stability, agglomeration, solubility, and chemical reactivity within various matrices. Understanding and controlling the surface charge facilitates the modulation of AgNPs behavior in various environmental and biological systems. Such control is pivotal for optimizing their biomedical applications, particularly in enhancing targeting specificity, cellular uptake, and the transport of therapeutic agents. Surface functionalization of silver nanoparticles, through stabilizing agents, surfactants, or polymer coatings, directly controls their surface charge and enhances the dispersion of colloidal silver particles due to electrostatic repulsion[144,145]. Citrate, sodium dodecylbenzenesulfonate (LAS), and polyvinylpyrrolidone are commonly employed agents in the synthesis of negatively charged silver nanoparticles, whereas positively charged-AgNPs are produced using cationic surfactants such as cetyltrimethylammonium bromide (CTAB), chitosan, and dodecyltrimethylammoniumchloride (DTAC).

The surface charge also exerts a significant influence on the biological properties and activities of silver nanoparticles. It has been reported that positively charged AgNPs exhibit enhanced antibacterial efficacy, often at lower concentrations, compared to their negatively charged or neutral AgNPs[146,147]. Furthermore, surface charge is a determinant of AgNPs toxicity, as confirmed by the study of T. Silva et al.[148], which investigated the potential role of surface charge in the toxicological responses of AgNPs against two model organisms, a eukaryote (Daphnia magna) and a prokaryote (Escherichia coli). The toxicity profiles indicated the important role of coating materials in surface charge-modifying for the environmental and biomedical uses of AgNPs. As coating agents significantly minimize the release and toxic effects of silver ions ($Ag^+$). Notably, negatively charged coatings have demonstrated superior efficacy in reducing Ag ion-associated toxicity. Similarly, the surface charge of AgNPs impacts their bioaccumulation dynamics, as J. Zhang et al.[149] reported in their evaluation of bioaccumulation of positively and negatively charged-AgNPs in freshwater algae (Chlorella vulgaris). The positively charged-AgNPs accumulate more efficiently, likely due to the electrical interaction potential with the negatively charged algal cells (mutual attraction), while the energy barrier is formed due to the electrostatic repulsion forces between the negatively charged-AgNPs and the living cells.

### I.4.2. Methods and Approaches for silver nanoparticles Manufacturing

Current research and technological advancements related to silver nanoparticles are accelerating rapidly. According to Web of Science Core estimates, over the past five years, more than 54,070 scientific documents (including research articles and patents) have been on the subject, representing over 10% of all scientific output within the nanomaterials category[150]. Published research is directed toward developing methods and techniques to improve the production yield of highly stable AgNPs with precisely tunable morphological and size characteristics. Within nanotechnology, the processes, procedures, and protocols for synthesizing AgNPs rely on two fundamental approaches that integrate various physical, chemical, and biological techniques: top-down and bottom-up approaches.

The top-down approach manufactures silver nanoparticles from solid or aerosolized bulk silver, which is reduced to the nanoscale dimensions through physical processes such as grinding, cutting, chopping, and milling. In contrast, the bottom-up approach involves various chemical and biological techniques that frame the atomic and ionic states of silver and transform

them into more complex silver nanostructures. Both chemical and biological techniques involve the reduction of silver ions, followed by the self-assembly of atoms to form new nuclei that subsequently grow into nanoscale particles. Figure I.8 provides a schematic representation of these two synthesis approaches.

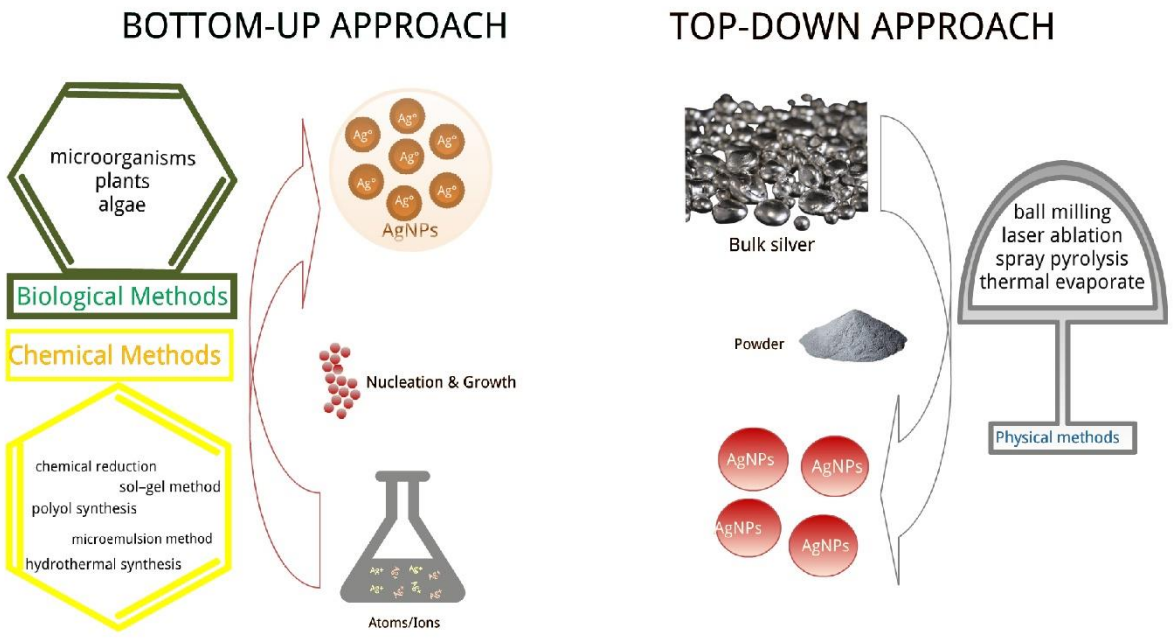


**FIGURE.I. 8**.Schematic diagram of the top-down and bottom-up approaches to AgNPs synthesis.

### *1. Physical techniques*

Physical techniques are employed to generate significant quantities of highly purified silver nanoparticles characterized by uniform dispersion, narrow size distribution, and freedom from solvent-derived contaminants. This type of synthesis relies on the exploitation of physical factors such as electrical discharge, electromagnetic radiation, ultraviolet radiation, plasma, and thermal energy. Among the physical techniques, evaporation–condensation and laser ablation are considered the most promising and approved for AgNPs production[151,152]. Evaporation–condensation is typically performed using a tubular furnace under atmospheric pressure. The silver metal is first evaporated inside a boat crucible into a carrier gas stream and then condensed onto various substrates so that the Ag atoms coalesce and cluster into Ag-nanoparticles. However, this method has several technical drawbacks, including the substantial spatial requirements of tubular furnace systems, high power consumption exceeding several

kilowatts, and the long time necessary to achieve the required temperatures for thermal stability operating[153] .

Laser ablation of bulk silver in solutions is another prominent technique to synthesize high-purity, monodisperse colloidal AgNPs. This technology is relatively green eco-friendly due to its lack of chemical reagents and solvents[154]. Furthermore, its key advantages include the ease and precise control of the shape, size, and concentration of AgNPs through adjusting several parameters such as laser fluence and speed, the wavelength directed to the silver metal, the number of laser pulses, beam spot size, the ablation time, and the synthesis medium[155]. Nevertheless, sophisticated instrumentation, high temperatures, and high external energy requirements contribute to high synthesis costs and low productivity, limiting the transition of laser ablation technology to economic industrial applications. These factors limit the green nature of this process, especially given the significant attention paid to green synthesis principles to address energy and economic requirements. Notably, LS Kibis et al.[156] reported that the laser ablation of silver in aqueous and air media can promote the formation of $Ag_2O$ rather than Ag-nanoparticles due to the presence of oxygen despite the use of noble gas jets in the ablation zone.

***2. Chemical techniques***

To date, chemical processes have been widely employed for the synthesis of silver nanoparticles, and they are the most effective and practical in terms of simplicity, cost, and speed. Several chemical synthesis techniques have been developed, including chemical reduction, electrochemical reduction, sol-gel, microemulsion, and polyol[157]. These processes share the production of AgNPs through chemical transformations of three essential components: silver precursors (silver salts), reducing agents, and capping/stabilizing agents.

Among the above techniques, chemical reduction in aqueous solutions or solvents is the most extensively utilized. This process generally proceeds through three sequential steps, whereby silver ions are first reduced from silver salts like (silver nitrate, silver acetate, and silver tetrafluoroborate to metallic silver ($Ag^0$) via electron transfer facilitated by reducing agents[158]. This is followed by a growth process, as the concentration of reduced silver atoms increases, leading to the formation of nuclei, which in turn grow into oligomeric clusters and then grow later into larger nanoparticles. A wide variety of organic and inorganic reducing agents can be used, such as elemental hydrogen, hydrogen peroxide, sodium borohydride, sodium citrate, thioglycerol borohydride, N-dimethylformamide, ascorbic acid, formaldehyde, aniline, 2-mercaptoethanol, and others[159,160]. Finally, the formed AgNPs are stabilized and

protected from binding and agglomeration by capping and stabilizing agents. These agents contain chemical functionalities that bind and adsorb to the AgNPs surface, forming an organic coat, such as chitosan, tannic acid, polyvinylpyrrolidone (PVP), oleylamine, and polyvinyl alcohol (PVA)[161].

Despite the numerous advantages of chemical techniques, particularly their ability to produce AgNPs with desired structural and size characteristics, there are significant limitations related to environmental and biological safety[162]. Many of the chemical reagents used in synthesis are toxic, and residual substances may remain on the AgNPs surface even after purification. For instance, inorganic reducing agents and certain solvents have been associated with long-term toxicity when introduced into the human body. High levels of exposure to sodium borohydride can result in pulmonary edema and neurological damage. Likewise, cytotoxic effects on healthy cells have been demonstrated when silver nanoparticles coated with agents such as PVA are used in drug delivery systems[163]. The presence of hazardous chemicals on the surface of AgNPs limits their application in sensitive fields such as antimicrobial and antiviral therapies, targeted drug delivery, and wound dressings. Therefore, there is growing scientific interest in developing alternative, environmentally friendly synthesis methods that reduce toxicity and enhance biocompatibility while maintaining control over AgNPs characteristics.

### *3. Biological techniques*

Given the shortcomings and limitations of physicochemical techniques for synthesizing silver nanoparticles and the increasing awareness of environmental and energy issues, biologically-inspired synthesis techniques have emerged as a less complex, more cost-effective, environmentally benign, and non-toxic alternative. Biosynthesis is a new and rapidly developing branch of nanotechnology that leverages natural biological entities such as enzymes, proteins, bacteria, phytochemicals, and biopolymers to serve as reducing and capping agents, replacing traditional hazardous and toxic chemicals.

The bionanotechnology synthesis branch is known as "green synthesis," which refers to the straightforward, cost-, energy-, and time-efficient process of engineering and developing safe and less toxic nanoparticles. This is exemplified by biologically derived silver nanoparticles, which exhibit high biocompatibility and low cytotoxicity toward eukaryotic cells, largely due to the biological templates that cover the nanoparticle surface and are naturally present in living organisms[157,164]. Additionally, unlike conventional techniques, biologically inspired synthesis holds promise for the integration of silver particles into biomedical

technology and promising future economic prospects, including scalability, high yield, and lower production costs.

### *3.1. microorganisms-based biosynthesis of AgNP*

Recently, the sustainable synthesis of naturally inspired silver nanoparticles using microorganisms has become a highly promising and extensively researched technique. This growing interest is attributed to inherent advantages of microorganisms, including their ease of cultivation and control, rapid proliferation under a wide range of environmental conditions, and their adaptability and proliferation in mineral-rich habitats. Various microorganisms, including fungi, bacteria, yeasts, algae, and even viruses, have demonstrated potential as bioplatforms for silver nanoparticle production[158]. AgNPs synthesized by microbial biosystems are typically classified according to their formation site or pathway into two distinct categories: in vitro (extracellular synthesis) and in vivo (intracellular synthesis).

The in vitro pathway is the most practical and convenient, largely due to the facilitated recovery of the formed silver nanoparticles. In this process, extracellular enzymes such as β-glucosidase, protease, and chitinase are secreted by microbial organisms into the culture medium. $Ag^{+}$ ions can be reduced to $Ag^{0}$ nanoparticles by the catalytic activity of these enzymes, particularly those nicotinamide adenine dinucleotide (NADH)-dependent[163,165] . Meanwhile, microbial proteins and peptides stabilize the formed particles through interactions with amino group residues.

Conversely, in the in vivo synthesis pathway, the reduction of silver ions occurs inside the microbial cells. This method was developed following the discovery by RM. Slawson et al.[166], who identified the silver-resistant bacterium Pseudomonas aeruginosa AG259, isolated from silver mines. They observed the intracellular accumulation of silver nanoparticles within the periplasmic space. In this context, $Ag^{+}$ ions are initially electrostatically trapped and diffused on the cell surface by the carboxyl groups present in cell wall-associated enzymes. Subsequently, $Ag^{+}$ are enzymatically reduced to $Ag^{0}$ and assemble into nanoparticles within the cytoplasm[167,168].

However, although microorganism-based technologies as biofactories for the synthesis of bioactive AgNPs without toxic byproducts are promising, several challenges remain. These include microbial culture contamination risks, limited control over the morphology and size of the NPs, as well as the incomplete and precise understanding of the synthesis mechanism and the bioactive compounds involved.

### *3.2. Plant-based biosynthesis of AgNP*

Currently, plant-based biosynthesis and plant extracts have opened new horizons for the development of non-toxic silver nanoparticles, offering superior properties that meet the diverse demands of a wide array of applications. Plants, both at the surface and internal tissue levels, possess a remarkable ability to hyperaccumulate and reduce metal ions, a trait that has been ingeniously harnessed for nanoparticle synthesis[169]. In this regard, J. L. Gardea-Torresdey et al.[170] first demonstrated the plant-based synthesis of AgNPs using alfalfa sprouts. In their work, silver ions introduced into the agar medium migrated through the roots to the plant shoots in their oxidized form, where they were subsequently reduced and assembled into NPs. This groundbreaking discovery highlighted the immense potential of plants and their extracts as natural factories for the biosynthesis of silver nanoparticles.

Numerous reports over the years have highlighted the effective applications of the use of extracts from many parts of various plant species, such as seeds, stems, rhizomes, twigs, leaves, latex, fruits, peels, flowers, and crowns[171]. Plant biomass is inherently rich in a complex network of bioactive molecules such as proteins, enzymes, antioxidant metabolites, polysaccharides, and amino acids. These molecules collectively contribute to the reduction of silver ions, the nucleation and growth of metallic silver ($Ag^0$) into NPs, and the stabilization of their surfaces. Plant extracts provide natural, non-toxic bioactive reducing and stabilizing agents capable of controlling the growth and stability of silver crystals[161,163]. Their ability to mediate the rapid, one-step synthesis of AgNPs aligns perfectly with the growing need for scalable, eco-friendly, and health-conscious production methods.

The abundance, diversity, and rapid growth of plant life make this biosynthetic route highly sustainable. It offers a simple, cost-effective alternative to conventional chemical and microbial synthesis methods, eliminating the need for expensive culture media, sterile conditions, and reducing the biological hazards associated with microbial systems. Therefore, plant-based AgNPs synthesis represents not only a green approach but also a practical pathway toward the large-scale, responsible production of silver nanoparticles.

## I.4.3. Boraginaceae family assisted-Silver Nanoparticles synthesis

According to current taxonomic classifications, the Boraginaceae family, known as forget-me-nots and borages, consists of approximately 2,700 species across 148 genera of trees, shrubs, and herbaceous flowering plants. These species exhibit a broad global geographical distribution, where they primarily thrive in forests, rocky slopes, meadows, and sandy beaches in temperate and subtropical regions of Asia, Europe, and North and South Africa[172]. Some

species are also distributed to limited extents in Oceania and North America. Boraginaceae are distinguished by a number of phylogenetic and morphological traits, including a gynobasic style (attached to the ovary base), deep quadrilateral ovaries, coiled inflorescences resembling a scorpion's tail, and a fruit that splits into four nutlets, as shown in Figure I.9. They also have rounded stems, alternate phyllotaxy, floral symmetry with an equal number of petals and stamens, and the production of specialized secondary metabolites that play ecological and physiological roles[173,174].

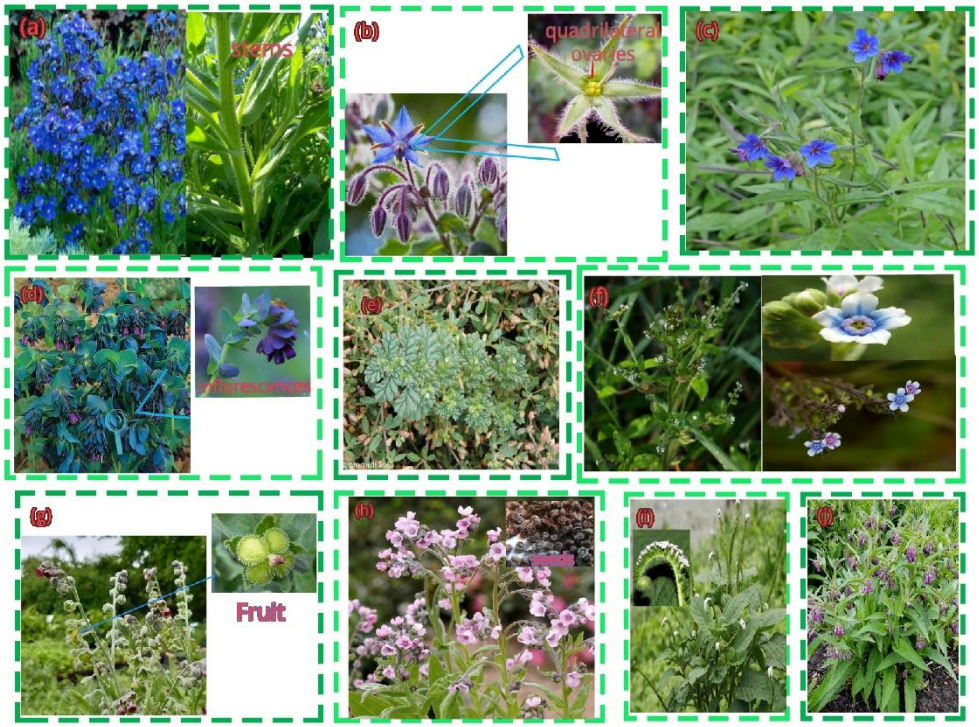


**FIGURE.I. 9.** Plants of the Boraginaceae with their common morphological and reproductive characteristics. a) Anchusa azurea; b) Borago ofcinalis; c) Buglossoides purpureocaerulea; d) Cerinthe major purpurascens; e) Coldenia procumbens L.; f) Cynoglossum lanceolatum Forssk; g) cynoglossum officinale; h) Cynoglossum amabile; i) Heliotropium indicum L.; and j) Symphytum ofcinale.

Although the notoriety of Boraginaceae species for producing hepatotoxic pyrrolizidine alkaloids, many taxa within the family have important uses in cosmetics, pharmaceuticals, and surgical compresses. This is primarily due to their rich profile of active compounds and metabolites, such as phenols, terpenoids, allantoin, flavonoids, sterols, anthocyanins, furans, and naphthoquinones[175,176]. Historically, the isolated constituents from this plant family have played an important role in the development of culinary practices and arts, traditional medicine, and the silk industry[177]. Shikonin and its naphthoquinone derivatives are the most well-known, imparting a distinctive red-purple pigment and exhibiting a wide spectrum of pharmacological

activities. These include antioxidants, antibacterials, antifungals, anti-inflammatories, anti-cancerous tumors, and antiplatelet activities. Research has also confirmed their promising therapeutic potential in wound-healing, contraceptive, and cardiotonic preparations[177,178].

The therapeutic properties and rich repertoire of bioactive phytochemicals exhibited by *Boraginaceae* plants have inspired numerous studies in recent years on the exploitation of extracts from various parts of these species in the sustainable and green synthesis of silver nanoparticles (Table.I.1). These biogenic-AgNPs demonstrate remarkable multifunctionality, notably in environmental and agrochemical remediation, showing promising results in degrading and removing pollutants, heavy metal sensing, and controlling insect pests. Furthermore, their biopharmaceutical activities have been explored in vitro and in vivo, including anticancer, antioxidant, antifungal, and antimicrobial effects. Their potent activities have been attributed to the synergistic interaction between AgNPs and Boraginaceae-derived bioactive compounds.

In this regard, S. Mollaet al.[178] successfully synthesized spherical silver nanoparticles with an average diameter of 7 nm through a single-step reduction process using an aqueous extract of *Lithospermum officinale* root. These AgNPs exhibited exceptional antioxidant activity, as demonstrated by their enhanced free radical scavenging capacity in vitro. Similarly, S. Nindawat and V. Agrawal [179] employed an aqueous extract of *Arnebia hispidissima* root to produce anisotropic silver nanoparticles (AHAgNPs) and evaluate their therapeutic activities. AHAgNPs displayed notable anti-DPPH and anti-$H_2O_2$ radical scavenging effects, along with selective cytotoxicity toward cervical cancer cells while sparing normal cells. Moreover, the *A. hispidissima*-derived silver particles demonstrated antimicrobial properties against both fungal and bacterial strains. These findings are corroborated by additional studies that discussed the microbial behavior of silver nanoparticles synthesized from other members of the Boraginaceae family, such as *Anchusa officinalis L., Heliotropium indicum L., Borago officinalis, and Trichodesma indicum*[180–184]. The AgNPs possess biological activity in killing the growth of microbes and inhibiting biofilms, underlining their applicability in medical and pharmaceutical settings for the prevention and treatment of pathogens and microbial infections.

Global concern is mounting over the impact of agricultural pests that cause significant crop losses and threaten the balance of ecosystems, including native plant and insect species. These pests, including worms, insects, and invasive weeds, have developed high resistance to conventional chemical pesticides, necessitating the development of alternative pest control strategies. Given the promising bioactivity demonstrated by AgNPs as antioxidant, antitoxic,

and antimicrobial properties, recent studies have particularly highlighted the potential development of new insecticides and herbicides based on silver nanoparticles. For instance, M. Hazaat al.[185] evaluated the insecticidal activity of *Borago officinalis* leaf-mediated AgNPs against the *Spodoptera littoralis* weevil. AgNPs significantly prolonged the larval period, and they possessed high larvicidal activity, with a concentration of 4.0 mg/g Ag NPs being sufficient to complete mortality (100%) of the larvae of this worm. In a parallel study, AA. Buhroo et al[186]. reported that *Trichodesma indicum*-synthesized AgNPs (20-50 nm in size) exhibited rapid biocidal action against *Mythimna separata* larvae; a treatment concentration of 500 ppm resulted in complete eradication of larvae within 72 hours.

**Table.I. 1.** Boraginaceae plants-assisted biogenic synthesis of silver nanoparticles uand their potential applications.

| *Boraginaceae* species | Part used | Particle size (nm) | Shape and morphology | Potential applications and activities | Ref |
|---|---|---|---|---|---|
| *Lithospermum offcinale* | Root | 7 | spherical | Antioxidant | [178] |
| *Lithospermum erythrorhizon* | Callus | 20-50 | spherical | cytotoxicity | [187] |
| *Borago officinalis* | leaves | 30-80 | spherical & hexagona | anticancer & antibacterial | [180] |
| *Borago officinalis* | leaves | 22 | spherical | Antimicrobial & antifungal | [181] |
| *Borago officinslis* | leaves | 40 | - | insecticides | [185] |
| *Anchusa Offcinalis* | leaves | 28.5 | spherical | Antimicrobial & anticancer | [182] |
| *Trichodesma indicum* | leaves | - | spherical | antibacterial & photocatalytic | [183] |
| *Trichodesma indicum* | leaves | 20-50 | spherical | insecticides | [186] |
| *Trichodesma indicum* | leaves & stem | 21 - 25 | spherical | anti-venom | [188] |
| *Heliotropium indicum L.* | leaves | 77-98 | spherical | Antimicrobial | [184] |
| *Heliotropium Curassavicum* | leaves | 5-30 | ellipsoidal & nearly spherical | antibacterial & antibiofilm | [189] |
| *Arnebia hispidissima* | leaves | 10-75 | rod, triangle, hexagon & polygon | antioxidant , antimicrobial & anticancer | [179] |
| *Cynoglossum furcatum* | leaves | 33 | spherical | antibacterial & anticancer | [190] |
| *Rotula aquatica* | leaves | - | - | antibacterial & photocatalytic | [191] |
| *Symphytum ofcinale* | leaves | 87.46 | irregular | antioxidant & anti-aging | [192] |

Among the most significant species within the Boraginaceae family, which is widely distributed across Mediterranean countries and commonly thrives on roadsides, field margins, forest edges, and in open, arid habitats in the northern region of Algeria, is *Cynoglossum*

*creticum* (*C. creticum*), also known as blue hound's tongue[193,194]. This species is an erect, branched, and biennial herbaceous plant belonging to the genus *Cynoglossum L*. Morphologically, *C. creticum* displays the typical vegetative characteristics of the Boraginaceae, with oblong to lanceolate, pubescent leaves arranged alternately along the stem, and inflorescences composed of small, bluish-purple, actinomorphic flowers (Figure. I.10).

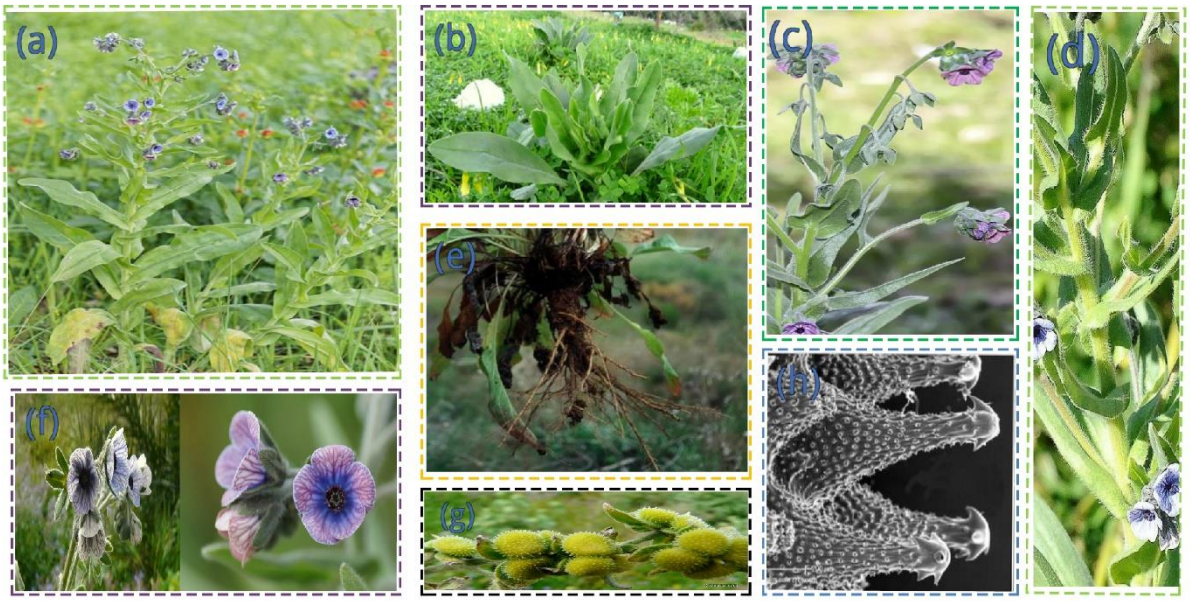


**FIGURE.I. 10.**Morphological and taxonomic details of Cynoglossum creticum. a) General form; b) basal leaves; c) inflorescences; d) stem, pubescence, and alternate lanceolate leaves; e) Mature base showing roots and remnants of dead basal leaves; f) flowers; g) seeds; and d) SEM image of the fruit surface (nutlet)[195].

Like the majority of species of its family, *C. creticum* is considered a toxic weed, particularly for livestock and equines, due to its high concentrations of pyrrolizidine alkaloids (PAs), especially in the countries where it has arrived as an invasive species, such as Southa [194,195]. Nonetheless, Mediterranean peoples have used this plant in folk medicine to dress wounds and treat throat infections and upper respiratory ailments[196]. Reports have presented the phytochemical profile, biological, and therapeutic properties *C. creticumt* (nt166,180). They have revealed a high content of active compounds, including allantoin and phenolic acids, especially in the aerial parts such as the leaves. Significant enzyme inhibitory activities have also been demonstrated, such as lipase, α-amylase, and cholinesterase, as well as antioxidant activities in free radical scavenging and metal chelation[196,197]. However, despite the high

content of natural secondary metabolites and the therapeutic potential of *Cynoglossum creticum*, it has not yet been exploited in nanomaterial biotechnology.

## I.5. Polyaniline Nanostructure (PANI-NS)

For the past two centuries, polyaniline has received significant attention as a conductive organic material with enormous industrial prospects. Its discovery dates back to 1834, when it was successfully synthesized during experiments by Friedrich Ferdinand Runge with aniline nitrate[198]. Prior to the establishment of the macromolecular concept by Hermann Staudinger in the 1920s, polyaniline was known and referred to according to its oxidation state as "aniline black"[199,200]. Brown et al.[201] were among the first to formally use the term "polyaniline" in 1947 in a published paper on the vapor phase-catalytic oxidation of aniline. However, the real breakthrough in the intensive understanding and development of polyaniline came in the 1980s, following the seminal discovery of intrinsically conducting organic polymers (ICPs) in 1977. This catalyzed a surge in research aimed at understanding the mechanisms of structure-induced electronic conduction, optimizing physicochemical structural processing and conductivity, and designing synthesis techniques and polymerization methods.

A major milestone came in 1987 when A.G. MacDiarmid proposed a structural model of polyaniline, consisting of alternating diaminobenzoide (reduced) and diaminoquinoid (oxidized) structural units[202]. Later in 1997, he also categorized polyaniline into three primary forms based on oxidation state and color (Figure. I.11): a fully reduced, colorless, and white leucoemeraldine base (LEB); a completely oxidized, purple-to-black pernigraniline base (PAB); and a blue emeraldine base (EB), which consists of both reduced and oxidized segments[203]. Among these, the latter is particularly significant due to its high environmental stability and is the only one that can be protonated to form the electrically conductive emeraldine salt (ES), typically green in color[204].

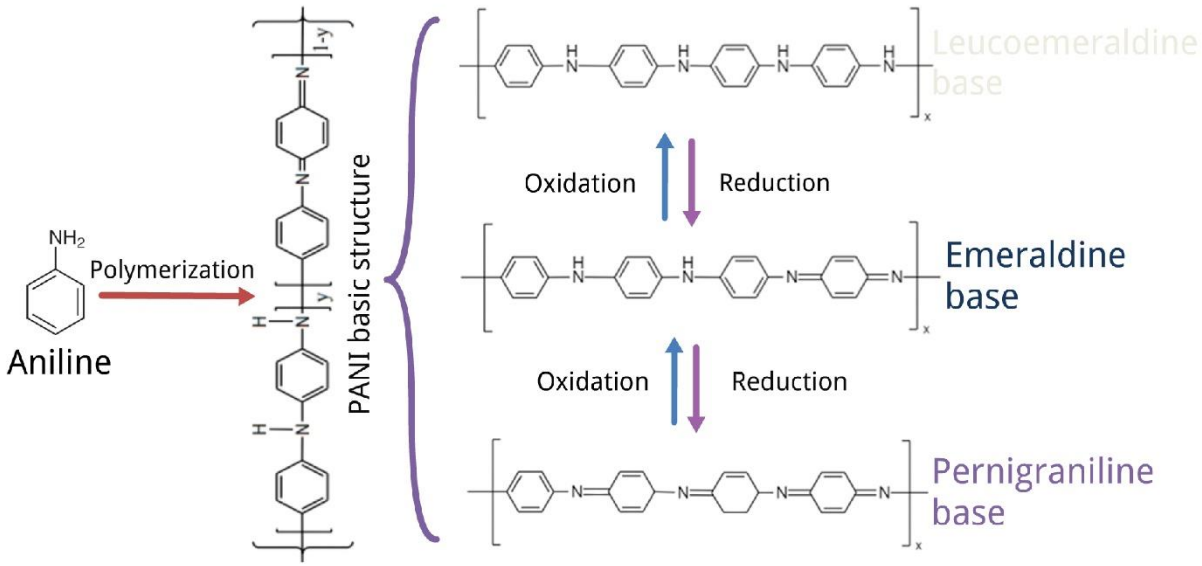


**FIGURE.I. 11.** Basic Molecular configuration of polyaniline ($0 \leq y \leq 1$) and corresponding redox states.

In fact, PANI is among the most interesting organic semiconductors in leading and multidisciplinary application areas. Its applications have been reported in solar cells, biofuel cells, supercapacitors, radar absorbers, electron field emitters, erasable optical data storage, anti-corrosion and antistatic coatings, electrorheological fluids, biosensors, smart membranes, and tissues[205–207]. This widespread utility is attributed to several advantageous properties: facile synthesis from inexpensive and widely available aniline monomer, relatively low cost and preparation time compared to other ICPs, as well as its high thermal, chemical, and environmental stability, and unique pH-dependentochromic behavior[208,209]. Furthermore, its ion-exchange, redox, and doping/dedoping characteristics also contribute to its superior electronic conductivity and high pseudocapacitance.

Nonetheless, polyaniline exhibits several inherent limitations that restrict its broader commercial deployment, especially in biomedical and biological fields. These include poor solubility and insolubility in most solvents, infusibility, non-biodegradability, limited mechanical flexibility, and processability challenges[210,211]. Additionally, its electrical conductivity is negatively affected by long life cycle. Addressing these shortcomings requires innovative strategies, such as chemical functionalization with organic carboxylic acids, nanocomposite formation, or the development of nanostructured PANI with tailored

morphologies. Structuring and dimensional design of polyaniline at nanoscale can offer new and improved properties, including enhanced chemical reactivity, increased molecular ordering, specific surface area, and specific discharge power-to-weight ratio, improved electrical conductivity due to the combination of ionic and electronic conductivity, and shorter ion transport pathways.

### I.5.1. Synthesis and Growth Control of Polyaniline Nanostructures

Like all nanomaterials, polyaniline nanostructures can be dimensionally classified into: zero-dimensional 0D-PANI such as nanospheres and nanoparticles[212]; one-dimensional structures such as PANI-nanotubes, PANI-nanofibers, PANI-nanowires, and PANI-nanorods[213,214]; and two-dimensional 2D-PANI such as nanosheets[215]; and complex micro/nanostructures-PANI exhibit unique morphological geometries such as feather-like, comb-shaped, honeycombs, rhizoid, and brain-like architectures[216] . The literature has reported numerous techniques and approaches for successfully oxidizing aniline and converting it to PANI with control and customization of the desired shape and structure at nanoscale. These include conventional polymerization methods, such as solution-phase, seeding, heterogeneous phase, interfacial, microsuspension, and electrochemical polymerization, as well as advanced approaches like radiolytic, sonochemical, plasma, rapid mixing reaction, and enzymatic synthesis[217–220].

However, the synthesis techniques are highly complex, and the successful formation of specific nanostructures critically depends on precise control of aniline oxidation parameters and associated physical and chemical processes, including initial concentration, oxidant type, pH, and temperature, all of which regulate nucleation and growth mechanisms during synthesis[213,221]. The choice of synthesis route plays a crucial role not only in determining the nanoscale shape of PANI but also in dictating its functional performance in various technological applications. Synthesis strategies can be classified into no template and template-based approaches. The latter are divided into two categories: soft-template synthesis (chemical) and hard-template synthesis (physical).

#### *1. Hard-template synthesis*

Hard-template synthesis is widely employed to produce one-dimensional (1D) nanostructured conductive polymers with precisely controlled lengths, diameters, and orientations. This method was first proposed by C.R. Martin et al.[222,223], and it quickly gained substantial adoption due to the improvements in electronic conductivity of PANI compared to its conventional bulk forms. In this approach, porous, nanochanneled materials serve as

templates into which aniline monomers are deposited, polymerized, and grown. Upon completion of the polymerization process, the template is either partially or completely removed to isolate and recover the nanostructured PANI. The most common utilized templates include monodisperse inorganic oxides such as anodic aluminum oxide (AAO), manganese oxide, silica, and zeolites. Additionally, porous and mesoporous membranes like particle track-etched membranes (PTMs), and polymeric microspheres, particularly those composed of polycarbonate (PC) or poly(vinyl alcohol) (PVA), are frequently employed[224,225].

The importance of templates lies in their narrow pore size distribution, which facilitates the control of polymer dimensions, allowing PANI to adopt the pore diameters and morphology of the template. Furthermore, these templates are commercially available in a variety of sizes and shapes and can be synthesized using well-established protocols[226]. However, there are several technical drawbacks associated with the hard-template approach, particularly the tedious and complex post-synthesis template removal processes, which are often performed by solvent etching or calcination. Template detachment also leads to the potential destruction of the nanostructure of PANI, the formation of aggregates, and the development of heterogeneous morphologies.

To address these drawbacks, alternative strategies involving in situ or self-removable templates have been proposed. Z. Zhang et al. [227] developed a self-template removal-based polyaniline synthesis. They employed the octahedral cuprous oxide ($CuO_2$) as both the template and a sacrificial component. Upon the addition of ammonium persulfate (APS) as the polymerization oxidant, it reacts with the $Cu_2O$ template to form soluble copper sulfate, eliminating the need for separate template-removal processes. Similarly, L.J. Pan et al.[228] proposed a template-based aniline polymerization technique utilizing manganese oxide nanowires ($MnO_2$-NW), which acted simultaneously as the template and the oxidative initiator. During polymerization, a thin PANI layer formed on the surface of the $MnO_2$-NW. These nanowires were subsequently reduced to soluble $Mn^{2+}$ ions and spontaneously removed, resulting in the development of hollow PANI nanotubes. A schematic representation of the proposed mechanism underlying this nanotube formation is illustrated in Figure. I.12(a-c). However, due to the redox behavior of the templates themselves, the reducibility of $Cu_2O$ or $MnO_2$ during the polymerization often results in the formation of PANI in its reduced emeraldine base (EB) form, which is electrically non-conductive. This poses a significant challenge for applications and highlights the need for further optimization in template-assisted PANI synthesis.

***2. Soft-template synthesis***

The soft template fabrication approach, often referred to in the literature as the self-assembly method, represents a more practical and cost-effective option for synthesizing low-dimensional nanostructured PANI. Unlike hard-template methods, soft-template synthesis eliminates the need for post-synthesis and template removal processes, as the synthesis is performed through a self-template (typically a micelle) formed in situ from aniline or its salts. These micellar structures arise through the interaction of aniline monomers with structure-directing agents such as reverse microemulsions, biopolymers, liquid crystals, organic acids, deoxyribonucleic acid (DNA), and surfactants[229–231]. In a typical polymerization, the soft template is formed by mixing aniline with surfactants in aqueous media at specific molar ratios, forming transparent micelles of aniline salt and surfactant due to the amphiphilic nature of the reactive (hydrophobic aniline and hydrophilic surfactant molecules). Upon addition of an oxidizing agent, the micelles self-assemble and acts as a transient scaffold that directs the nanostructural organization of PANI.

The selection of acid dopants with bulky and complex side groups and amphiphilic properties, which simultaneously act as surfactants and dopants, is among the most important factors in controlling the nanostructure in the soft-template synthesis. Sulfonic acid derivatives such as naphthalene sulfonic acid (NSA), β-naphthalene sulfonic acid (β-NSA), 2,4-dinitronaphthol-7-sulfonic acid (NONSA), perfluorooctane sulfonic acid (PFOSA), azobenzene sulfonic acid (ABSA), and p-methylbenzene sulfonic acid (MBSA), as well as carboxylic acids like salicylic acid, malic acid, oxalinic acid, glutaric acid, and benzene-1,2,4,5-tetracarboxylic acid (BTCA), are commonly employed[232–234]. M. Wan and his team first reported the synthesis of PANI nanotubes by soft-template synthesis in 2001[235]. A year later, the team examined the effect of the molar ratio of beta-naphthalene sulfonic acid (β-NSA) and aniline on the synthesis process and proposed the first theory explaining the PANI self-assembly mechanism[236]. The acidic structure-directing agent (dopant) acts as a surfactant that forms micelles with anilinium cations thanks to its hydrophilic $–SO_3H$ groups and hydrophobic $C_{10}H_7$ backbones. The micelles accrete and elongate into nanotubes and nanofibers, as illustrated in in the schematic in Figure.I.12(d). Dynamic light scattering (DLS) measurements revealed that the micelle diameters fall between the outer and inner diameters of the resulting nanotubes, supporting their role as structural templates.

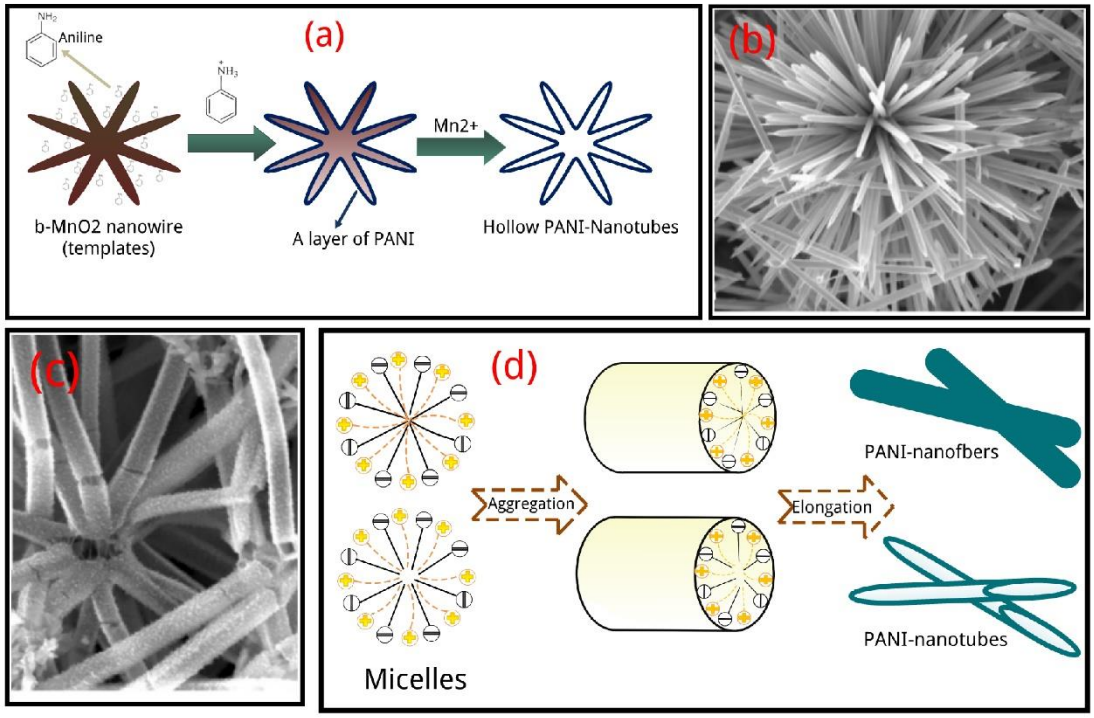


**FIGURE.I. 12.** a) schematic diagram of the potential formation mechanism of PANI nanotubes on a manganese oxide wire template; b-c) SEM images of manganese oxide ($MnO_2$) nonowires and hollow PAni nanotubes, respectively[228]; self-assembly mechanism of micelles to form PANI nano-tubes/fibers.

Subsequent reports by this research team further clarified the self-assembly process[237,238] . In experiments involving poly(3-thiopheneacetic acid) and salicylic acid, the role of the hydrophilic -COOH group of the dopants in the nanostructure growth mechanism was demonstrated, as it induces polymerization at the micelle/water interface. W. Wu et al.[234] synthesized homogeneous PANI nanotubes doped with various organic acids and observed that the number of –COOH groups in the surfactant determines the diameter of the micelles and the outer diameter of the PANI tubes, which increased with increasing –COOH numbers. They also suggested that the self-assembly of the nanotubes was a result of hydrogen bonding between the –OH groups of the carboxylic acids and the amine of PANI. Further refinement of the mechanism was proposed by G.H. Lim and H.J. Choi[239]. They believe that due to the hydrophilic nature of the oxidizing agent (APS), polymerization occurs at the interface, and anilinium cations tend to incline to fill the internal surface of the oxidant, forming lamellar-bilayer-micelles that grow into oligomers, which in turn form flakes. The flakes eventually self-assemble into PANI nanotube structures thanks to hydrogen bonding and π–π electron interactions.

***3. No template synthesis***

No template synthesis is the most straightforward approach for fabricating PANI nanostructures without relying on any scaffolds, whether soft or hard. Self-assembly occurs by changing the redox potential of the oxidizing agent, removing the need for an acidic dopant. This approach not only eliminates the template and its removal processes but rather simplifies the number of reagents and reactants, resulting in purer PANI. M. Trchova et al.[240] were the first to propose this type of synthesis. In 2006, they successfully synthesized PANI nanotubes in aqueous solution in the presence of only APS. This oxidative polymerization proceeded in two steps, with APS acting as the oxidant and subsequently acting as both dopant and oxidant. Initially, when the pH was above 4, the monomer was oxidized, and aniline oligomers were formed. As the reaction progressed, the oxidation reaction generated sulfuric acid ($H_2SO_4$) as a byproduct, causing the pH of the reaction medium to drop below 4. This acidification changed the reaction mechanism; the aniline was protonated to form anilinium cations and nucleated sites on the oligomer, stimulating the growth of PANI chains, which subsequently self-assembled and extended into nanotube structures.

This report motivated M. Wan and his research group, who developed the soft-template synthesis approach, to conduct further investigations on the synthesis of PANI with different oxidants in the absence of acidic dopants[241]. These included copper(II) chloride ($CuCl_2$), iron(III) chloride ($FeCl_3$), ferric sulfate ($Fe_2(SO_4)_3$), cerium(IV) sulfate ($Ce(SO_4)_2$), and APS. Interestingly, PANI nanofibers with notable conductivity were successfully obtained. The morphology and diameter of the nanofibers could be predicted and controlled by the redox potential of the oxidants; increasing the redox potential of the oxidants resulted in an increase in the diameter and size of the nanofibers. This strategy, which Wan's team termed "the dopant-free, template-free method (DFTFM)."[241,242]. To distinguish this approach from the soft template synthesis method, also referred to in much literature as "template-free synthesis," the no-template method was later renamed "the simplified template-free method (STFM)" [243]. Subsequently, X. Wang et al.[244] reported the possibility of controlling the morphology of PANI by introducing alkali agents. The presence of sodium hydroxide (NaOH) in varying molar proportions during the template-free oxidation of aniline with APS yielded different PANI morphologies: microparticles, hollow and solid microspheres, and nanotubes. P. Liu et al.[245] developed a sub-method under the STFM framework to synthesize PANI nanostructures containing nanofilms and nanotubes in two separate reactions at low reagent concentrations.

### I.5.2. Physicochemical and Biological Features of Polyaniline Nanostructure

Polyaniline is widely recognized as the second most widely applied intrinsically conductive polymers (ICPs) after polypyrrole (PPy), thanks to its tunable electrical conductivity and favorable dielectric properties[246]. Among oxidation states of PANI, only the semi-oxidized, fully protonated emeraldine salt form exhibits intrinsic electrical conductivity. This conductive behavior arises from the presence of delocalized radical cations (polarons) along the polymer chains. Increasing the number of these charge carriers in the backbone enhances the electrical conductivity, whereas their absence results in insulating structures, such as those found in pernigraniline and leucomeridine. At the nanoscale, PANI demonstrates significantly improved electrical conductivity compared to its macroscopic counterparts[242,247]. This enhancement is primarily attributed to the formation of interconnected conductive networks based on the low intrinsic resistance of the nanofibers, tubes, wires, or particles, which reduce grain boundaries and facilitate efficient charge transport.

The four-point probe method is commonly employed to estimate the electrical conductivity of PANI-based materials. The literature confirms that the electrical conductivity of PANI nano/micro-tubes and wires typically ranges from $10^{-2}$ to 1 S/cm[248]. Y. Long et al[249]. observed that the conductivity of PANI nanotubes synthesized through the self-assembly process in aqueous camphor sulfonic acid (CSA) medium was about $3 \times 10^{-2}$ S/cm. However, due to the moderate distribution of PANI nanotubes, the four-point measurement method cannot exclude the contact resistance between individual nanostructures; the measured resistance includes both the intrinsic resistance and the contact resistance[242,243].

To minimize the effect of the contact resistance in ensemble measurements, advanced techniques have been developed to characterize the electrical properties of a single nanostructure. These include isolating a single PANI nanotube or nanowire on an atomic force microscope (AFM) conductor tip and directly probing their current-voltage (I–V) characteristics[250]. S. Xiong et al.[247] also utilized a scanning probe microscope (SPM) to measure the I-V characteristics of individual PANI nanotubes with a diameter of 200 nm. The SPM tip served as the positive electrode, and the average conductivity of the PANI nanotube was 5.81 S/cm, approximately three times higher than the average conductivity of bulk PANI, which is estimated to be 1.75 S/cm. These findings reinforce the notion that nanoscale PANI structures possess superior electrical performance. These findings reinforce the notion that nanoscale PANI structures possess superior electrical performance. Furthermore, studies have shown that the conductivity of PANI nanotubes is inversely related to their diameter; as the diameter

increases, the conductivity tends to decrease and may approach the lower values characteristic of bulk PANI[244,248].

Conventional polyaniline is characterized by its high agglomeration, exceptional chemical and structural stability in both alkaline and acidic media, exhibiting high resistance to degradation due to its rigid π-conjugated backbone. However, bulk PANI suffers from poor processability due to its insolubility in water and organic solvents, and the agglomeration structure prevents effective dispersion. This hinders the integration of polyaniline into bio- and pharmaceutical-related applications[211]. The development of polyaniline nanofibers has improved processability, as these nanofibers can form stable aqueous colloidal dispersions without any additional chemical modification or surfactants. D. Li and R.B. Kaner,[251] demonstrated the possibility of forming pure aqueous PANI nanofiber colloids by controlling the pH at acidic conditions in post-synthesis purification processes. Positively charged nanofibers form interconnected networks and well-separated segments due to electrostatic repulsion forces, enabling self-colloidal stability. Additionally, A. Rahy et al.[252] succeeded in greenly synthesizing polyaniline nanofibers in the presence of sucralose and sucrose. The presence of the added disaccharide in the synthesis enabled the production of polyaniline nanofibers that are soluble in water and polar solvents such as alcohols, dimethyl sulfoxide (DMSO), and dimethylformamide (DMF). disaccharide facilitates the dissolution and stabilization of PANI fibers, acting as a bridge that connects with both the polymer chains and the solvent molecules through hydrogen bonds.

Biocompatibility is a critical prerequisite for materials intended for use in pharmaceuticals, medical devices, and equipment. Biocompatibility refers to the ability of a material to perform its intended function in contact with biological systems or coexist with living tissues and cells without causing inflammatory responses and adverse effects. Cytotoxicity assays provide essential tools used to estimate the biocompatibility and cellular response to materials. For polyaniline as a promising material for biomedical applications, several studies have evaluated their biological properties, biocompatibility, and cellular toxicity in vitro and in vivo. C.H. Wanga et al.[253] were the first to assess the biocompatibility of various oxidation states of PANI. They implanted films and powders of PANI under the skin of the dorsal surfaces of male Sprague-Dawley rats over a 50-week period. In vivo tissue response indicated insignificant inflammation in PANI samples, except for emeraldine films, which showed signs of an inflammatory response after 24 weeks; they were coated with fibrous tissue. Contrastingly, S. Kamalesh et al.[254] reported no signs of inflammation or neoplastic tissue over

a long-term study, where PANI-emeraldine films were subcutaneously implanted in similar animal models for up to 90 weeks, suggesting excellent long-term biocompatibility.

Meanwhile, in vitro (on human keratinocyte cell line NCTC 2544) and in vivo (on female Sprague-Dawley rats) studies conducted by M. Mattioli-Belmonte et al.[255] indicated that polyaniline films exhibited inflammatory damage. Nevertheless, polyaniline demonstrated cytocompatibility with various cell lines, including L929 and NIH-3T3 fibroblasts, H9c2 cardiomyocytes, and neural stem cells[256,257]. The behavior and toxicity of PANI, as well as the cell viability and growth, are not precisely defined due to conflicting results in the literature. L.E. Ibarra et al.[258] believe that PANI possesses no cytotoxicity due to its insolubility and that the primary factors contributing to cytotoxicity are monomer residues, aniline oligomers (e.g., benzidine), oxidizing agents, and strongly acidic dopants. APS, in particular, has been shown to exhibit significant cytotoxicity and may act synergistically with aniline cation to cause severe cell damage, impair cellular viability, and promote oxidative stress[259,260]. Additionally, the high levels of low-molecular-weight oligomers may carry carcinogenic risks. Interestingly, aqueous solutions of colloidal polyaniline have demonstrated relatively low cytotoxicity in some cases, with selective interactions observed between cell types. For instance, enhanced toxicity toward NIH/3T3 mouse embryonic fibroblasts compared to human HaCaT keratinocytes[261].

As previously mentioned in the nanomaterial classification section, NMs cause increased biological interactions, cellular uptake, bioavailability, and toxicity compared to their bulk counterparts, and this is also found with polyaniline nanostructures. The cytotoxicity of nanopolyaniline is primarily associated with altered mitochondrial membrane potential (MMP) and the generation of oxidative stress (ROS), leading to cell death[262]. Y.S. Li et al.[263] demonstrated that the toxicity of PANI-NS is dependent on the dose and incubation time, increased generation of caspase-3, a protein that induces cell death, was observed during cellular exposure. Additionally, L.E. Ibarra et al.[258] conducted comprehensive studies about the embryotoxicity and teratogenicity of polyaniline nanoparticles on Rhinella arenarum larvae and embryos. PANI nanoparticles are considered to pose no toxicity risk to R. arenarum, but they cause teratogenic effects related to their nanoscale size. Similarly, reports have revealed that the high surface area and low size and dimensions of polyaniline nanostructures contribute to their potentially hazardous effects on living tissues[262]. Y. Zhang et al.[264] explored the impact of PANI-NMs sizes on both in vivo acute oral toxicity (in ICR mice) and in vitro cytotoxicity (in BV2 microglial cells). Low-molecular-weight polyaniline nanofibers induced acute in vitro cytotoxicity, notable oral toxicity, and minor damage to liver and kidney tissue. In contrast,

high-molecular-weight PANI nanospheres demonstrated no significant oral or tissue toxicity. This discrepancy was linked to the high surface area of the nanofibers and their excellent stability in a culture medium, compared to nanospheres, which tend to aggregate.

To address and minimize the toxicological risks associated with PANI-NS, particularly nanofibers, recent research has focused on eco-friendly manufacturing approaches and the use of bioactive dopants to replace conventional toxic reagents. These strategies aim to reduce residual impurities and improve the compatibility of PANI-NS with living systems, enhancing the application of PANI-NS in tissue engineering, drug delivery, and regenerative medicine[265,266]. In this regard, Z. Daraeinejad and I. Shabani synthesized polyaniline nanofibers doped with taurine, an aminosulfonic acid naturally present as a nutrient in mammalian tissues and promotes neural stem cell proliferation. This biodopant not only enhanced the biocompatibility of the PANI nanofibers and prevented cytotoxicity to 3T3 fibroblast cells but also promoted cell proliferation and viability[267]. Beyond biocompatibility, PANI nanofibers possess unique characteristics such as high porosity, large surface area, and electrical conductivity that make them ideal as biofunctional carrier matrices for enzyme immobilization, drug loading, and biosensing. S. Ghosh et al.[268] confirmed the precise enzyme loading and immobilization capabilities of PANI nanofibers, where the immobilization of L-asparaginase on the nanofibers increased its stability and resistance to denaturation under various conditions.

## I.6. Silver/Polyaniline nanocomposites (Ag/PANI-NCs): preparation strategies and biological activities

Hybrid organic-inorganic nanocomposite systems have attracted extensive academic interest due to their synergistic organic-inorganic properties and novel functionalities distinct from those of the individual components. Among these systems, nanocomposites based on π-conjugated polymers and noble metal nanoparticles, particularly polyaniline and silver nanoparticles (AgNPs), are a model of great interest due to their enhanced applications in data storage, energy storage, catalysis, adhesive and conductive coatings, bio- and chemical sensing, and drug delivery. These composites maintain the intrinsic properties of both the original PANI and AgNPs, but exhibit enhanced effects due to synergistic interactions, manifested in enhanced optical, electrical, and dielectric properties. Due to their superior thermal and electrical conductivity, silver can act as a conductive junction between the chains, interacting with the delocalized π-electrons, enhancing the electrical behavior of the composites[269,270]. There are

several techniques for preparing nanocomposites based on PANI and silver nanoparticles, including mechanical blending of the two phases, physical mixing in solution, reduction of silver precursors with PANI, synthesis of silver nanoparticles in the presence of PANI, incorporation of silver nanoparticles into the oxidative polymerization of aniline, and direct oxidation of aniline with silver compounds or salts.

Among the most widely employed strategies for synthesizing polyaniline-silver nanocomposites, the insitu simultaneous polymerization and reduction approach has been the most interesting approach recently investigated. This approach is simpler and relies on a one-step redox reaction wherein aniline monomers are oxidized by silver precursors, producing concurrent PANI and AgNPs with synergistic advantages. N.V. Blinova et al.[271] were among the first to demonstrate this approach, employing $AgNO_3$ as the oxidant in nitric acid solutions to initiate the polymerization of aniline. Nanocomposites consisting of PANI nanofibers and silver in the form of nanoparticles and microscopic sheets were produced. Subsequent studies have further expanded upon this approach by exploring alternative acidic media to facilitate polymerization[272,273]. Sulfonic acids such as sulfamic, methanesulfonic, styrenesulfonic, and camphorsulfonic acids have proven particularly effective as doped mediums, enabled homogeneous polymerization and improved product yield. Notably, composites consisting of AgNPs accompanied by emeraldine rods synthesized in methanesulfonic acid exhibited high electrical conductivity, reaching values up to 880 $S \cdot cm^{-1}$[272].

Despite its potential, the routine preparation of PANI–Ag composites via direct redox polymerization of aniline with silver salts remains technically challenging. This is primarily due to the relatively high reduction potential of aniline (1.0 V) compared to that of silver ions (0.799 V), which renders the redox-driven polymerization thermodynamically sluggish. As a result, the induction period alone can extend over several weeks[274,275]. This has prompted research to propose other procedures that enhance the redox activity [275]of silver precursors and accelerate polymerization kinetics. These include the use of co-oxidants as well as physical activation techniques such as ultraviolet (UV) irradiation, sonication, γ-irradiation, photolysis, radiolysis, and asymmetric square-wave[276–278]. For instance, Q. Jia et al.[279] reported the successful one-step synthesis of AgNPs-PANINFs composites using silver nitride and APS in nitric acid. The resulting nanocomposites exhibited potent antimicrobial activity against bacterial and yeast strains, attributed to the synergistic effect of PANI and AgNPs. PANI serves to stabilize and protect the AgNPs from aggregation, while the AgNPs induce a redox imbalance and a decrease in osmotic pressure in cells, which kills bacteria.

Multiple studies have confirmed the synergistic antibacterial effect of the individual components in PANI/Ag composites synthesized using this approach[280,281]. M. Shaban et al.[282] further elucidated the antibacterial mechanism of Ag/PANI nanocomposites synthesized under artificial visible light irradiation. The Ag/PANI composite exhibits high bactericidal activity against both Gram-negative and Gram-positive bacteria. The antimicrobial mechanism involves electrostatic attraction adsorption between the positively charged Ag/PANI NCs and the negatively charged bacterial surface. This interaction facilitates the penetration of composites into the cytoplasmic membrane, leading to disruption of vital functions, rupture of cell walls, leakage of intracellular contents, and eventual cell lysis. Figure.I.13 illustrates the potential mechanism of electrostatic attraction.

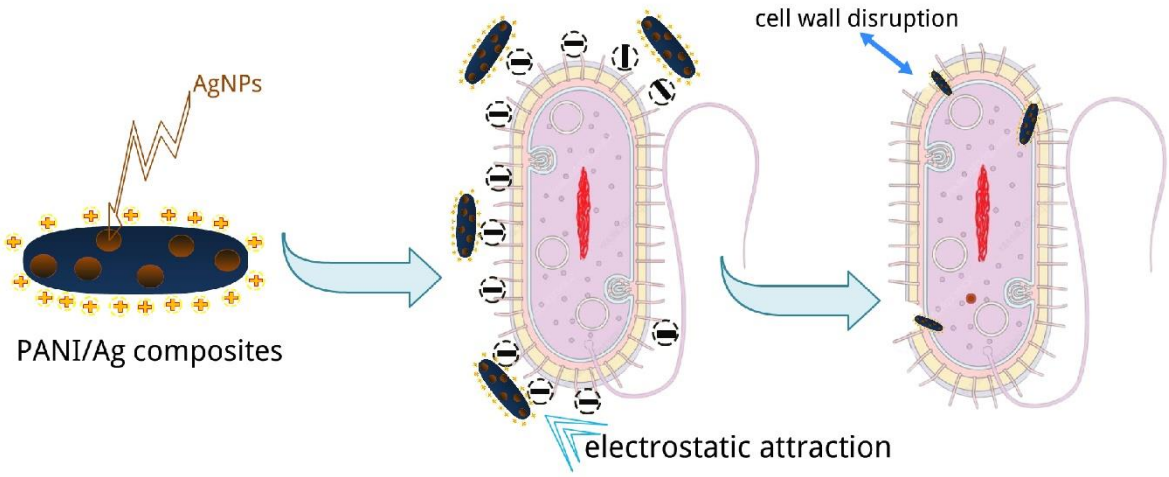


**FIGURE.I. 13.**schematic illustrating the electrostatic attraction-related antibacterial activity of PANI/Ag composites.

Polyaniline-silver composites can be prepared via an in situ oxidative polymerization carried out in two-step. In this approach, aniline is oxidized in the presence of pre-synthesized AgNPs. During the polymerization, polyaniline (PANI) chains form and grow on the surface of the AgNPs, leading to the development of a core–shell structure[283]. The synthesis mechanism is primarily driven by electrostatic interactions between the anilinium cations and Ag. Capping agents, such as citrate and polyethylene glycol, confer a negative surface charge on AgNPs, enabling them to attract and absorb positively charged aniline cations, resulting in the formation

of silver-aniline complexes. Polymerization is initiated upon the addition of the oxidizing agent to the reaction mixture, triggering nucleation on the AgNPs surface[284,285]. The subsequent growth of PANI chains merges with the nanoparticles.

The presence of AgNPs enhances the conductivity of the composites compared to pristine PANI due to electron tunneling through AgNPs, which increases electron mobility and charge transfer between the Ag and the quinoid unit[285]. In this regard, H. Zengin et al.[286] observed the formation of covalent bonds between carbon atoms in the PANI rings and AgNPs, potentially contributing to the enhanced electrical conductivity. They also investigated the antibacterial properties of PANI/AgNPs films. Microbiological viability assays demonstrated that all tested bacterial strains were not colonized on PANI and PANI/Ag films over 72 h, indicating their antimicrobial properties. Furthermore, Mark et al.[287] explored the application of PANI/AgNPs composites as coatings for tissue engineering scaffolds, using Nile tilapia skin. In their study, AgNPs were synthesized using Cymbopogon nardus essential oil and subsequently dispersed in an aniline cation monomer. The fish skin scaffolds were then immersed in this solution prior to polymerization. The PANI/AgNPs coating exhibited significant antibacterial activity against both planktonic and biofilm-forming species. This prevented bacterial penetration into Nile tilapia skin tissues and its contamination, supporting the long-term use as a xenograft. This antibacterial efficacy of the PANI/AgNPs coat is mainly due to the synergistic effect of AgNPs embedded in the PANI matrix, which locally inhibit bacterial growth and biofilm formation.

A third approach for synthesizing PANI/AgNPs composites involves the in situ chemical reduction of silver salts in the presence of PANI, which functions either as a structural template or as a reducing agent. This approach leverages the unique properties of PANI, particularly its nanostructured form (PANI-NS), which offers a high surface area, cavity-rich porosity, and surface chemistry rich in functional amine groups[237,288]. Polyaniline has been widely reported to act as both a reducing agent and binding agent in the direct, one-step synthesis of AgNPs. Thermodynamically, due to the higher reduction potential of PANI compared to $Ag^{+}$, NPs can be formed through redox reactions, where the redox-active sites on PANI donate electrons and reduce silver ions[289]. During synthesis reactions, silver ions ($Ag^{+}$) adsorb onto the PANI surface via coordination with electron-rich secondary and tertiary amines in the chains. Subsequent electron transfer results in the reduction of $Ag^{+}$ to $Ag^{0}$, followed by NPs growth and clustering. Additionally, strong interactions such as coordination bonds can form between silver and terminal quinoid imine (N═) groups, contributing to the formation of a hybrid network[270] .

The morphology, particle size, and distribution of AgNPs within the PANI matrix are significantly influenced by several factors, including the redox state of PANI, the nature and concentration of dopant acids, and reaction conditions[289,290]. S. Bouazza et al.[291] demonstrated that leucoemeraldine exhibits enhanced silver-reducing capacity compared to other PANI forms due to a greater availability of free redox-active sites. Furthermore, incorporation of Ag into the PANI framework also impacts the thermal, optical, and catalytic properties of composites. The embedded Ag acts as heat sinks and can control the thermal kinetics of the chains, thereby improving the thermal stability of the composites[270]. Optically, the PANI/Ag composites exhibit enhanced localized surface plasmon resonance (LSPR) of silver, enabling high catalytic activity and excellent sensitivity as a surface-enhanced Raman scattering (SERS) substrate[288,289]. However, despite the promising potential of this approach for producing PANI/Ag nanocomposites, comprehensive evaluations of the biological activity of the synthesized composites have not been studied. Furthermore, green synthesis principles and techniques were not employed to incorporate AgNPs into the PANI matrix, which is expected to improve biocompatibility, antibacterial and antioxidant activities, and reduce bioavailability and associated toxicity.

## I.7. Conclusions

Nanotechnology continues to evolve as a revolutionary scientific and transformative industrial domain, attracting substantial academic and commercial interest. As a multidisciplinary field, nanotechnology integrates physical, chemical, and biological principles and concepts to engineer and design nanoscale systems and materials. The unique characteristics demonstrated at this scale, such as tunable electronic behavior, quantum effects, and enhanced surface chemistry and area, have spurred the translation of nanotechnology knowledge across various industries, manifested in the development of innovative nanomaterial-based products. These materials offer significant economic benefits, including improved performance, reduced production and energy costs, and respectful environmental considerations. Among the most promising emerging nanostructures are silver nanoparticles and nano-polyaniline, which represent inorganic and organic nanomaterials, respectively. These have shown exceptional utility in a wide array of fields, including catalysis, sensing, energy storage, solar energy conversion, antimicrobial textiles, food preservation, bioimaging, tissue engineering, and targeted drug and gene delivery.

This chapter provided a comprehensive theoretical overview of nanotechnology and nanomaterials, tracing the historical development of the field and exploring the fundamental characteristics that define and classify nanostructures. Special attention was paid to discussing the importance of silver nanoparticles, nano-polyaniline, and their hybrid composites. This importance is reflected in the superior optical, surface, conductive, and biological properties offered by these structures. The chapter also highlighted key fabrication strategies, emphasizing green synthesis methods that employ renewable, less toxic, and environmentally benign precursors. While green synthesis offers significant advantages such as biocompatibility and environmental sustainability, its development is still accompanied by significant scientific and practical challenges. These challenges include a lack of standardization in synthesis protocols and limited scalability. These limitations underscore the need for further interdisciplinary research to improve green synthesis processes, as well as to explore underutilized plant natural resources that themselves pose unaddressed challenges, such as toxic weeds. The following experimental chapters attempt to exploit this type of resource to enhance green nanotechnology by synthesizing silver nanoparticles, polyaniline nanostructures, and their composites, suggesting potential biopharmaceutical and analytical applications.

## References


1. Clinton BP. Science in the 21st Century. *Science*. 1997;276(5321):1951-1951. doi:10.1126/science.276.5321.1951

2. Khatoon UT, Velidandi A. An Overview on the Role of Government Initiatives in Nanotechnology Innovation for Sustainable Economic Development and Research Progress. *Sustainability*. 2025;17(3):1250. doi:10.3390/su17031250

3. Díaz-Marcos J, Mendoza Gonzálvez J. Shaping the future of nanotechnology: a perspective on education, dissemination and ethics. *Front Nanotechnol*. 2025;7:1524578. doi:10.3389/fnano.2025.1524578

4. Coccia M, Finardi U, Margon D. Current trends in nanotechnology research across worldwide geo-economic players. *J Technol Transf*. 2012;37(5):777-787. doi:10.1007/s10961-011-9219-6

5. Kamarulzaman NA, Lee KE, Siow KS, Mokhtar M. Public benefit and risk perceptions of nanotechnology development: Psychological and sociological aspects. *Technology in Society*. 2020;62:101329. doi:10.1016/j.techsoc.2020.101329

6. Ghasemi I, Abdi E, Yaghmaei O, Nemati R. Nanotechnology Markets in Global Competition: A Review. *ILSHS*. 2015;57:74-84. doi:10.18052/www.scipress.com/ILSHS.57.74

7. Ulucan-Karnak F, Kuru Cİ, Sağın FG. Critical evaluation of publications and patents in nanobiotechnology-based research in the last decade. *Turkish Journal of Biochemistry*. 2024;48(6):606-619. doi:10.1515/tjb-2023-0144

8. Dong H, Gao Y, Sinko PJ, Wu Z, Xu J, Jia L. The nanotechnology race between China and the United States. *Nano Today*. 2016;11(1):7-12. doi:10.1016/j.nantod.2016.02.001

9. Rambaran T, Schirhagl R. Nanotechnology from lab to industry – a look at current trends. *Nanoscale Adv*. 2022;4(18):3664-3675. doi:10.1039/D2NA00439A

10. Pandiarajan J. Diverse Manifolds of Biogenic Nanoparticles in Synthesis, Characterization, and Applications. In: Saglam N, Korkusuz F, Prasad R, eds. *Nanotechnology Applications in Health and Environmental Sciences*. Nanotechnology in the Life Sciences. Springer International Publishing; 2021:1-28. doi:10.1007/978-3-030-64410-9_1

11. Schaming D, Remita H. Nanotechnology: from the ancient time to nowadays. *Found Chem*. 2015;17(3):187-205. doi:10.1007/s10698-015-9235-y

12. Zhu B, Wang H, Leow WR, Cai Y, Loh XJ, Han M, Chen X. Silk Fibroin for Flexible Electronic Devices. *Advanced Materials*. 2016;28(22):4250-4265. doi:10.1002/adma.201504276

13. Walter P, Welcomme E, Hallégot P, Zaluzec NJ, Deeb C, Castaing J, Veyssière P, Bréniaux R, Lévêque JL, Tsoucaris G. Early Use of PbS Nanotechnology for an Ancient Hair Dyeing Formula. *Nano Lett*. 2006;6(10):2215-2219. doi:10.1021/nl061493u

14. Barhoum A, García-Betancourt ML, Jeevanandam J, Hussien EA, Mekkawy SA, Mostafa M, Omran MM, S. Abdalla M, Bechelany M. Review on Natural, Incidental, Bioinspired, and Engineered Nanomaterials: History, Definitions, Classifications, Synthesis, Properties, Market, Toxicities, Risks, and Regulations. *Nanomaterials*. 2022;12(2):177. doi:10.3390/nano12020177

15. Deshmukh K. Nanotechnology in Ancient Era. In: Khoobchandani M, Saxena A, eds. *Biotechnology Products in Everyday Life*. EcoProduction. Springer International Publishing; 2019:3-14. doi:10.1007/978-3-319-92399-4_1

16. Skovmøller A, Brøns C, Sargent ML. Egyptian blue: modern myths, ancient realities. *J Roman archaeol*. 2016;29:371-387. doi:10.1017/S1047759400072184

17. Nicola M, Gobetto R, Masic A. Egyptian blue, Chinese blue, and related two-dimensional silicates: from antiquity to future technologies. Part A: general properties and historical uses. *Rend Fis Acc Lincei*. 2023;34(2):369-413. doi:10.1007/s12210-023-01153-5

18. Brun N, Mazerolles L, Pernot M. Microstructure of opaque red glass containing copper. *J Mater Sci Lett*. 1991;10(23):1418-1420. doi:10.1007/BF00735696

19. Sharon M, ed. *History of Nanotechnology: From Pre-Historic to Modern Times*. 1st ed. Wiley; 2019. doi:10.1002/9781119460534

20. Kumar N, Dixit A. Nanotechnology: Science and Technology at New Length Scale with Implications in Defense. In: *Nanotechnology for Defence Applications*. Springer International Publishing; 2019:35-79. doi:10.1007/978-3-030-29880-7_2

21. drinking-cup | British Museum. Accessed August 1, 2025. https://www.britishmuseum.org/collection/object/H_1958-1202-1

22. Barchiesi D. Lycurgus Cup: inverse problem using photographs for characterization of matter. *J Opt Soc Am A*. 2015;32(8):1544. doi:10.1364/JOSAA.32.001544

23. Drozdov A, Andreev M, Kozlov M, Petukhov D, Klimonsky S, Pettinari C. Lycurgus cup: the nature of dichroism in a replica glass having similar composition. *Journal of Cultural Heritage*. 2021;51:71-78. doi:10.1016/j.culher.2021.07.002

24. Verney-Carron A, Sessegolo L, Chabas A, Lombardo T, Rossano S, Perez A, Valbi V, Boutillez C, Muller C, Vaulot C, Trichereau B, Loisel C. Alteration of medieval stained glass windows in atmospheric medium: review and simplified alteration model. *npj Mater Degrad*. 2023;7(1):49. doi:10.1038/s41529-023-00367-0

25. Delgado J, Vilarigues M, Ruivo A, Corregidor V, Silva RCD, Alves LC. Characterisation of medieval yellow silver stained glass from Convento de Cristo in Tomar, Portugal. *Nuclear Instruments and Methods in Physics Research Section B: Beam Interactions with Materials and Atoms*. 2011;269(20):2383-2388. doi:10.1016/j.nimb.2011.02.059

26. Tariq LR, Jafaar AM. A Review of Nanotechnology in Self-Healing of Ancient and Heritage Buildings.

27. Verhoeven JD, Zowada T. Comparison of Two Swords of Antiquity: The Japanese Sword and the Muslim Crucible Damascus Sword. *Metallogr Microstruct Anal*. 2023;12(6):934-943. doi:10.1007/s13632-023-01018-1

28. Bayda S, Adeel M, Tuccinardi T, Cordani M, Rizzolio F. The History of Nanoscience and Nanotechnology: From Chemical–Physical Applications to Nanomedicine. *Molecules*. 2019;25(1):112. doi:10.3390/molecules25010112

29. Adhikari R. Ayurvedic Bhasmas: Overview on Nanomaterialistic Aspects, Applications, and Perspectives. In: Adhikari R, Thapa S, eds. *Infectious Diseases and Nanomedicine I*. Vol 807. Advances in Experimental Medicine and Biology. Springer India; 2014:23-32. doi:10.1007/978-81-322-1777-0_3

30. Loveshikha, Kapil P, Gehlot A, Sharma OP. A Comprehensive Review on Sameer Pannaga Rasa: An Ayurvedic Formulation. *IRJAY*. 2022;05(03):49-55. doi:10.47223/IRJAY.2022.5306

31. Meena R, Vardhan P, Pamnani GC. Netra Putpaka Kriya Kalpa: An Ayurvedic Perspective on Ocular Treatment. *irjay*. 2024;7(2):41-44. doi:10.48165/IRJAY.2024.70208

32. Jayadevan A, Ravi R Chavan. Pharmaceutico-Analytical Study of Agnikumara Rasa - A Kupipakwa Kalpana. *J Ayurveda Integr Med Sci*. 2022;7(7):73-79. doi:10.21760/jaims.7.7.10

33. X. The Bakerian Lecture. —Experimental relations of gold (and other metals) to light. *Phil Trans R Soc*. 1857;147:145-181. doi:10.1098/rstl.1857.0011

34. Mie G. Beiträge zur Optik trüber Medien, speziell kolloidaler Metallösungen. *Annalen der Physik*. 1908;330(3):377-445. doi:10.1002/andp.19083300302

35. Muhammud AM, Gupta NK. Nanostructured $SiO_2$ material: synthesis advances and applications in rubber reinforcement. *RSC Adv*. 2022;12(29):18524-18546. doi:10.1039/D2RA02747J

36. Ruska E. The development of the electron microscope and of electron microscopy. *Rev Mod Phys*. 1987;59(3):627-638. doi:10.1103/RevModPhys.59.627

37. Syed J. Scanning Electron Microscopy in Oral Research. *J Pak Dent Assoc*. 2018;26(4):189-195. doi:10.25301/JPDA.264.189

38. Liu J (Jimmy). Advances and Applications of Atomic-Resolution Scanning Transmission Electron Microscopy. *Microsc Microanal*. 2021;27(5):943-995. doi:10.1017/S1431927621012125

39. Feynman R. There's Plenty of Room at the Bottom. In: *Feynman And Computation*. CRC Press; 2002.

40. TANIGUCHI N. On the Basic Concept of "Nano-Technology." *Proc Intl Conf Prod Eng Tokyo, Part II, 1974*. Published online 1974. Accessed August 1, 2025. https://cir.nii.ac.jp/crid/1572261550373135488

41. Taniguchi N. Current Status in, and Future Trends of, Ultraprecision Machining and Ultrafine Materials Processing. *CIRP Annals*. 1983;32(2):573-582. doi:10.1016/S0007-8506(07)60185-1

42. Drexler KE. Molecular engineering: An approach to the development of general capabilities for molecular manipulation. *Proc Natl Acad Sci USA*. 1981;78(9):5275-5278. doi:10.1073/pnas.78.9.5275

43. Drexler KE. Nanotechnology: From Feynman to Funding. *Bulletin of Science, Technology & Society*. 2004;24(1):21-27. doi:10.1177/0270467604263113

44. Binnig G, Rohrer H, Gerber Ch, Weibel E. Surface Studies by Scanning Tunneling Microscopy. *Phys Rev Lett*. 1982;49(1):57-61. doi:10.1103/PhysRevLett.49.57

45. Binnig G, Quate CF, Gerber Ch. Atomic Force Microscope. *Phys Rev Lett*. 1986;56(9):930-933. doi:10.1103/PhysRevLett.56.930

46. Kroto HW, Heath JR, O'Brien SC, Curl RF, Smalley RE. C60: Buckminsterfullerene. *Nature*. 1985;318(6042):162-163. doi:10.1038/318162a0

47. Pinkard A, Champsaur AM, Roy X. Molecular Clusters: Nanoscale Building Blocks for Solid-State Materials. *Acc Chem Res*. 2018;51(4):919-929. doi:10.1021/acs.accounts.8b00016

48. Iijima S. Helical microtubules of graphitic carbon. *Nature*. 1991;354(6348):56-58. doi:10.1038/354056a0

49. Reibold M, Paufler P, Levin AA, Kochmann W, Pätzke N, Meyer DC. Carbon nanotubes in an ancient Damascus sabre. *Nature*. 2006;444(7117):286-286. doi:10.1038/444286a

50. Crewe AV, Wall J, Welter LM. A High-Resolution Scanning Transmission Electron Microscope. *Journal of Applied Physics*. 1968;39(13):5861-5868. doi:10.1063/1.1656079

51. Huang Z, Chen H, Yan L, Roco MC. Longitudinal Nanotechnology Development (1991--2002): National Science Foundation Funding and its Impact on Patents. *J Nanopart Res*. 2005;7(4-5):343-376. doi:10.1007/s11051-005-5468-3

52. Chen H, Roco MC, Son J, Jiang S, Larson CA, Gao Q. Global nanotechnology development from 1991 to 2012: patents, scientific publications, and effect of NSF funding. *J Nanopart Res*. 2013;15(9):1951. doi:10.1007/s11051-013-1951-4

53. Nizam NUM, Hanafiah MM, Woon KS. A Content Review of Life Cycle Assessment of Nanomaterials: Current Practices, Challenges, and Future Prospects. *Nanomaterials*. 2021;11(12):3324. doi:10.3390/nano11123324

54. Foulkes R, Man E, Thind J, Yeung S, Joy A, Hoskins C. The regulation of nanomaterials and nanomedicines for clinical application: current and future perspectives. *Biomater Sci*. 2020;8(17):4653-4664. doi:10.1039/D0BM00558D

55. Piret J, Boivin G. Pandemics Throughout History. *Front Microbiol*. 2021;11:631736. doi:10.3389/fmicb.2020.631736

56. Mohamed NA, Zupin L, Mazi SI, Al-Khatib HA, Crovella S. Nanomedicine as a Potential Tool against Monkeypox. *Vaccines*. 2023;11(2):428. doi:10.3390/vaccines11020428

57. Schoenmaker L, Witzigmann D, Kulkarni JA, Verbeke R, Kersten G, Jiskoot W, Crommelin DJA. mRNA-lipid nanoparticle COVID-19 vaccines: Structure and stability. *International Journal of Pharmaceutics*. 2021;601:120586. doi:10.1016/j.ijpharm.2021.120586

58. Singh V, Yadav P, Mishra V. Recent Advances on Classification, Properties, Synthesis, and Characterization of Nanomaterials. In: Srivastava N, Srivastava M, Mishra PK, Gupta VK, eds. *Green Synthesis of Nanomaterials for Bioenergy Applications*. 1st ed. Wiley; 2020:83-97. doi:10.1002/9781119576785.ch3

59. Jeevanandam J, Barhoum A, Chan YS, Dufresne A, Danquah MK. Review on nanoparticles and nanostructured materials: history, sources, toxicity and regulations. *Beilstein J Nanotechnol*. 2018;9:1050-1074. doi:10.3762/bjnano.9.98

60. Almuhammady AK, Salem KFM, Alloosh MT, Saleh MM, Alnaddaf LM, Al-Khayri JM. Nanomaterials Fundamentals: Classification, Synthesis and Characterization. In: Al-Khayri JM, Ansari MI, Singh AK, eds. *Nanobiotechnology*. Springer International Publishing; 2021:77-99. doi:10.1007/978-3-030-73606-4_4

61. Goswami P, He K, Li J, Pan Y, Roberts AP, Lin W. Magnetotactic bacteria and magnetofossils: ecology, evolution and environmental implications. *npj Biofilms Microbiomes*. 2022;8(1):43. doi:10.1038/s41522-022-00304-0

62. Llopis Monferrer N, Leynaert A, Tréguer P, Gutiérrez-Rodríguez A, Moriceau B, Gallinari M, Latasa M, L'Helguen S, Maguer J, Safi K, Pinkerton MH, Not F. Role of small Rhizaria and diatoms in the pelagic silica production of the Southern Ocean. *Limnology & Oceanography*. 2021;66(6):2187-2202. doi:10.1002/lno.11743

63. Mitroo D, Wu J, Colletti PF, Lee SS, Walker MJ, Brune WH, Williams BJ, Fortner JD. Atmospheric Reactivity of Fullerene ($C_{60}$ ) Aerosols. *ACS Earth Space Chem*. 2018;2(2):95-102. doi:10.1021/acsearthspacechem.7b00116

64. Wang Y. Nanogeochemistry: Nanostructures, emergent properties and their control on geochemical reactions and mass transfers. *Chemical Geology*. 2014;378-379:1-23. doi:10.1016/j.chemgeo.2014.04.007

65. Yaghobee S, Bayani M, Samiei N, Jahedmanesh N. What are the nanobacteria? *Biotechnology & Biotechnological Equipment*. 2015;29(5):826-833. doi:10.1080/13102818.2015.1052761

66. Schmiedl G, Milker Y, Mackensen A. Climate forcing of regional deep-sea biodiversity documented by benthic foraminifera. *Earth-Science Reviews*. 2023;244:104540. doi:10.1016/j.earscirev.2023.104540

67. Calvo-Olvera A, De Donato-Capote M, Pool H, Rojas-Avelizapa NG. In vitro toxicity assessment of fungal-synthesized cadmium sulfide quantum dots using bacteria and seed germination models. *Journal of Environmental Science and Health, Part A*. 2021;56(6):713-722. doi:10.1080/10934529.2021.1899718

68. Mika F, Matějková-Plšková J, Jiwajinda S, Dechkrong P, Shiojiri M. Photonic Crystal Structure and Coloration of Wing Scales of Butterflies Exhibiting Selective Wavelength Iridescence. *Materials*. 2012;5(5):754-771. doi:10.3390/ma5050754

69. Seago AE, Oberprieler R, Saranathan VK. Evolution of Insect Iridescence: Origins of Three-Dimensional Photonic Crystals in Weevils (Coleoptera: Curculionoidea). *Integrative and Comparative Biology*. 2019;59(6):1664-1672. doi:10.1093/icb/icz040

70. Vukusic P, Sambles JR. Photonic structures in biology. *Nature*. 2003;424(6950):852-855. doi:10.1038/nature01941

71. Das S, Shanmugam N, Kumar A, Jose S. Review: Potential of biomimicry in the field of textile technology. *Bioinspired, Biomimetic and Nanobiomaterials*. 2017;6(4):224-235. doi:10.1680/jbibn.16.00048

72. Wilts BD, Saranathan V. A Literal Elytral Rainbow: Tunable Structural Colors Using Single Diamond Biophotonic Crystals in *Pachyrrhynchus congestus* Weevils. *Small*. 2018;14(46):1802328. doi:10.1002/smll.201802328

73. Salvadores Farran N, Wang L, Pirih P, Wilts BD. Orientation-dependent photonic bandgaps in gold-dust weevil scales and their titania bioreplicates. *Beilstein J Nanotechnol*. 2025;16:1-10. doi:10.3762/bjnano.16.1

74. Albalawi F, Hussein MZ, Fakurazi S, Masarudin MJ. Engineered Nanomaterials: The Challenges and Opportunities for Nanomedicines. *IJN*. 2021;Volume 16:161-184. doi:10.2147/IJN.S288236

75. Garner KL, Suh S, Keller AA. Assessing the Risk of Engineered Nanomaterials in the Environment: Development and Application of the nanoFate Model. *Environ Sci Technol*. 2017;51(10):5541-5551. doi:10.1021/acs.est.6b05279

76. Zhao J, Lin M, Wang Z, Cao X, Xing B. Engineered nanomaterials in the environment: Are they safe? *Critical Reviews in Environmental Science and Technology*. 2021;51(14):1443-1478. doi:10.1080/10643389.2020.1764279

77. Senchukova M. A Brief Review about the Role of Nanomaterials, Mineral-Organic Nanoparticles, and Extra-Bone Calcification in Promoting Carcinogenesis and Tumor Progression. *Biomedicines*. 2019;7(3):65. doi:10.3390/biomedicines7030065

78. Zan G, Wu Q. Biomimetic and Bioinspired Synthesis of Nanomaterials/Nanostructures. *Advanced Materials*. 2016;28(11):2099-2147. doi:10.1002/adma.201503215

79. Li W, Chen Y, Jiao Z. Efficient Anti-Fog and Anti-Reflection Functions of the Bio-Inspired, Hierarchically-Architectured Surfaces of Multiscale Columnar Structures. *Nanomaterials*. 2023;13(9):1570. doi:10.3390/nano13091570

80. Li HY, Feng JK, Xiang L, Huang J, Xie B. Facile synthesis of bio-inspired anemone-like VS4 nanomaterials for long-life supercapacitors with high energy density. *Journal of Power Sources*. 2020;457:228031. doi:10.1016/j.jpowsour.2020.228031

81. Liu W, Zou M, Qin S, Cheng Y, Ma Y, Sun Y, Zhang X. Recent Advances of Cell Membrane-Coated Nanomaterials for Biomedical Applications. *Adv Funct Materials*. 2020;30(39):2003559. doi:10.1002/adfm.202003559

82. Li J, Guo Z, Liu W. Biomimetic Superhydrophobic Materials Construct from Binary Structure: A Review on Design, Properties, and Applications. *Adv Materials Inter*. 2023;10(2):2201847. doi:10.1002/admi.202201847

83. Guo Z, Liu W. Biomimic from the superhydrophobic plant leaves in nature: Binary structure and unitary structure. *Plant Science*. 2007;172(6):1103-1112. doi:10.1016/j.plantsci.2007.03.005

84. Baalousha M, Yang Y, Vance ME, Colman BP, McNeal S, Xu J, Blaszczak J, Steele M, Bernhardt E, Hochella MF. Outdoor urban nanomaterials: The emergence of a new, integrated, and critical field of study. *Science of The Total Environment*. 2016;557-558:740-753. doi:10.1016/j.scitotenv.2016.03.132

85. Kumar P, Pirjola L, Ketzel M, Harrison RM. Nanoparticle emissions from 11 non-vehicle exhaust sources – A review. *Atmospheric Environment*. 2013;67:252-277. doi:10.1016/j.atmosenv.2012.11.011

86. Gleiter H. Nanostructured materials: basic concepts and microstructure. *Acta Materialia*. 2000;48(1):1-29. doi:10.1016/S1359-6454(99)00285-2

87. Pokropivny VV, Skorokhod VV. Classification of nanostructures by dimensionality and concept of surface forms engineering in nanomaterial science. *Materials Science and Engineering: C*. 2007;27(5-8):990-993. doi:10.1016/j.msec.2006.09.023

88. Zhu S, Song Y, Wang J, Wan H, Zhang Y, Ning Y, Yang B. Photoluminescence mechanism in graphene quantum dots: Quantum confinement effect and surface/edge state. *Nano Today*. 2017;13:10-14. doi:10.1016/j.nantod.2016.12.006

89. Edvinsson T. Optical quantum confinement and photocatalytic properties in two-, one- and zero-dimensional nanostructures. *R Soc open sci*. 2018;5(9):180387. doi:10.1098/rsos.180387

90. Ha H, Amicucci C, Matteini P, Hwang B. Mini review of synthesis strategies of silver nanowires and their applications. *Colloid and Interface Science Communications*. 2022;50:100663. doi:10.1016/j.colcom.2022.100663

91. Jain K, Mehandzhiyski AY, Zozoulenko I, Wågberg L. PEDOT:PSS nano-particles in aqueous media: A comparative experimental and molecular dynamics study of particle size, morphology and z-potential. *Journal of Colloid and Interface Science*. 2021;584:57-66. doi:10.1016/j.jcis.2020.09.070

92. Gong S, Cheng W. One-Dimensional Nanomaterials for Soft Electronics. *Adv Elect Materials*. 2017;3(3):1600314. doi:10.1002/aelm.201600314

93. Shi B, Lu S, Yang H, Mahmood S, Sun C, Malek NANN, Kamaruddin WHA, Saidin S, Zhang C. One-dimensional nanomaterials for nerve tissue engineering to repair spinal cord injury. *BMEMat*. 2025;3(1):e12111. doi:10.1002/bmm2.12111

94. Ge Y, Shi Z, Tan C, Chen Y, Cheng H, He Q, Zhang H. Two-Dimensional Nanomaterials with Unconventional Phases. *Chem*. 2020;6(6):1237-1253. doi:10.1016/j.chempr.2020.04.004

95. Ee HS, Kang JH, Brongersma ML, Seo MK. Shape-Dependent Light Scattering Properties of Subwavelength Silicon Nanoblocks. *Nano Lett*. 2015;15(3):1759-1765. doi:10.1021/nl504442v

96. Wang X, Ahmad M, Sun H. Three-Dimensional ZnO Hierarchical Nanostructures: Solution Phase Synthesis and Applications. *Materials*. 2017;10(11):1304. doi:10.3390/ma10111304

97. Yun Q, Lu Q, Zhang X, Tan C, Zhang H. Three-Dimensional Architectures Constructed from Transition-Metal Dichalcogenide Nanomaterials for Electrochemical Energy Storage and Conversion. *Angew Chem Int Ed*. 2018;57(3):626-646. doi:10.1002/anie.201706426

98. Guo Z, Chen Y, Wang Y, Jiang H, Wang X. Advances and challenges in metallic nanomaterial synthesis and antibacterial applications. *J Mater Chem B*. 2020;8(22):4764-4777. doi:10.1039/D0TB00099J

99. Nizami MZI, Xu VW, Yin IX, Lung CYK, Niu JY, Chu CH. Ceramic Nanomaterials in Caries Prevention: A Narrative Review. *Nanomaterials*. 2022;12(24):4416. doi:10.3390/nano12244416

100. Fujioka-Kobayashi M, Tsuru K, Nagai H, Fujisawa K, Kudoh T, Ohe G, Ishikawa K, Miyamoto Y. Fabrication and evaluation of carbonate apatite-coated calcium carbonate bone substitutes for bone tissue engineering. *J Tissue Eng Regen Med*. Published online August 29, 2018. doi:10.1002/term.2742

101. Chen BM, Cheng TL, Roffler SR. Polyethylene Glycol Immunogenicity: Theoretical, Clinical, and Practical Aspects of Anti-Polyethylene Glycol Antibodies. *ACS Nano*. 2021;15(9):14022-14048. doi:10.1021/acsnano.1c05922

102. Perumal S, Atchudan R, Lee W. A Review of Polymeric Micelles and Their Applications. *Polymers*. 2022;14(12):2510. doi:10.3390/polym14122510

103. Kaur J, Mishra V, Singh SK, Gulati M, Kapoor B, Chellappan DK, Gupta G, Dureja H, Anand K, Dua K, Khatik GL, Gowthamarajan K. Harnessing amphiphilic polymeric micelles for diagnostic and therapeutic applications: Breakthroughs and bottlenecks. *Journal of Controlled Release*. 2021;334:64-95. doi:10.1016/j.jconrel.2021.04.014

104. Zhang X, Hou Y, Zhang F, Luo G. Protein Extraction from Grape Seeds by Reverse Micelles: Optimization of the Forward Extraction. *OALib*. 2017;04(06):1-12. doi:10.4236/oalib.1103376

105. Arabestani MR, Bigham A, Kamarehei F, Dini M, Gorjikhah F, Shariati A, Hosseini SM. Solid lipid nanoparticles and their application in the treatment of bacterial infectious diseases. *Biomedicine & Pharmacotherapy*. 2024;174:116433. doi:10.1016/j.biopha.2024.116433

106. Kondel R, Shafiq N, Kaur IP, Singh MP, Pandey AK, Ratho RK, Malhotra S. Effect of Acyclovir Solid Lipid Nanoparticles for the Treatment of Herpes Simplex Virus (HSV)

Infection in an Animal Model of HSV-1 Infection. *PNT*. 2019;7(5):389-403. doi:10.2174/2211738507666190829161737

107. Lesiak B, Kövér L, Tóth J, Zemek J, Jiricek P, Kromka A, Rangam N. C sp2/sp3 hybridisations in carbon nanomaterials – XPS and (X)AES study. *Applied Surface Science*. 2018;452:223-231. doi:10.1016/j.apsusc.2018.04.269

108. Marsden BJ, Jones AN, Hall GN, Treifi M, Mummery PM. Graphite as a core material for Generation IV nuclear reactors. In: *Structural Materials for Generation IV Nuclear Reactors*. Elsevier; 2017:495-532. doi:10.1016/B978-0-08-100906-2.00014-8

109. Reyes-Gasga J, Elechiguerra JL, Liu C, Camacho-Bragado A, Montejano-Carrizales JM, Jose Yacaman M. On the structure of nanorods and nanowires with pentagonal cross-sections. *Journal of Crystal Growth*. 2006;286(1):162-172. doi:10.1016/j.jcrysgro.2005.09.028

110. Kumar SK, Krishnamoorti R. Nanocomposites: Structure, Phase Behavior, and Properties. *Annu Rev Chem Biomol Eng*. 2010;1(1):37-58. doi:10.1146/annurev-chembioeng-073009-100856

111. Anastasiadis SH, Chrissopoulou K, Stratakis E, Kavatzikidou P, Kaklamani G, Ranella A. How the Physicochemical Properties of Manufactured Nanomaterials Affect Their Performance in Dispersion and Their Applications in Biomedicine: A Review. *Nanomaterials*. 2022;12(3):552. doi:10.3390/nano12030552

112. Xu M, Li J, Iwai H, Mei Q, Fujita D, Su H, Chen H, Hanagata N. Formation of Nano-Bio-Complex as Nanomaterials Dispersed in a Biological Solution for Understanding Nanobiological Interactions. *Sci Rep*. 2012;2(1):406. doi:10.1038/srep00406

113. Murdock RC, Braydich-Stolle L, Schrand AM, Schlager JJ, Hussain SM. Characterization of Nanomaterial Dispersion in Solution Prior to In Vitro Exposure Using Dynamic Light Scattering Technique. *Toxicological Sciences*. 2008;101(2):239-253. doi:10.1093/toxsci/kfm240

114. Kosmulski M, Mączka E. Zeta potential in dispersions of titania nanoparticles in moderately polar solvents stabilized with anionic surfactants. *Journal of Molecular Liquids*. 2022;355:118972. doi:10.1016/j.molliq.2022.118972

115. Jose A, Mathew T, Fernández-Navas N, Querebillo CJ. Porous Inorganic Nanomaterials: Their Evolution towards Hierarchical Porous Nanostructures. *Micro*. 2024;4(2):229-280. doi:10.3390/micro4020016

116. Wu Y, Ge P, Xu W, Li M, Kang Q, Zhang X, Xie J. Cancer-targeted and intracellular delivery of Bcl-2-converting peptide with functional macroporous silica nanoparticles for biosafe treatment. *Materials Science and Engineering: C*. 2020;108:110386. doi:10.1016/j.msec.2019.110386

117. Li SR, Huo FY, Wang HQ, Wang J, Xu C, Liu B, Bu LL. Recent advances in porous nanomaterials-based drug delivery systems for cancer immunotherapy. *J Nanobiotechnol*. 2022;20(1):277. doi:10.1186/s12951-022-01489-4

118. Al-Shehri BM, Khder AERS, Ashour SS, Hamdy MS. A review: the utilization of mesoporous materials in wastewater treatment. *Mater Res Express*. 2019;6(12):122002. doi:10.1088/2053-1591/ab52af

119. Schlumberger C, Thommes M. Characterization of Hierarchically Ordered Porous Materials by Physisorption and Mercury Porosimetry—A Tutorial Review. *Adv Materials Inter*. 2021;8(4):2002181. doi:10.1002/admi.202002181

120. Biswas P, Polash SA, Dey D, Kaium MdA, Mahmud AR, Yasmin F, Baral SK, Islam MdA, Rahaman TI, Abdullah A, Ema TI, Khan DA, Bibi S, Chopra H, Kamel M, Najda A, Fouda MMA, Rehan UM, Mheidat M, Alsaidalani R, Abdel-Daim MM, Hasan MdN. Advanced implications of nanotechnology in disease control and environmental perspectives. *Biomedicine & Pharmacotherapy*. 2023;158:114172. doi:10.1016/j.biopha.2022.114172

121. Moreno-Horn M, Gebel T. Granular biodurable nanomaterials: No convincing evidence for systemic toxicity. *Critical Reviews in Toxicology*. 2014;44(10):849-875. doi:10.3109/10408444.2014.938802

122. Donaldson K, Stone V, Tran CL, Kreyling W, Borm PJA. Nanotoxicology. *Occup Environ Med*. 2004;61(9):727.1-728. doi:10.1136/oem.2004.013243

123. McCunney RJ, Yong M. Coal Miners and Lung Cancer: Can Mortality Studies Offer a Perspective on Rat Inhalation Studies of Poorly Soluble Low Toxicity Particles? *Front Public Health*. 2022;10:907157. doi:10.3389/fpubh.2022.907157

124. Roller M, Pott F. Lung Tumor Risk Estimates from Rat Studies with Not Specifically Toxic Granular Dusts. *Annals of the New York Academy of Sciences*. 2006;1076(1):266-280. doi:10.1196/annals.1371.064

125. Pleus RC, Murashov V, eds. *Physicochemical Properties of Nanomaterials*. Pan Stanford Publishing; 2018.

126. Kumar A, Dhawan A. Genotoxic and carcinogenic potential of engineered nanoparticles: an update. *Arch Toxicol*. 2013;87(11):1883-1900. doi:10.1007/s00204-013-1128-z

127. An H, Liu Q, Ji Q, Jin B. DNA binding and aggregation by carbon nanoparticles. *Biochemical and Biophysical Research Communications*. 2010;393(4):571-576. doi:10.1016/j.bbrc.2010.02.006

128. Kamat JP, Devasagayam TPA, Priyadarsini KI, Mohan H, Mittal JP. Oxidative damage induced by the fullerene C60 on photosensitization in rat liver microsomes. *Chemico-Biological Interactions*. 1998;114(3):145-159. doi:10.1016/S0009-2797(98)00047-7

129. Liu Q, Xu C, Ji G, Liu H, Mo Y, Tollerud DJ, Gu A, Zhang Q. Sublethal effects of zinc oxide nanoparticles on male reproductive cells. *Toxicology in Vitro*. 2016;35:131-138. doi:10.1016/j.tiv.2016.05.017

130. Adebayo OA, Akinloye O, Adaramoye OA. Cerium oxide nanoparticle elicits oxidative stress, endocrine imbalance and lowers sperm characteristics in testes of balb/c mice. *Andrologia*. 2018;50(3):e12920. doi:10.1111/and.12920

131. Tarannum N, Divya D, Gautam YK. Facile green synthesis and applications of silver nanoparticles: a state-of-the-art review. *RSC Adv*. 2019;9(60):34926-34948. doi:10.1039/C9RA04164H

132. Barillo DJ, Marx DE. Silver in medicine: A brief history BC 335 to present. *Burns*. 2014;40:S3-S8. doi:10.1016/j.burns.2014.09.009

133. Wood CM. Silver. In: *Fish Physiology*. Vol 31. Elsevier; 2011:1-65. doi:10.1016/S1546-5098(11)31023-0

134. López-Álvarez IA, Reyes-Domínguez IA, Vilasó-Cadre JE, Flores-Carlos LF, Ramírez-Rodríguez A, Cruz R, Juárez-Tapia JC. Silver froth flotation using xanthogen formate-type collectors for the valorization of a hydrometallurgical waste. *MRS Advances*. 2024;9(22):1728-1735. doi:10.1557/s43580-024-01002-z

135. Industrial Demand for Silver Reaches Record Levels - Google Scholar. Accessed August 4, 2025. https://scholar.google.com/scholar?hl=en&as_sdt=2005&sciodt=0%2C5&cites=12909645474155164435&scipsc=&q=Industrial+Demand+for+Silver+Reaches+Record+Levels&btnG=

136. World Silver Survey 2025. https://silverinstitute.org/. Accessed August 4, 2025. https://silverinstitute.org/world-silver-survey-2025/

137. Raman S, Arunagirinathan RS. Silver Nanowires in Stretchable Resistive Strain Sensors. *Nanomaterials*. 2022;12(11):1932. doi:10.3390/nano12111932

138. Ilawe NV, Oviedo MB, Wong BM. Effect of quantum tunneling on the efficiency of excitation energy transfer in plasmonic nanoparticle chain waveguides. *J Mater Chem C*. 2018;6(22):5857-5864. doi:10.1039/C8TC01466C

139. Noguez C. Surface Plasmons on Metal Nanoparticles: The Influence of Shape and Physical Environment. *J Phys Chem C*. 2007;111(10):3806-3819. doi:10.1021/jp066539m

140. Shipunova VO, Belova MM, Kotelnikova PA, Shilova ON, Mirkasymov AB, Danilova NV, Komedchikova EN, Popovtzer R, Deyev SM, Nikitin MP. Photothermal Therapy with HER2-Targeted Silver Nanoparticles Leading to Cancer Remission. *Pharmaceutics*. 2022;14(5):1013. doi:10.3390/pharmaceutics14051013

141. Zhao LJ, Yu RJ, Ma W, Han HX, Tian H, Qian RC, Long YT. Sensitive detection of protein biomarkers using silver nanoparticles enhanced immunofluorescence assay. *Theranostics*. 2017;7(4):876-883. doi:10.7150/thno.17575

142. Hassan A, Ali S, Bae J, Lee CH. All printed antenna based on silver nanoparticles for 1.8 GHz applications. *Appl Phys A*. 2016;122(8):768. doi:10.1007/s00339-016-0286-2

143. Hazra Chowdhury A, Debnath R, Manirul Islam Sk, Saha T. Impact of Nanoparticle Shape, Size, and Properties of Silver Nanocomposites and Their Applications. In: Inamuddin, Thomas S, Kumar Mishra R, Asiri AM, eds. *Sustainable Polymer Composites and Nanocomposites*. Springer International Publishing; 2019:1067-1091. doi:10.1007/978-3-030-05399-4_37

144. Hedberg J, Lundin M, Lowe T, Blomberg E, Wold S, Wallinder IO. Interactions between surfactants and silver nanoparticles of varying charge. *Journal of Colloid and Interface Science*. 2012;369(1):193-201. doi:10.1016/j.jcis.2011.12.004

145. Skoglund S, Lowe TA, Hedberg J, Blomberg E, Wallinder IO, Wold S, Lundin M. Effect of Laundry Surfactants on Surface Charge and Colloidal Stability of Silver Nanoparticles. *Langmuir*. 2013;29(28):8882-8891. doi:10.1021/la4012873

146. Qiao Z, Yao Y, Song S, Yin M, Luo J. Silver nanoparticles with pH induced surface charge switchable properties for antibacterial and antibiofilm applications. *J Mater Chem B*. 2019;7(5):830-840. doi:10.1039/C8TB02917B

147. Abbaszadegan A, Ghahramani Y, Gholami A, Hemmateenejad B, Dorostkar S, Nabavizadeh M, Sharghi H. The Effect of Charge at the Surface of Silver Nanoparticles on Antimicrobial Activity against Gram-Positive and Gram-Negative Bacteria: A Preliminary Study. Hazan R, ed. *Journal of Nanomaterials*. 2015;2015(1):720654. doi:10.1155/2015/720654

148. Silva T, Pokhrel LR, Dubey B, Tolaymat TM, Maier KJ, Liu X. Particle size, surface charge and concentration dependent ecotoxicity of three organo-coated silver nanoparticles: Comparison between general linear model-predicted and observed toxicity. *Science of The Total Environment*. 2014;468-469:968-976. doi:10.1016/j.scitotenv.2013.09.006

149. Zhang J, Xiang Q, Shen L, Ling J, Zhou C, Hu J, Chen L. Surface charge-dependent bioaccumulation dynamics of silver nanoparticles in freshwater algae. *Chemosphere*. 2020;247:125936. doi:10.1016/j.chemosphere.2020.125936

150. Duman H, Eker F, Akdaşçi E, Witkowska AM, Bechelany M, Karav S. Silver Nanoparticles: A Comprehensive Review of Synthesis Methods and Chemical and Physical Properties. *Nanomaterials*. 2024;14(18):1527. doi:10.3390/nano14181527

151. Zhang H, Zou G, Liu L, Li Y, Tong H, Sun Z, Zhou YN. A comparative study of silver nanoparticles synthesized by arc discharge and femtosecond laser ablation in aqueous solution. *Appl Phys A*. 2016;122(10):896. doi:10.1007/s00339-016-0424-x

152. Smetana AB, Klabunde KJ, Sorensen CM. Synthesis of spherical silver nanoparticles by digestive ripening, stabilization with various agents, and their 3-D and 2-D superlattice formation. *Journal of Colloid and Interface Science*. 2005;284(2):521-526. doi:10.1016/j.jcis.2004.10.038

153. Abbasi E, Milani M, Fekri Aval S, Kouhi M, Akbarzadeh A, Tayefi Nasrabadi H, Nikasa P, Joo SW, Hanifehpour Y, Nejati-Koshki K, Samiei M. Silver nanoparticles: Synthesis methods, bio-applications and properties. *Critical Reviews in Microbiology*. Published online June 17, 2014:1-8. doi:10.3109/1040841X.2014.912200

154. Werner D, Hashimoto S, Tomita T, Matsuo S, Makita Y. Examination of Silver Nanoparticle Fabrication by Pulsed-Laser Ablation of Flakes in Primary Alcohols. *J Phys Chem C*. 2008;112(5):1321-1329. doi:10.1021/jp075401g

155. Naser H, Alghoul MA, Hossain MK, Asim N, Abdullah MF, Ali MS, Alzubi FG, Amin N. The role of laser ablation technique parameters in synthesis of nanoparticles from different target types. *J Nanopart Res*. 2019;21(11):249. doi:10.1007/s11051-019-4690-3

156. Kibis LS, Stadnichenko AI, Pajetnov EM, Koscheev SV, Zaykovskii VI, Boronin AI. The investigation of oxidized silver nanoparticles prepared by thermal evaporation and radio-frequency sputtering of metallic silver under oxygen. *Applied Surface Science*. 2010;257(2):404-413. doi:10.1016/j.apsusc.2010.07.002

157. Pryshchepa O, Pomastowski P, Buszewski B. Silver nanoparticles: Synthesis, investigation techniques, and properties. *Advances in Colloid and Interface Science*. 2020;284:102246. doi:10.1016/j.cis.2020.102246

158. Meher A, Tandi A, Moharana S, Chakroborty S, Mohapatra SS, Mondal A, Dey S, Chandra P. Silver nanoparticle for biomedical applications: A review. *Hybrid Advances*. 2024;6:100184. doi:10.1016/j.hybadv.2024.100184

159. Pastoriza-Santos I, Liz-Marzán LM. Reduction of silver nanoparticles in DMF. Formation of monolayers and stable colloids. *Pure and Applied Chemistry*. Published online 2000.

160. Suriati G, Mariatti M, Azizan A. Synthesis of Silver Nanoparticles by Chemical Reduction Method: Effect of Reducing Agent and Surfactant Concentration. *Int J Automot Mech Eng*. 2022;10:1920-1927. doi:10.15282/ijame.10.2014.9.0160

161. Restrepo CV, Villa CC. Synthesis of silver nanoparticles, influence of capping agents, and dependence on size and shape: A review. *Environmental Nanotechnology, Monitoring & Management*. 2021;15:100428. doi:10.1016/j.enmm.2021.100428

162. De Lima R, Seabra AB, Durán N. Silver nanoparticles: a brief review of cytotoxicity and genotoxicity of chemically and biogenically synthesized nanoparticles. *J of Applied Toxicology*. 2012;32(11):867-879. doi:10.1002/jat.2780

163. Vishwanath R, Negi B. Conventional and green methods of synthesis of silver nanoparticles and their antimicrobial properties. *Current Research in Green and Sustainable Chemistry*. 2021;4:100205. doi:10.1016/j.crgsc.2021.100205

164. Husain S, Nandi A, Simnani FZ, Saha U, Ghosh A, Sinha A, Sahay A, Samal SK, Panda PK, Verma SK. Emerging Trends in Advanced Translational Applications of Silver Nanoparticles: A Progressing Dawn of Nanotechnology. *JFB*. 2023;14(1):47. doi:10.3390/jfb14010047

165. Alfryyan N, Kordy MGM, Abdel-Gabbar M, Soliman HA, Shaban M. Characterization of the biosynthesized intracellular and extracellular plasmonic silver nanoparticles using Bacillus cereus and their catalytic reduction of methylene blue. *Sci Rep*. 2022;12(1):12495. doi:10.1038/s41598-022-16029-1

166. Slawson RobinM, Trevors JackT, Lee H. Silver accumulation and resistance in Pseudomonas stutzeri. *Arch Microbiol*. 1992;158(6). doi:10.1007/BF00276299

167. Otari SV, Patil RM, Ghosh SJ, Thorat ND, Pawar SH. Intracellular synthesis of silver nanoparticle by actinobacteria and its antimicrobial activity. *Spectrochimica Acta Part A: Molecular and Biomolecular Spectroscopy*. 2015;136:1175-1180. doi:10.1016/j.saa.2014.10.003

168. Nie P, Zhao Y, Xu H. Synthesis, applications, toxicity and toxicity mechanisms of silver nanoparticles: A review. *Ecotoxicology and Environmental Safety*. 2023;253:114636. doi:10.1016/j.ecoenv.2023.114636

169. Verbruggen N, Hermans C, Schat H. Molecular mechanisms of metal hyperaccumulation in plants. *New Phytologist*. 2009;181(4):759-776. doi:10.1111/j.1469-8137.2008.02748.x

170. Gardea-Torresdey JL, Gomez E, Peralta-Videa JR, Parsons JG, Troiani H, Jose-Yacaman M. Alfalfa Sprouts: A Natural Source for the Synthesis of Silver Nanoparticles. *Langmuir*. 2003;19(4):1357-1361. doi:10.1021/la020835i

171. Chung IM, Park I, Seung-Hyun K, Thiruvengadam M, Rajakumar G. Plant-Mediated Synthesis of Silver Nanoparticles: Their Characteristic Properties and Therapeutic Applications. *Nanoscale Res Lett*. 2016;11(1):40. doi:10.1186/s11671-016-1257-4

172. Chacón J, Luebert F, Hilger HH, Ovchinnikova S, Selvi F, Cecchi L, Guilliams CM, Hasenstab-Lehman K, Sutorý K, Simpson MG, Weigend M. The borage family (Boraginaceae s.str.): A revised infrafamilial classification based on new phylogenetic evidence, with emphasis on the placement of some enigmatic genera. *TAXON*. 2016;65(3):523-546. doi:10.12705/653.6

173. Riedl H. Boraginaceae. *Flora Malesiana - Series 1, Spermatophyta*. 1997;13(1):43-144.

174. Ovchinnikova S, Tajetdinova D, Tojibaev K. Taxonomic analysis of the family Boraginaceae in the "Flora of Uzbekistan." Chepinoga VV, Ma KP, eds. *BIO Web Conf*. 2021;38:00095. doi:10.1051/bioconf/20213800095

175. Gupta PSP, Vishwakarma K, Soni P, Jadhao AB, Das K, Kumar S, Soni P. Medicinally Important Plants of Boraginaceae Family. Published online 2024.

176. Dresler S, Szymczak G, Wójcik M. Comparison of some secondary metabolite content in the seventeen species of the Boraginaceae family. *Pharmaceutical Biology*. 2017;55(1):691-695. doi:10.1080/13880209.2016.1265986

177. Gautam S, Lapčík L, Lapčíková B. Pharmacological Significance of Boraginaceae with Special Insights into Shikonin and Its Potential in the Food Industry. *Foods*. 2024;13(9):1350. doi:10.3390/foods13091350

178. Mollaei S, Habibi B, Amani Ghadim A, Shakouri M. A green approach for the synthesis of silver nanoparticles using Lithospermum officinale root extract and evaluation of their antioxidant activity. *JPST*. 2017;3(4). doi:10.22104/jpst.2018.2652.1103

179. Nindawat S, Agrawal V. Fabrication of silver nanoparticles using *Arnebia hispidissima* (Lehm.) A. DC. root extract and unravelling their potential biomedical applications. *Artificial Cells, Nanomedicine, and Biotechnology*. 2019;47(1):166-180. doi:10.1080/21691401.2018.1548469

180. Singh H, Du J, Yi TH. Green and rapid synthesis of silver nanoparticles using *Borago officinalis* leaf extract: anticancer and antibacterial activities. *Artificial Cells, Nanomedicine, and Biotechnology*. 2017;45(7):1310-1316. doi:10.1080/21691401.2016.1228663

181. Kumavat SR, Mishra S. Green synthesis of silver nanoparticles using Borago officinalis leaves extract and screening its antimicrobial and antifungal activity. *Int Nano Lett*. 2021;11(4):355-370. doi:10.1007/s40089-021-00345-x

182. Keskin C, Aslan S, Baran MF, Baran A, Eftekhari A, Adıcan MT, Ahmadian E, Arslan S, Mohamed AJ. Green Synthesis and Characterization of Silver Nanoparticles Using Anchusa Officinalis: Antimicrobial and Cytotoxic Potential. *IJN*. 2025;Volume 20:4481-4502. doi:10.2147/IJN.S511217

183. Kathiravan V. Green synthesis of silver nanoparticles using different volumes of Trichodesma indicum leaf extract and their antibacterial and photocatalytic activities. *Res Chem Intermed*. 2018;44(9):4999-5012. doi:10.1007/s11164-018-3405-1

184. Gopinathan M, Balasubramanian M. GREEN SYNTHESIS AND CHARACTERIZATION OF SILVER NANOPARTICLES USING HELIOTROPIUM INDICUM L. LEAVES EXTRACT AND ANTIMICROBIAL ACTIVITY. *JASR*. 2022;13(01):365-373. doi:10.55218/JASR.202213143

185. Hazaa M, Alm-Eldin M, Ibrahim AE, Elbarky N, Salama M, Sayed R, Sayed W. Biosynthesis of Silver Nanoparticles using Borago officinslis leaf extract, characterization and larvicidal activity against cotton leaf worm, Spodoptera littoralis (Bosid). *Int J Trop Insect Sci*. 2021;41(1):145-156. doi:10.1007/s42690-020-00187-8

186. Buhroo AA, Nisa G, Asrafuzzaman S, Prasad R, Rasheed R, Bhattacharyya A. Biogenic silver nanoparticles from Trichodesma indicum aqueous leaf extract against Mythimna separata and evaluation of its larvicidal efficacy. *Journal of Plant Protection Research*. 2017;57(2):194-200. doi:10.1515/jppr-2017-0026

187. Shkryl Y, Rusapetova T, Yugay Y, Egorova A, Silant'ev V, Grigorchuk V, Karabtsov A, Timofeeva Y, Vasyutkina E, Kudinova O, Ivanov V, Kumeiko V, Bulgakov V. Biosynthesis and Cytotoxic Properties of Ag, Au, and Bimetallic Nanoparticles Synthesized Using Lithospermum erythrorhizon Callus Culture Extract. *IJMS*. 2021;22(17):9305. doi:10.3390/ijms22179305

188. Suman B, Eswari B, Divya BJ, Pallavi V, Venkataswamy M, Kemparaj K, Thyagaraju K. Effect of silver nanoparticles synthesized of trichodesma indicum against naja naja (cobra) venom. *IJPSR*. 9(8).

189. Satyavani K, Gurudeeban S, Deepak V, Ramanathan T. Heliotropium curassavicum mediated silver nanoparticles for environmental application. *Res J Chem Environ*. 2013;17:27-33.

190. Kamalanathan J, Venkatesh R, Swetha S, Sampath S, Ahmed MZ, Alqahtani AS, Suresh MS, Asaithambi P. Microwave-assisted green synthesis of silver nanoparticles using *Cynoglossum furcatum* extract: biomedical evaluation against A431 skin cancer cell line. *Materials Technology*. 2024;39(1):2401260. doi:10.1080/10667857.2024.2401260

191. Francis S, Koshy EP, Mathew B. Optical and Catalytic Properties of Silver and Gold Nanoparticles Using Biomedical plant, Rotula aquatica through Microwave Irradiation. 2021;9(3).

192. Singh H, Du J, Singh P, Yi TH. Role of green silver nanoparticles synthesized from Symphytum officinale leaf extract in protection against UVB-induced photoaging. *J Nanostruct Chem*. 2018;8(3):359-368. doi:10.1007/s40097-018-0281-6

193. Bowe LM, Yatskievych G. *Cynoglossum creticum* in the North American Flora. *Lundellia*. 2016;19(1):39-46. doi:10.25224/1097-993X-19.1.39

194. Fan Y, Wang M, Zhang Q, Ouyang S, Mao W, Xu C, Wang M, Long C. Traditional uses, phytochemistry, pharmacology, toxicity and clinical application of traditional Chinese medicine Cynoglossum amabile: a review. *Front Pharmacol*. 2024;15:1325283. doi:10.3389/fphar.2024.1325283

195. Selvi F, Sutorý K. A synopsis of the genus *Cynoglossum* (Boraginaceae-Cynoglosseae) in Italy. *Plant Biosystems - An International Journal Dealing with all Aspects of Plant Biology*. 2012;146(2):461-479. doi:10.1080/11263504.2012.667842

196. Menghini L, Ferrante C, Zengin G, Mahomoodally MF, Leporini L, Locatelli M, Cacciagrano F, Recinella L, Chiavaroli A, Leone S, Brunetti L, Orlando G. Multiple pharmacological approaches on hydroalcoholic extracts from different parts of *Cynoglossum creticum* Mill. (Boraginaceae). *Plant Biosystems - An International Journal Dealing with all Aspects of Plant Biology*. 2019;153(5):633-639. doi:10.1080/11263504.2018.1527790

197. Dallali D, Fakhfakh J, Paris C, Aoiadni N, Philippot S, Risler A, Varbanov M, Allouche N. HPLC-HESI-MS/MS Analysis of Phenolic Compounds from Cynoglossum tubiflorus Leaf Extracts: An Assessment of Their Cytotoxic, Antioxidant, and Antibacterial Properties. *Plants*. 2024;13(6):909. doi:10.3390/plants13060909

198. Runge FF. Ueber einige Produkte der Steinkohlendestillation. *Annalen der Physik*. 1834;107(5):65-78.

199. Endemann H. ON A PHOTOGRAPHIC PROCESS BY MEANS OF ANILINE BLACK. *J Am Chem Soc*. 1886;8(8):189-191. doi:10.1021/ja02129a015

200. Green AG, Woodhead AE. CCXLIII.—Aniline-black and allied compounds. Part I. *J Chem Soc, Trans*. 1910;97(0):2388-2403. doi:10.1039/CT9109702388

201. Brown OW, Frishe WC. Catalytic Oxidation of Aniline in the Vapor Phase. *J Phys Chem*. 1947;51(6):1394-1400. doi:10.1021/j150456a013

202. Macdiarmid AG, Chiang JC, Richter AF, Epstein AJ. Polyaniline: a new concept in conducting polymers. *Synthetic Metals*. 1987;18(1-3):285-290. doi:10.1016/0379-6779(87)90893-9

203. MacDiarmid AG. Polyaniline and polypyrrole: Where are we headed? *Synthetic Metals*. 1997;84(1-3):27-34. doi:10.1016/S0379-6779(97)80658-3

204. Chen X, Yuan CA, Wong CKY, Zhang G. Molecular modeling of the conductivity changes of the emeraldine base polyaniline due to protonic acid doping. In: *2012 13th International Thermal, Mechanical and Multi-Physics Simulation and Experiments in Microelectronics and Microsystems*. IEEE; 2012:1/4-4/4. doi:10.1109/ESimE.2012.6191741

205. Zahid M, Anum R, Siddique S, Shakir HF, Rehan Z. Polyaniline-based nanocomposites for electromagnetic interference shielding applications: A review. *Journal of Thermoplastic Composite Materials*. 2023;36(4):1717-1761. doi:10.1177/08927057211022408

206. Lapkin DA, Korovin AN, Malakhov SN, Emelyanov AV, Demin VA, Erokhin VV. Optical Monitoring of the Resistive States of a Polyaniline-Based Memristive Device. *Adv Elect Materials*. 2020;6(10):2000511. doi:10.1002/aelm.202000511

207. Abu-Thabit NY. Electrically conducting polyaniline smart coatings and thin films for industrial applications. In: *Advances in Smart Coatings and Thin Films for Future Industrial and Biomedical Engineering Applications*. Elsevier; 2020:585-617. doi:10.1016/B978-0-12-849870-5.00026-4

208. Kang Q, Takehara H, Ichiki T. Effect of pH on the properties of protonated polyaniline-based films for pH sensing applications. *J of Applied Polymer Sci*. 2024;141(12):e55110. doi:10.1002/app.55110

209. Chandrakanthi N, Careem MA. Thermal stability of polyaniline. *Polymer Bulletin*. 2000;44(1):101-108. doi:10.1007/s002890050579

210. Jaymand M. Recent progress in chemical modification of polyaniline. *Progress in Polymer Science*. 2013;38(9):1287-1306. doi:10.1016/j.progpolymsci.2013.05.015

211. Kheilnezhad B, Firoozabady AS, Aidun A. An Overview of Polyaniline in Tissue Engineering.

212. Lee T, Kim I, Cheong DY, Roh S, Jung HG, Lee SW, Kim HS, Yoon DS, Hong Y, Lee G. Selective colorimetric urine glucose detection by paper sensor functionalized with polyaniline nanoparticles and cell membrane. *Analytica Chimica Acta*. 2021;1158:338387. doi:10.1016/j.aca.2021.338387

213. Wang J, Zhang D. One-Dimensional Nanostructured Polyaniline: Syntheses, Morphology Controlling, Formation Mechanisms, New Features, and Applications. *Adv Polym Technol*. 2013;32(S1). doi:10.1002/adv.21283

214. Li D, Huang J, Kaner RB. Polyaniline Nanofibers: A Unique Polymer Nanostructure for Versatile Applications. *Acc Chem Res*. 2009;42(1):135-145. doi:10.1021/ar800080n

215. Wang Y, Chu X, Zhu Z, Xiong D, Zhang H, Yang W. Dynamically evolving 2D supramolecular polyaniline nanosheets for long-stability flexible supercapacitors. *Chemical Engineering Journal*. 2021;423:130203. doi:10.1016/j.cej.2021.130203

216. Li Y, Zheng JL, Feng J, Jing XL. Polyaniline micro-/nanostructures: morphology control and formation mechanism exploration. *Chemical Papers*. 2013;67(8). doi:10.2478/s11696-013-0347-3

217. Bhadra S, Khastgir D, Singha NK, Lee JH. Progress in preparation, processing and applications of polyaniline. *Progress in Polymer Science*. 2009;34(8):783-810. doi:10.1016/j.progpolymsci.2009.04.003

218. Xing S, Zhao C, Jing S, Wang Z. Morphology and conductivity of polyaniline nanofibers prepared by 'seeding' polymerization. *Polymer*. 2006;47(7):2305-2313. doi:10.1016/j.polymer.2006.02.008

219. Abdolahi A, Hamzah E, Ibrahim Z, Hashim S. Synthesis of Uniform Polyaniline Nanofibers through Interfacial Polymerization. *Materials*. 2012;5(8):1487-1494. doi:10.3390/ma5081487

220. Kurisu M, Kissner R, Imai M, Walde P. Application of an enzymatic cascade reaction for the synthesis of the emeraldine salt form of polyaniline. *Chem Pap*. 2021;75(10):5071-5085. doi:10.1007/s11696-021-01620-z

221. Stejskal J, Sapurina I, Trchová M. Polyaniline nanostructures and the role of aniline oligomers in their formation. *Progress in Polymer Science*. 2010;35(12):1420-1481. doi:10.1016/j.progpolymsci.2010.07.006

222. Martin CR, Parthasarathy R, Menon V. Template synthesis of electronically conductive polymers - A new route for achieving higher electronic conductivities. *Synthetic Metals*. 1993;55(2-3):1165-1170. doi:10.1016/0379-6779(93)90218-L

223. Parthasarathy RV, Martin CR. Template-Synthesized Polyaniline Microtubules. *Chem Mater*. 1994;6(10):1627-1632. doi:10.1021/cm00046a011

224. Lee W, Park SJ. Porous Anodic Aluminum Oxide: Anodization and Templated Synthesis of Functional Nanostructures. *Chem Rev*. 2014;114(15):7487-7556. doi:10.1021/cr500002z

225. Gao Y, Li X, Gong J, Fan B, Su Z, Qu L. Polyaniline Nanotubes Prepared Using Fiber Mats Membrane as the Template and their Gas-response Behavior. *J Phys Chem C*. 2008;112(22):8215-8222. doi:10.1021/jp711601f

226. Jackowska K, Bieguński AT, Tagowska M. Hard template synthesis of conducting polymers: a route to achieve nanostructures. *J Solid State Electrochem*. 2008;12(4):437-443. doi:10.1007/s10008-007-0453-7

227. Zhang Z, Sui J, Zhang L, Wan M, Wei Y, Yu L. Synthesis of Polyaniline with a Hollow, Octahedral Morphology by Using a Cuprous Oxide Template. *Advanced Materials*. 2005;17(23):2854-2857. doi:10.1002/adma.200501114

228. Pan LJ, Pu L, Shi Y, Song SY, Xu Z, Zhang R, Zheng YD. Synthesis of Polyaniline Nanotubes with a Reactive Template of Manganese Oxide. *Advanced Materials*. 2007;19(3):461-464. doi:10.1002/adma.200602073

229. Parveen A, Manjunatha S, Kumar MM, Roy AS. Agile soft template array fabrication of one-dimensional (1D) polyaniline nanocomposite fibers for hydrogen storage. *RSC Adv*. 2024;14(35):25347-25358. doi:10.1039/D4RA04710A

230. Wang ZG, Zhan P, Ding B. Self-Assembled Catalytic DNA Nanostructures for Synthesis of Para-directed Polyaniline. *ACS Nano*. 2013;7(2):1591-1598. doi:10.1021/nn305424e

231. Chen J, Bai L, Yang M, Guo H, Xu Y. Biocatalyzed synthesis of conducting polyaniline in reverse microemulsions. *Synthetic Metals*. 2014;187:108-112. doi:10.1016/j.synthmet.2013.10.026

232. Wei Z, Wan M. Synthesis and characterization of self-doped poly(aniline- *co* -aminonaphthalene sulfonic acid) nanotubes. *J of Applied Polymer Sci*. 2003;87(8):1297-1301. doi:10.1002/app.11541

233. Zhang Z, Wei Z, Zhang L, Wan M. Polyaniline nanotubes and their dendrites doped with different naphthalene sulfonic acids. *Acta Materialia*. 2005;53(5):1373-1379. doi:10.1016/j.actamat.2004.11.030

234. Wu W, Pan D, Li Y, Zhao G, Jing L, Chen S. Facile fabrication of polyaniline nanotubes using the self-assembly behavior based on the hydrogen bonding: a mechanistic study and application in high-performance electrochemical supercapacitor electrode. *Electrochimica Acta*. 2015;152:126-134. doi:10.1016/j.electacta.2014.11.130

235. Qiu H, Wan M, Matthews B, Dai L. Conducting Polyaniline Nanotubes by Template-Free Polymerization. *Macromolecules*. 2001;34(4):675-677. doi:10.1021/ma001525e

236. Wei Z, Zhang Z, Wan M. Formation Mechanism of Self-Assembled Polyaniline Micro/Nanotubes. *Langmuir*. 2002;18(3):917-921. doi:10.1021/la0155799

237. Zhang L, Wan M. Self-Assembly of Polyaniline—From Nanotubes to Hollow Microspheres. *Adv Funct Materials*. 2003;13(10):815-820. doi:10.1002/adfm.200304458

238. Zhang Z, Wang L, Deng J, Wan M. Self-assembled nanostructures of polyaniline doped with poly(3-thiopheneacetic acid). *Reactive and Functional Polymers*. 2008;68(6):1081-1087. doi:10.1016/j.reactfunctpolym.2008.02.010

239. Lim GH, Choi HJ. Synthesis of self-assembled rectangular-shaped polyaniline nanotubes and their physical characteristics. *Journal of Industrial and Engineering Chemistry*. 2017;47:51-55. doi:10.1016/j.jiec.2016.11.035

240. Trchová M, Šeděnková I, Konyushenko EN, Stejskal J, Holler P, Ćirić-Marjanović G. Evolution of Polyaniline Nanotubes: The Oxidation of Aniline in Water. *J Phys Chem B*. 2006;110(19):9461-9468. doi:10.1021/jp057528g

241. Ding H, Wan M, Wei Y. Controlling the Diameter of Polyaniline Nanofibers by Adjusting the Oxidant Redox Potential. *Advanced Materials*. 2007;19(3):465-469. doi:10.1002/adma.200600831

242. Wan M. A Template-Free Method Towards Conducting Polymer Nanostructures. *Advanced Materials*. 2008;20(15):2926-2932. doi:10.1002/adma.200800466

243. Ding H, Shen J, Wan M, Chen Z. Formation Mechanism of Polyaniline Nanotubes by a Simplified Template-Free Method. *Macro Chemistry & Physics*. 2008;209(8):864-871. doi:10.1002/macp.200700624

244. Wang X, Liu N, Zhang WJ. Studies on Multi Morphology of Polyaniline Guided by Alkali. *SSP*. 2007;121-123:429-432. doi:10.4028/www.scientific.net/SSP.121-123.429

245. Liu P, Zhu Y, Torres J, Lee SH, Yun M. Facile and template-free method toward chemical synthesis of polyaniline film/nanotube structures. *J Polym Sci Part A: Polym Chem*. 2017;55(24):3973-3979. doi:10.1002/pola.28749

246. Shahid MdA, Rahman MdM, Hossain MdT, Hossain I, Sheikh MdS, Rahman MdS, Uddin N, Donne SW, Hoque MdIU. Advances in Conductive Polymer-Based Flexible Electronics for Multifunctional Applications. *J Compos Sci*. 2025;9(1):42. doi:10.3390/jcs9010042

247. Xiong S, Wang Q, Chen Y. Study on electrical conductivity of single polyaniline microtube. *Materials Letters*. 2007;61(14-15):2965-2968. doi:10.1016/j.matlet.2006.10.049

248. Delvaux M, Duchet J, Stavaux PY, Legras R, Demoustier-Champagne S. Chemical and electrochemical synthesis of polyaniline micro- and nano-tubules. *Synthetic Metals*. 2000;113(3):275-280. doi:10.1016/S0379-6779(00)00226-5

249. Long Y, Zhang L, Ma Y, Chen Z, Wang N, Zhang Z, Wan M. Electrical Conductivity of an Individual Polyaniline Nanotube Synthesized by a Self-Assembly Method. *Macromol Rapid Commun*. 2003;24(16):938-942. doi:10.1002/marc.200300039

250. Jafarzadeh S, Claesson PM, Sundell PE, Pan J, Thormann E. Nanoscale Electrical and Mechanical Characteristics of Conductive Polyaniline Network in Polymer Composite Films. *ACS Appl Mater Interfaces*. 2014;6(21):19168-19175. doi:10.1021/am505161z

251. Li D, Kaner RB. Processable stabilizer-free polyaniline nanofiber aqueous colloids. *Chem Commun*. 2005;(26):3286. doi:10.1039/b504020e

252. Rahy A, Rguig T, Cho SJ, Bunker CE, Yang DJ. Polar solvent soluble and hydrogen absorbing polyaniline nanofibers. *Synthetic Metals*. 2011;161(3-4):280-284. doi:10.1016/j.synthmet.2010.11.036

253. Wang CH, Dong YQ, Sengothi K, Tan KL, Kang ET. In-vivo tissue response to polyaniline. *Synthetic Metals*. 1999;102(1-3):1313-1314. doi:10.1016/S0379-6779(98)01006-6

254. Kamalesh S, Tan P, Wang J, Lee T, Kang ET, Wang CH. Biocompatibility of electroactive polymers in tissues. *J Biomed Mater Res*. 2000;52(3):467-478. doi:10.1002/1097-4636(20001205)52:3<467::AID-JBM4>3.0.CO;2-6

255. Mattioli-Belmonte M, Giavaresi G, Biagini G, Virgili L, Giacomini M, Fini M, Giantomassi F, Natali D, Torricelli P, Giardino R. Tailoring Biomaterial Compatibility: In Vivo Tissue Response versus in Vitro Cell Behavior. *Int J Artif Organs*. 2003;26(12):1077-1085. doi:10.1177/039139880302601205

256. Humpolíček P, Radaszkiewicz KA, Kašpárková V, Stejskal J, Trchová M, Kuceková Z, Vičarová H, Pacherník J, Lehocký M, Minařík A. Stem cell differentiation on conducting polyaniline. *RSC Adv*. 2015;5(84):68796-68805. doi:10.1039/C5RA12218J

257. Rejmontová P, Capáková Z, Mikušová N, Maráková N, Kašpárková V, Lehocký M, Humpolíček P. Adhesion, Proliferation and Migration of NIH/3T3 Cells on Modified Polyaniline Surfaces. *IJMS*. 2016;17(9):1439. doi:10.3390/ijms17091439

258. Ibarra LE, Tarres L, Bongiovanni S, Barbero CA, Kogan MJ, Rivarola VA, Bertuzzi ML, Yslas EI. Assessment of polyaniline nanoparticles toxicity and teratogenicity in

aquatic environment using Rhinella arenarum model. *Ecotoxicology and Environmental Safety*. 2015;114:84-92. doi:10.1016/j.ecoenv.2015.01.013

259. Humpolíček P, Kašpárková V, Pacherník J, Stejskal J, Bober P, Capáková Z, Radaszkiewicz KA, Junkar I, Lehocký M. The biocompatibility of polyaniline and polypyrrole: A comparative study of their cytotoxicity, embryotoxicity and impurity profile. *Materials Science and Engineering: C*. 2018;91:303-310. doi:10.1016/j.msec.2018.05.037

260. Kašpárková V, Humpolíček P, Stejskal J, Capáková Z, Bober P, Skopalová K, Lehocký M. Exploring the Critical Factors Limiting Polyaniline Biocompatibility. *Polymers*. 2019;11(2):362. doi:10.3390/polym11020362

261. Kucekova Z, Humpolicek P, Kasparkova V, Perecko T, Lehocký M, Hauerlandová I, Sáha P, Stejskal J. Colloidal polyaniline dispersions: Antibacterial activity, cytotoxicity and neutrophil oxidative burst. *Colloids and Surfaces B: Biointerfaces*. 2014;116:411-417. doi:10.1016/j.colsurfb.2014.01.027

262. Oh WK, Kim S, Kwon O, Jang J. Shape-Dependent Cytotoxicity of Polyaniline Nanomaterials in Human Fibroblast Cells. *J Nanosci Nanotech*. 2011;11(5):4254-4260. doi:10.1166/jnn.2011.3662

263. Li YS, Chen BF, Li XJ, Zhang WK, Tang HB. Cytotoxicity of Polyaniline Nanomaterial on Rat Celiac Macrophages In Vitro. Lee MH, ed. *PLoS ONE*. 2014;9(9):e107361. doi:10.1371/journal.pone.0107361

264. Zhang Y, Zhou M, Dou C, Ma G, Wang Y, Feng N, Wang W, Fang L. Synthesis and biocompatibility assessment of polyaniline nanomaterials. *Journal of Bioactive and Compatible Polymers*. 2019;34(1):16-24. doi:10.1177/0883911518809110

265. Kuang Y, Liu N, Ye S, Li X, Chen X, Qi L, Zhu P, Liu R, Wu X. Ce doped polyaniline nanoparticles for absorption and photoacoustic imaging response to GSH in vitro and in vivo. *Bioactive Materials*. 2022;17:197-203. doi:10.1016/j.bioactmat.2022.01.022

266. Minisy IM, Salahuddin NA, Ayad MM. In vitro release study of ketoprofen-loaded chitosan/polyaniline nanofibers. *Polym Bull*. 2021;78(10):5609-5622. doi:10.1007/s00289-020-03385-z

267. Daraeinejad Z, Shabani I. Enhancing biocompatibility of polyaniline-based scaffolds by using a bioactive dopant. *Synthetic Metals*. 2021;271:116642. doi:10.1016/j.synthmet.2020.116642

268. Ghosh S, Chaganti SR, Prakasham RS. Polyaniline nanofiber as a novel immobilization matrix for the anti-leukemia enzyme l-asparaginase. *Journal of Molecular Catalysis B: Enzymatic*. 2012;74(1-2):132-137. doi:10.1016/j.molcatb.2011.09.009

269. Neelgund GM, Hrehorova E, Joyce M, Bliznyuk V. Synthesis and characterization of polyaniline derivative and silver nanoparticle composites. *Polymer International*. 2008;57(10):1083-1089. doi:10.1002/pi.2445

270. Salem MA, Elsharkawy RG, Hablas MF. Adsorption of brilliant green dye by polyaniline/silver nanocomposite: Kinetic, equilibrium, and thermodynamic studies. *European Polymer Journal*. 2016;75:577-590. doi:10.1016/j.eurpolymj.2015.12.027

271. Blinova NV, Stejskal J, Trchová M, Sapurina I, Ćirić-Marjanović G. The oxidation of aniline with silver nitrate to polyaniline–silver composites. *Polymer*. 2009;50(1):50-56. doi:10.1016/j.polymer.2008.10.040

272. Bober P, Trchová M, Prokeš J, Varga M, Stejskal J. Polyaniline–silver composites prepared by the oxidation of aniline with silver nitrate in solutions of sulfonic acids. *Electrochimica Acta*. 2011;56(10):3580-3585. doi:10.1016/j.electacta.2010.08.041

273. Blinova NV, Bober P, Hromádková J, Trchová M, Stejskal J, Prokeš J. Polyaniline–silver composites prepared by the oxidation of aniline with silver nitrate in acetic acid solutions. *Polymer International*. 2010;59(4):437-446. doi:10.1002/pi.2718

274. Wankhede YB, Kondawar SB, Thakare SR, More PS. Synthesis And Characterization Of Silver Nanoparticles embedded In Polyaniline Nanocomposite. *Adv Mater Lett*. 2013;4(1):89-93. doi:10.5185/amlett.2013.icnano.108

275. Biswas S, Dutta B, Bhattacharya S. Consequence of silver nanoparticles embedment on the carrier mobility and space charge limited conduction in doped polyaniline. *Applied Surface Science*. 2014;292:420-431. doi:10.1016/j.apsusc.2013.11.154

276. Wang X, Shen Y, Xie A, Chen S. One-step synthesis of Ag@PANI nanocomposites and their application to detection of mercury. *Materials Chemistry and Physics*. 2013;140(2-3):487-492. doi:10.1016/j.matchemphys.2013.03.058

277. Singh RP, Tiwari A, Pandey AC. Silver/Polyaniline Nanocomposite for the Electrocatalytic Hydrazine Oxidation. *J Inorg Organomet Polym*. 2011;21(4):788-792. doi:10.1007/s10904-011-9554-y

278. De Barros RA, De Azevedo WM. Polyaniline/silver nanocomposite preparation under extreme or non-classical conditions. *Synthetic Metals*. 2008;158(21-24):922-926. doi:10.1016/j.synthmet.2008.06.021

279. Jia Q, Shan S, Jiang L, Wang Y, Li D. Synergistic antimicrobial effects of polyaniline combined with silver nanoparticles. *J of Applied Polymer Sci*. 2012;125(5):3560-3566. doi:10.1002/app.36257

280. Tamboli MS, Kulkarni MV, Patil RH, Gade WN, Navale SC, Kale BB. Nanowires of silver–polyaniline nanocomposite synthesized via in situ polymerization and its novel functionality as an antibacterial agent. *Colloids and Surfaces B: Biointerfaces*. 2012;92:35-41. doi:10.1016/j.colsurfb.2011.11.006

281. Poyraz S, Cerkez I, Huang TS, Liu Z, Kang L, Luo J, Zhang X. One-Step Synthesis and Characterization of Polyaniline Nanofiber/Silver Nanoparticle Composite Networks as Antibacterial Agents. *ACS Appl Mater Interfaces*. 2014;6(22):20025-20034. doi:10.1021/am505571m

282. Shaban M, Rabia M, Fathallah W, El-Mawgoud NA, Mahmoud A, Hussien H, Said O. Preparation and Characterization of Polyaniline and Ag/ Polyaniline Composite Nanoporous Particles and Their Antimicrobial Activities. *J Polym Environ*. 2018;26(2):434-442. doi:10.1007/s10924-017-0937-1

283. Zhang C, Govindaraju S, Giribabu K, Huh YS, Yun K. AgNWs-PANI nanocomposite based electrochemical sensor for detection of 4-nitrophenol. *Sensors and Actuators B: Chemical*. 2017;252:616-623. doi:10.1016/j.snb.2017.06.039

284. Gupta K, Jana PC, Meikap AK. Optical and electrical transport properties of polyaniline–silver nanocomposite. *Synthetic Metals*. 2010;160(13-14):1566-1573. doi:10.1016/j.synthmet.2010.05.026

285. Mishra S, Shimpi NG, Sen T. The effect of PEG encapsulated silver nanoparticles on the thermal and electrical property of sonochemically synthesized polyaniline/silver nanocomposite. *J Polym Res*. 2013;20(1):49. doi:10.1007/s10965-012-0049-5

286. Zengin H, Aksin G, Zengin G, Kahraman M, Kilic IH. Preparation and Characterization of Conductive Polyaniline/Silver Nanocomposite Films and Their Antimicrobial Studies. *Polymer Engineering & Sci*. 2019;59(S1). doi:10.1002/pen.24902

287. Guimarães ML, Da Silva FAG, Da Costa MM, De Oliveira HP. Coating of conducting polymer-silver nanoparticles for antibacterial protection of Nile tilapia skin xenografts. *Synthetic Metals*. 2022;287:117055. doi:10.1016/j.synthmet.2022.117055

288. Da Silva BN, Vieira MF, Izumi CMS. In situ preparation of silver nanoparticles on polyaniline nanofibers for SERS applications. *Synthetic Metals*. 2022;291:117171. doi:10.1016/j.synthmet.2022.117171

289. Mondal S, Rana U, Malik S. Facile Decoration of Polyaniline Fiber with Ag Nanoparticles for Recyclable SERS Substrate. *ACS Appl Mater Interfaces*. 2015;7(19):10457-10465. doi:10.1021/acsami.5b01806

290. Stejskal J, Trchová M, Kovářová J, Brožová L, Prokeš J. The reduction of silver nitrate with various polyaniline salts to polyaniline–silver composites. *Reactive and Functional Polymers*. 2009;69(2):86-90. doi:10.1016/j.reactfunctpolym.2008.11.004

291. Bouazza S, Alonzo V, Hauchard D. Synthesis and characterization of Ag nanoparticles–polyaniline composite powder material. *Synthetic Metals*. 2009;159(15-16):1612-1619. doi:10.1016/j.synthmet.2009.04.025

# *Chapter II*

## *Biological synthesis and characterization of Cynoglossum creticum-mediated silver nanoparticles*

## II.1. Introduction

The remarkable diversity, abundance, and rapid growth of plant life, in combined with their unique biological capacity to hyperaccumulate and reduce metal ions, provide promising opportunities for the development of sustainable biosynthetic approaches. In particular, many herbaceous species found throughout the Mediterranean basin present underexplored potential for applications in nanotechnology. One such species is *Cynoglossum criticum*, a biennial plant belonging to the Boraginaceae family, notorious for being toxic to livestock and herbivores. Native to regions such as northern Algeria, this plant thrives disturbed and marginal habitats, field edges, and roadsides. Despite its negative perception, *C. criticum* has been subjected to phytochemical investigations, such as a report by S. Dresler et al.[1] on the content of secondary metabolites, and a study by L. Menghini et al.[2] on the extraction of various parts of its plant. *C. criticum*, particularly its aerial parts, specifically the leaves, have been shown to contain a rich profile of bioactive compounds, such as phenolic acids with important therapeutic and biological properties.

From the perspective of sustainable biotechnology, this neglected biomass represents an untapped resource rather than a waste product. Its abundance and rich phytochemical composition make *C. criticum* an attractive candidate for environmentally friendly applications, particularly in the field of nanoparticle biosynthesis. Building on this premise, the present chapter will explore the potential of *C. criticum* leaves as a green platform for the biosynthesis of silver nanoparticles (Ccl-AgNPs). Specifically, it focuses on optimizing the aqueous extraction and nanoparticle synthesis processes, followed by a comprehensive physicochemical characterization of the resulting nanoparticles using spectroscopic and imaging techniques.

## II.2. Experimental

### II.2.1. Chemicals and reagents

The following reagents of analytical and titration grades were used without any further purification: silver nitrate (BP USP 99.8-100.5%), Folin-Ciocalteu reagent, sodium carbonate ( ACS reagent, ≥99.5%) , gallic acid (titration, 97.5-102.5% ), aluminium nitrate (ACS specification, 98.0-102.0% ), potassium acetate (ACS reagent, ≥99.0%), quercetin (≥95%, HPLC), Iron(III) chloride hexahydrate (puriss. p.a., reag. Ph. Eur., ≥99%), potassium iodide (ACS , ≥99.0%), iodine (≥99.99% ), sodium hydroxide (ACS reagent, ≥97.0%, pellets), and 4-

(Dimethylamino)benzaldehyde (ACS reagent grade, 99%) provided by Sigma-Aldrich (Sigma-Aldrich, St. Louis, MO, USA).

### II.2.2. Collection of *Cynoglossum creticum* and optimization of extraction process

The basal leaves of *Cynoglossum criticum* were gathered in early April from the Azzaba district of Skikda, northeastern Algeria (coordinates: 36° 44′ 21.98″ N, 7° 6′ 19.01″ E). Botanical identification was provided by Pr. Hamdi Bendif from the Department of Biology, IIslamic University, Saudi Arabia. Immediately after collection, the leaves were purified to remove any surface residues and possible contaminants, using potable water and distilled water, respectively. They were then dried under ventilated and shaded conditions to minimize photodegradation and thermal loss of bioactive constituents. Once completely dried, the leaves were electronically ground into a homogenized fine powder, which was subsequently stored in a tightly sealed container in cool, dry, and dark location.

The level of plant phytochemicals, especially secondary metabolites, in the plant extract is a critical practical variable influencing the efficiency of the biosynthesis process. Optimal selection of extraction parameters enhances the maximum yield of these bioactive compounds[3,4]. In this study, aqueous extractions of *C. creticum* leaves were performed under controlled experimental conditions to investigate the influence of different variables on extraction efficiency. Specifically, varying amounts of dried leaf powder were added to conical flasks containing 200 mL of distilled water, corresponding to weight-to-volume ratios of 0.5%, 1.0%, and 2.0% (w/v). Extractions were carried out at temperatures ranging from ambient room temperature to 70°C, with continuous stirring, for different time intervals. In each experiment, one of three parameters (i.e., plant powder mass, extraction time, or temperature) was varied, resulting in a total of 11 distinct extracts coded CclE1–CclE11, as shown in Table.II.1. Upon completion of each extraction, the mixtures were cooled to room temperature, and the residual microvegetation was separated from the supernatant via triple vacuum filtration using Whatman No. 1 filter paper. The clarified extracts were then stored at 4°C until further analysis.

**TABLE.II.1.** Experimental circumstances used for extracting C. creticum leaves.

| Extract code | weight to volume ratio (% w/v) | Temperature (°C) | Time (min) |
|---|---|---|---|
| CclE1 | 0.5 | Room Temperature | 60 |
| CclE2 | 0.5 | 50 | 60 |
| CclE3 | 0.5 | 70 | 60 |
| CclE4 | 1 | Room Temperature | 60 |
| CclE5 | 1 | 50 | 60 |
| CclE6 | 1 | 70 | 60 |
| CclE7 | 2 | Room Temperature | 60 |
| CclE8 | 2 | 50 | 60 |
| CclE9 | 2 | 70 | 60 |
| CclE10 | 1 | 70 | 30 |
| CclE11 | 1 | 70 | 120 |

***1. Total phenolic and flavonoid content measurement***

Quantitative tests of total phenolic and total flavonoid contents were performed to establish the optimal experimental parameters for the aqueous extraction of bioactive phytochemicals compounds from C. creticum leaves. Prior to these tests, the extracts were concentrated under reduced pressure using a rotary evaporator (EV400H-SERIES, LabTech Company, Sorisole, Italy) maintained at 45 °C.

The standard Folin-Ciocalteau assay was chosen to quantify the total polyphenol content (TPC) of aqueous extracts of CclEx[5]. In brief, 20 µL of serially diluted of Ccl-extracts were added to 100 µL of 1 mg/mL Folin-Ciocalteau reagent (diluted in distilled water), followed after 4 minutes by the addition of 75 µL of sodium carbonate solution (75 g/L). The reaction mixtures were left in the opaque incubator for 2 h at room temperature before recording the absorbance at 765 nm using an EnSpire 96-well microplate reader (PerkinElmer, MA, USA). TPC was calculated from a gallic acid standard calibration curve ($y = 0.03x + 0.205$, $R^2 = 0.9672$) and expressed as micrograms of gallic acid equivalents per milligram of dried extract (µg GAE/mg extract).

Total flavonoid content (TFC) was quantified spectrophotometrically through the complexation colorimetric method AlCl3-flavonoid, with modifications suitable for a 96-well microplate[6]. First, 130 µL of methanol was mixed with 50 µL of 1 mg/mL aqueous Ccl-extracts, followed by sequential addition of 10 µL each of 9.8% potassium acetate and 10% aluminum nitrate, respectively. After 40 min of incubation at room temperature, the absorbance of the complexes was measured at 415 nm. Finally, quercetin was employed as the reference standard, and the TFC value was calculated from the linear regression of the calibration curve ($y = 0.049x + 0.005$ ($R^2 = 0.9957$) and expressed as micrograms of quercetin equivalents/milligram dry weight extracts (µg QE/mg extract). All TPC and TFC measurements were performed in triplicate ($n = 3$).

***2. Phytochemistry assessment***

To elucidate the biologically active secondary metabolites potentially responsible for the bioreduction of metal ions and the concomitant stabilization and coating of nanoparticles, preliminary screening tests were conducted on the optimal aqueous extract of the Cynoglossum criticum leaves. Standardized qualitative assays were employed, wherein the presence of distinct classes of metabolites was inferred on the basis of observable colorimetric transitions and/or the formation of precipitates. Specifically, the screening targeted tannins,[7] alkaloids[8], pyrrolizidine alkaloids[9], flavonoids[10], saponins[11], quinones[10], anthraquinones[10], and sterols-terpenes[12,13], as these categories of bioactive compounds are frequently implicated in redox-mediated nanoparticle synthesis and surface modification. To ensure the reliability of the results, the experiments were tri-repeated.

### II.2.3. Bio-manufacture of silver nanoparticles (Ccl-AgNPs)

A one-step biosynthesis was performed to prepare Ccl-AgNPs using silver nitrate as the primary metal salt source of $Ag^+$ ions and Cynoglossum creticum leaf extract, which functioned simultaneously as a reducing and stabilizing agent. Practically, the synthesis began by introducing a measured volume Ccl-extract to a 250-ml Erlenmeyer flask containing 1 mM aqueous $AgNO_3$ solution under continuous magnetic stirring. To establish the most favorable synthesis conditions, the reaction was optimized using a one-variable-at-a-time (OVAT) technique wherein individual parameters were varied systematically while others were held constant. Specifically, the volumetric ratio of $AgNO_3$ to Ccl-extract, reaction temperature (ranging from ambient to 80°C), and reaction time (monitored at 15-minute intervals to study the reaction kinetics). The progression of the reduction reaction and evolution of the NPs under these experimental conditions was monitored and analyzed by recording absorption spectra using a UV-Vis spectrometer (UV-1900i, Shimadzu Corporation). Upon determination of the optimal conditions, the produced Ccl-AgNPs were collected through centrifugation for 20 minutes, effectively separating the colloidal NPs from unreacted components and surplus biomolecules in the supernatant. The obtained solid pellet was subjected to repeated washing with distilled water (three cycles), followed by drying at 60°C to yield purified Ccl-AgNPs powder suitable for subsequent physicochemical and biological characterization and applications.

### II.2.3. Characterization and analysis of Ccl-AgNPs

***1. Fourier transform infrared (FTIR) spectroscopic measurement***

Spectroscopic measurements of the CCl-extract and Ccl-AgNPs were performed using a FTIR spectrometer from Shimadzu Corporation (Japan), equipped with a QATRTM-S single-reflection ATR accessory fitted with a high-strength diamond crystal . Spectra were recorded at a resolution of 1 $cm^{-1}$, providing sufficient spectral detail to identify subtle vibrational modes across the mid-infrared region spanning 4000–400 $cm^{-1}$.

***2. X-ray diffraction study***

X-ray diffraction (XRD) analysis was performed to investigate the phase structure, crystallinity, and crystal size of Ccl-AgNPs utilizing a Bruker D8 ADVANCE instrument equipped with DAVINCI design technology (Bruker AXS, Germany). The instrument was operated at an accelerating voltage of 40 kV and a current of 40 mA, using Cu Kα radiation with a wavelength of 1.5406 Å as the incident beam source. Data were collected over a diffraction angle (2θ) range of 10° to 90°, which includes most of the characteristic Bragg reflections of crystalline materials. A step sizes and total time/step of 0.02° and 19.1 s, respectively, were used to ensure high angular resolution and accurate peak identification.

***3. SEM- EDS examinations***

The morphological features as well as the qualitative and semi-quantitative elemental composition of the Ccl-AgNPs were analyzed using an environmental scanning electron microscope (ESEM) coupled with energy dispersive X-ray spectroscopy (EDS) measurements (Quattro S-ESEM , Thermo Fisher Scientific, Waltham, MA, USA).

***4. Thermal resiliency and phase transition assessment***

Thermal stability of the synthesized Ccl-AgNPs was assessed using thermogravimetric analysis (TGA), performed on a Mettler Toledo TGA-DSC 3+ Thermal Analyzer (Mettler Toledo, Switzerland). The measurements were conducted under a controlled nitrogen atmosphere in order to prevent oxidative degradation and ensure accurate assessment of intrinsic thermal behavior. The analysis was carried out over a broad temperature range, extending from 25 to 1000 °C, with a constant heating rate of 10 °C/min. This experimental setup allowed the detection of decomposition stages, and phase transitions.

## II.3. Results and discussion

### II.3.1. Extraction process of *Cynoglossum criticum* leaves

Plant polyphenols, particularly flavonoids, have attracted significant scientific interest due to their role as natural physiological response modulators, largely attributable to their

multifunctional structural properties, such as free radical scavenging and metal chelation capacities. Furthermore, among the different classes of phytochemicals, polyphenols exhibit the strongest reducing potential, making them the primary participants in biosynthesis[14] . At the plant tissue level, free polyphenols and flavonoids are predominantly localized in vacuoles, whereas insoluble forms are found in the plant cell wall. Consequently, the choice of an appropriate extraction process is critical, as it must enable solvent penetration into cellular compartments to effectively solubilize and recover these secondary metabolites[15]. According to O.R. Alara et al.[16], the efficiency of phytochemical extraction is strongly influenced by multiple experimental factors, and the use of non-statistically significant variables often results in inconsistent or unreliable outcomes. Based on this evidence, this applied part focused on optimizing the most influential parameters governing the extraction process to maximize yield and preserve the quality of the recovered polyphenols. These parameters are extraction temperature, solid-to-liquid ratio, and extraction duration.

Table. II.2. and Figure.II.1 present TPC and TFC values as a function of various extraction parameters. The results demonstrate that elevating the extraction temperature from room temperature to 50 and 70°C (extracts 1-9) significantly enhanced the recovery of phenolic compounds. This improvement is attributed to the reduction in the surface tension and viscosity of water, which allows for greater permeability of the solvent into plant pores and increased solubility of phenolics[17]. Heating also weakens and breaks down the intermolecular interactions (hydrogen bonds and van der Waals) between phenols and both polysaccharides and proteins due to softening of plant tissues, which enhances and accelerates the diffusion rate of polyphenols into the solvent[14,18].

**TABLE.II.2 .**Results of single-factor aqueous extraction experiments. TPC and TFC are reported as the mean ± SD of three measurements.

| Extract | Experimental conditions | Total phenolic content (µg GAE/ml) | Total Flavonoids content (µg QE/ml) |
|---|---|---|---|
| CclE1 | 0.5 (% w/v) ; room T; and 60 (min) | 9.09±3.22 | 6.944±0.14 |
| CclE2 | 0.5 (% w/v) ; 50 °C; and 60 (min) | 36.35±0.77 | 24.16±0.73 |
| CclE3 | 0.5 (% w/v) ; 70 °C; and 60 (min) | 94.49±0.44 | 38.33±1.76 |
| CclE4 | 1 (% w/v) ; room T; and 60 (min) | 38,90± 0.74 | 24.16±0.29 |
| CclE5 | 1 (% w/v) ; 50 °C; and 60 (min) | 97.62±1.45 | 44.23±0.44 |
| CclE6 | 1 (% w/v) ; 70 °C; and 60 (min) | 181.549±0.44 | 109.58±0.29 |
| CclE7 | 2 (% w/v) ; room T; and 60 (min) | 59.78±2.50 | 31.66±0.44 |
| CclE8 | 2 (% w/v) ; 50 °C; and 60 (min) | 149.78±1.80 | 56.38±1.62 |
| CclE9 | 2 (% w/v) ; 70 °C; and 60 (min) | 185.17±2.56 | 112.84±0.55 |
| CclE10 | 1 (% w/v) ; 70 °C; and 30 (min) | 71.64±0.77 | 32.91±1.32 |
| CclE11 | 1 (% w/v) ; 70 °C; and 120 (min) | 177.52±1,52 | 102.98±0.41 |

Similarly, the effect of the sample-to-solvent ratio on the polyphenol concentrations was investigated. The results showed a marked enhancement in the mean TPC and TFC values with increasing the solids content from 0.5% to 1.0% (w/v); for example, extracts obtained at 70°C exhibited a jump in TPC values from 94.49 µg GAE/mg to 181.59 µg GAE/mg (Table. II.2). These findings align with the mass transfer principle, whereby higher the solids-to-solvent ratio increases the concentration gradient and diffusion rate of the extracted phytocompounds into the solvent[19]. Increasing the solvent volume dilutes the extracted polyphenols. However, further increasing the solid content to 2.0% (w/v) produced no significant gains in TPC and TFC (185.17 µg GAE/mg and 112.84 µg QE/mg, respectively), suggesting a saturation effect. Reports confirmed that the extraction yield increased exponentially as the function of solids-to-solvent ratio increased. Once equilibrium was reached between the solid matrix and solvent, additional solute transfer was limited, leading to a stable and maximum yield[20,21]. K. Stamatopoulos et al.[22] observed stable yields when the olive leaf-to-solvent ratio exceeded 1:8, supporting the extraction efficiency plateaus beyond a critical threshold.

Furthermore, the impact of extraction duration on phenolic and flavonoid recovery was examined under a fixed solids-to-solvent ratio and the temperature conditions at 1.0% (w/v) and 80°C, respectively. Short extraction times, i.e., 30 min, yielded relatively low TPC and TFC values (71.64 µg GAE/mg and 32.91 µg QE/mg, respectively). Extending the incubation time to 60 minutes resulted in a more than twofold increase in TPC and nearly a threefold increase in TFC. However, doubling the extraction time to 120 minutes did not result in any improvement in phenolic yield but rather resulted in a decline. This reduction is attributed to the degradation of phenolic compounds due to prolonged overexposure to high temperatures, as the heat catalyzed the simultaneous decomposition and oxidation of phenolic compounds[23,24]. These results indicate that the relatively high extraction temperature of 70°C requires moderate extraction times to avoid thermal degradation of bioactive compounds. Consequently, conditions of 01% (w/v) leaf powder-to-distilled water, extracted at 70 °C for 60 min, were identified as the optimal parameters in subsequent experiments.

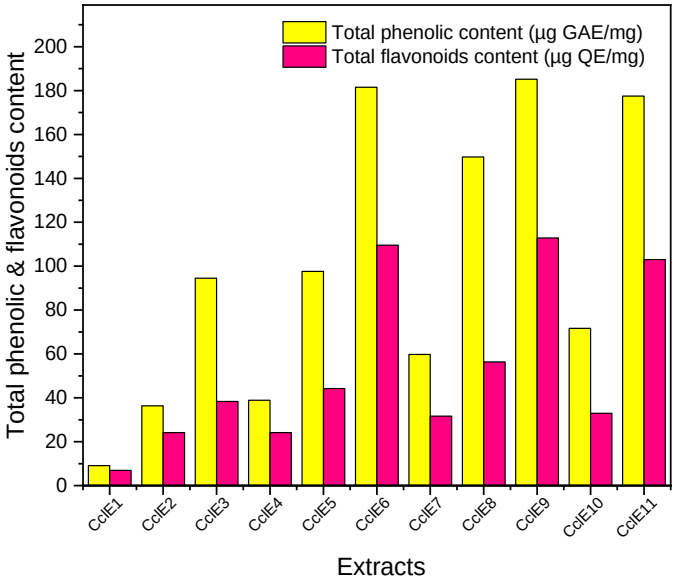


**FIGURE.II.1.** Columns of TPC and TFC values in Ccl-leaf extracts under the experimental conditions.

### II.3.2. Screening of active phytochemicals in Ccl-extract

Phytochemical screening represents a fundamental preliminary step in botany research, as it relies on simple and uncomplicated standard chemical techniques for the rapid identification of bioactive compounds.The results of phytochemical analysis (TableII.3 and Figure.II.2) revealed that the aqueous extract of Cynoglossum criticum leaves contained the following secondary metabolite constituents: tannins, saponins, flavonoids, quinones, alkaloids, and steroids/terpenes, while anthraquinones and pyrrolizidine alkaloids were absent. The detection of these metabolites supports the extensive traditional ethnomedicinal applications of C. criticum, since secondary metabolites act as defensive and preventive system agents against pathogens and disease. Their pharmacological relevance is well established: Alkaloids exhibit anticholinesterase, analgesic, and antibacterial properties and have been used to treat malaria[25,26]; flavonoids possess potent anti-inflammatory and immunomodulatory properties and are effective in preventing age-related toxicological pathways associated with neurodegenerative diseases[27]. Furthermore, tannins have been shown to interact irreversibly with bacterial membrane proteins and inactivate them, causing an imbalance in osmotic pressure and subsequent bacterial cell death[28] . Quinones have demonstrated promising antiviral activities against several viruses, including Coxsackievirus A16 (CVA16), dengue, and human immunodeficiency virus (HIV)[29,30]. Similarly, water-soluble saponins act as preformed natural barriers against pathogens and inhibitors of induced defense responses[31].

**TABLE.II.3.** Preliminary phytochemical examination of Ccl-extract.

| Phyto-constituents | Chemical tests | Result |
|---|---|---|
| tannins | Ferric chloride test | + |
| alkaloid | Wagner's reagent | + |
| pyrrolizidine alkaloids | Van Urk reaction | - |
| saponins | Foam test | + |
| flavonoids | Sodium Hydroxide test | + |
| quinones | Sulfuric acid test | + |
| anthraquinon | Borntragor's Test | - |
| sterols /terpenes | Liebermann-Buchard test | + |

Interestingly, the absence of pyrrolizidine alkaloids (PAs) from the extract is of particular importance, as it eliminates concerns about hepatotoxicity and supports the extract's safety in bioapplications. It is also worth noting that PAs are naturally occurring in Boraginaceae species; they do not possess intrinsic toxicity. Instead, their toxicity arises from the hepatic metabolic activation of 1,2-unsaturated PAs, where they are converted into reactive pyrrole metabolites. These derivatives are capable of inducing hepatocellular injury, liver fibrosis, and hepatic veno-occlusive disease, particularly upon chronic or high-dose exposure[32,33]. Therefore, the lack of PAs in C. criticum extract enhances its medicinal value, in line with the principles of green chemistry, by providing bioactive components without toxicological liabilities. This phytochemical profile not only underscores the therapeutic potential of C. criticum but also reinforces its role as a promising source of secondary metabolites with biocatalytic properties capable of donating hydrogen atoms or electrons, reducing metal ions, and producing nanoparticles[34].

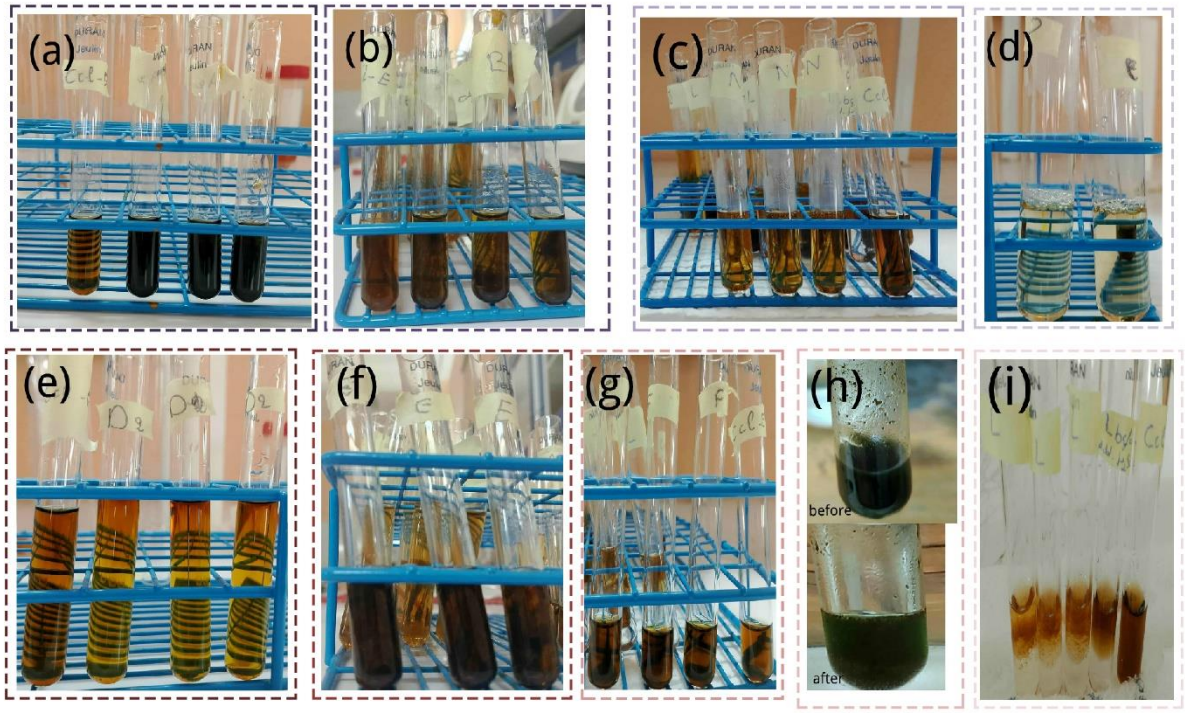


**FIGURE.II.2.** Phytochemical profiling of secondary metabolites in Ccl-extract. a) a greenish-black color signifies the presence of tannins; b) a red-orange precipitate denotes alkaloids; c) the lack of blue-violet color indicates the absence of pyrrolizidine alkaloids; d) persistent foam confirms the presence of saponins; e) yellow fluorescence reveals flavonoids; f) a red coloration indicates the presence of quinones; g) the absence of pink precipitate confirms the absence of anthraquinones; h) a blue coloration signifies the presence of steroids/terpenes; and i) a brown ring verifies the presence of steroids.

### II.3.3. Optimization of Ccl-AgNPs synthesis

A systematic investigation was conducted to examine the sustainable feasibility of employing Ccl-extract as a biogenic mediator for silver nanoparticle (AgNP) synthesis in the absence of any supplementary chemical reagents. During the course of the reaction, a pronounced and time-dependent color change was observed in the reaction mixture: the initial pale-yellow solution, formed when the aqueous $AgNO_3$ solution was mixed with Ccl-extract, gradually turned reddish-brown within minutes, then blackish-brown as the reaction advanced (Figure.II.3(a-c)). This visual color transformation is a qualitative first indicator of the formation of silver nanoparticles in the colloidal suspension. The origin of color evolution arises from the distinctive optical characteristics of AgNPs, specifically as the surface free conduction-band electrons undergo oscillations in resonance with the incident electromagnetic radiation at a specific frequency, known as surface plasmon resonance (SPR)[35].

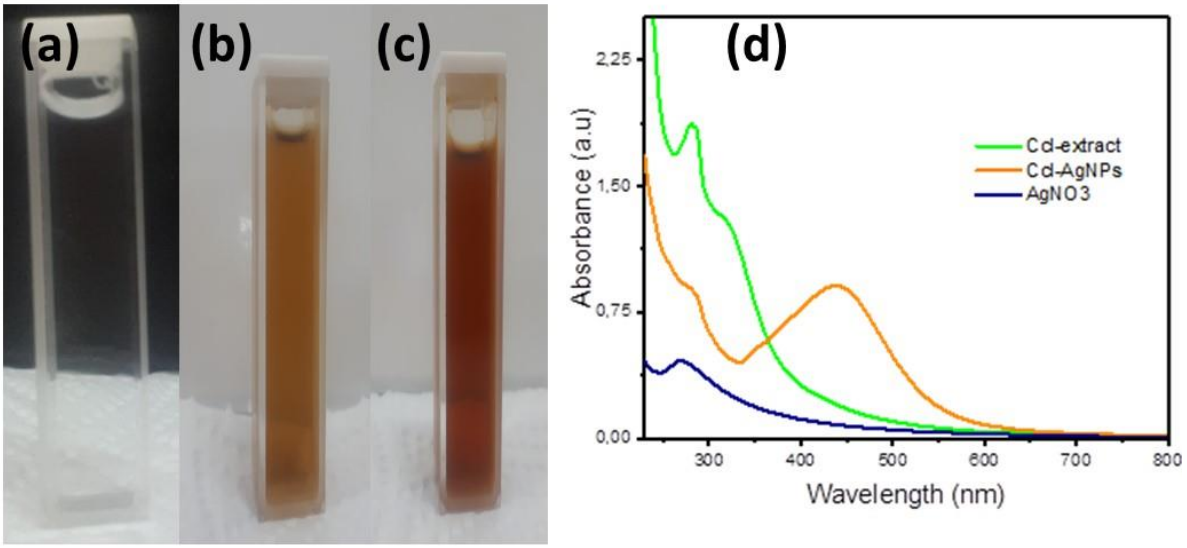


**FIGURE.II. 3**.(a) Silver nitrate solution; (b) solutioncolor of Ccl-extract ;(c) the developed Ccl-AgNPs colloidal; and (d) UV-vis spectra of these solutions.

For further investigation, UV-vis spectroscopy was used as a primary screening technique to monitor the formation of AgNPs during synthesis and to investigate their optical properties. Figure.II.3(d) illustrates the UV-vis spectra recorded for the Ccl-extract, silver precursor ($AgNO_3$), and the formed Ccl-AgNPs within the wavelength range of 200–800 nm. The absorption spectrum of the Ccl-extract exhibited a characteristic absorption peak at 281 nm accompanied by a minor hump near 325 nm. These features are attributed to the π-π* and n-π* electron transitions associated with conjugated C=C bonds, carbonyl groups, and hydroxyl functionalities, which are characteristic of flavonoid and phenolic constituents present in C. creticum leaves[36].

The spectrum of the $AgNO_3$ precursor (Figure.II.3(d)) revealed a strong absorption peak centered at 269 nm in the UV region, which corresponds to the characteristic electron transitions of nitrate. In contrast, after the biological reduction of $Ag^+$ ions, the spectrum of Ccl-AgNPS displayed a prominent and clear absorption peak at approximately 435 nm, along with a smaller hump near 350 nm attributed to the surface plasmon resonance (SPR). The appearance of the SPR band is a visual signature confirming the formation of nanoparticles. The SPR band of AgNPs is typically observed within the 350-450 nm range[37]. Furthermore, the changes in the peak position (λmax) and band intensity are strongly related to the nanoparticle size, shape, and degree of polydispersity, which in turn are affected by variations in reaction parameters such as temperature, initial reactant concentrations and types, and the surrounding dielectric

environment, etc.[38] Given the high sensitivity of the spectral properties to the reaction parameters, the role and effect of each of the main experimental variables were explored individually using a "one variable at a time" (OVAT) approach.

***1. Influence of silver nitrate amount***

The impact of silver nitrate concentration on the synthesis process was investigated by varying the volume ratio of $AgNO_3$ to Ccl-extract, while maintaining the extract volume fixed. The studied ratios ranged from 1:1 to 6:1 ($AgNO_3$: Ccl-extract), and the reaction mixtures were stirred for 1 h at 50°C. The surface plasmon resonance (SPR) behavior was monitored by recording UV–vis spectra of the reacted colloidal mixture (Figure.II.4(a)). At the lowest silver precursor level (1:1), the absorption profile closely mirrored that of the pure extract (Figure.II.3(d)), showing a dominant peak at 218 nm with the absence of a distinct SPR band, signifying no nanoparticle formation under these conditions. However, the relative increase in silver ions concentration resulted in a gradual decrease in the extract-associated absorption intensity at 281 nm, consistent with the reduction of $Ag^+$ ions by the phytochemicals. Meanwhile, a new SPR band developed around 435 nm. The sharpness and intensity of this peak increased significantly with precursor availability, reaching a maximum at a 5:1 ratio ($AgNO_3$: CCl-extract), indicating a suitable balance between $Ag^+$ ions and bioreductants. In contrast, further increasing the $AgNO_3$ ratio (beyond 5:1) resulted in a decline in SPR band intensity, possibly due to reduced NPs stability and the occurrence of agglomerations.

***2. Influence of Ccl-extract Concentration***

In addition to the silver precursor, the Ccl-extract plays a critical role due to its dual synthetic role. Therefore, it is necessary to find a suitable concentration that ensures efficient reduction of silver ions while simultaneously achieving sufficient stability of AgNPs. Following OVAT steps, a fixed concentration of silver nitrate (1 mM) was treated with varying ratios of Ccl-extract ($Ag^+$ extract: Ccl-extract ranging from 5:1 to 5:4) under constant experimental conditions of temperature and reaction time.

As demonstrated in the test results (Figure.II.4(b)), increasing the Ccl-extract concentration is accompanied by a sharp decrease in the absorption intensity at 435 nm, eventually disappearing completely at 5:4 ($Ag^+$:Ccl-extract), indicating a failure to reduce $Ag^+$ ions. This phenomenon is explained by the chemical composition of plant leaves, which are the richest source of phenolic and flavonoid compounds, which in turn possess redox-active hydroxyl groups capable of donating electrons, enabling them to reduce silver ions. They also act as ligands on the surface of the generated AgNPs. However, at high levels of these compounds, their functional groups preferentially interact with each other through hydrogen

bonds or π–π stacking, rather than with saturated $Ag^+$ ions[39]. These interactions hinder the reduction process and instead promote the formation of Ag-hydro-complexes, preventing the development of a stable colloidal solution of AgNPs[40,41]. Based on these observations, the $Ag^+$: Ccl-extract ratio of 5:1 was identified as the most suitable and was chosen for subsequent investigations.

***3. Reaction times effect***

Reaction kinetics testing was performed to determine the optimal reduction contact time that efficiently promotes crystal formation and nanoparticle stability. Figure.II.4(c) illustrates the UV-vis spectra of the reaction mixture, collected at regular intervals (0–105 min, every 15 min) during the synthesis process. It is noteworthy that the characteristic SPR band of the AgNPs appeared as early as 15 min; however, the band at this stage was weak, broad, and poorly defined, suggesting limited formation of nucleated particles with an inhomogeneous size distribution. As the reaction proceeded, the SPR band intensity gradually increased up to 75 min, indicating enhanced nucleation and growth of the AgNPs in the colloidal solution. This increase in absorbance is associated with both the increasing concentration of the NPs and the gradual enlargement of their size, consistent with Gustav Mie's theory of plasmon resonance in metallic nanostructures[42]. After 75 min, the SPR band showed a marked decline in intensity accompanied by a slight redshift, particularly evident at 105 min. These spectral changes are generally attributed to the agglomeration of the NPs and the decreased stability of the colloidal system, resulting from preferential crystal face growth along the (111) planes via deposition of atoms on the less stable cubic (100) faces rather than continued nucleation and formation of new crystallites[40]. Therefore, 75 min represents the optimal reaction time for the synthesis of Ccl-AgNPs.

***4. Reaction temperature influence***

The thermal environment of the reaction plays a crucial role in controlling the nucleation and growth dynamics of NPs during the synthesis process. In this regard, temperature-dependent experiments were performed over a range from ambient conditions to 80 °C under optimized conditions. As can be seen in Figure.II.4(d), the appearance of a characteristic SPR band at all examined temperatures confirmed the successful formation of Ccl-AgNPs. Upon heating, the absorption spectra exhibited both an increase in intensity and a noticeable broadening, accompanied by a blue shift of the maximum absorption wavelength (λmax) from 438 nm at room temperature to 424 nm at 80 °C. This broadening of the absorption spectrum is explained by the enhanced phonon-electron scattering rate, which affects the damping of plasmon oscillations[43].

The observed blueshift in λmax is linked to the preferential formation of smaller, more dispersed NPs at elevated temperatures. This is explained kinetically by the acceleration of the reduction rate of $Ag^+$ ions under heating, which lowers the activation energy barrier for nucleation and produces a larger number of nuclei in a shorter period of time. Thermodynamically, it is due to the lower surface energy per atom of smaller NPs formed under fast nucleation conditions. The increased nucleation density inhibits subsequent particle growth through competition for precursor $Ag^+$ ions, ultimately producing smaller nanoparticles with narrower size distributions[44,45]. Conversely, the reduction of silver ions is slower at low temperatures, resulting in fewer nucleation and extended crystal growth. This environment facilitates Ostwald ripening and particle coalescence, increasing the average particle size[46]. Overall, low temperatures promote growth in nanosynthesis systems, while high temperatures shift the balance toward nucleation-dominated regimes[47]. Based on these findings, the most favorable temperature for Ccl-AgNPs synthesis was established at 80°C.

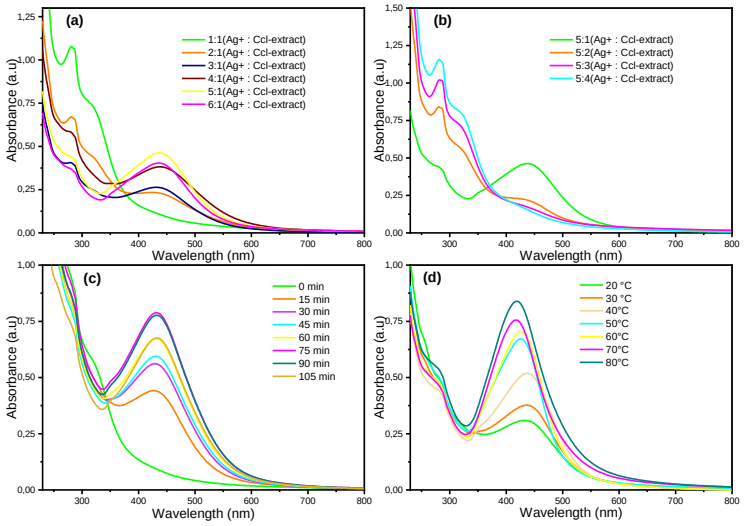


**FIGURE.II. 4.** UV–vis absorption spectra of the synthesized Ccl-AgNPs recorded under different experimental conditions. (a) varying the concentration of silver nitrate; (b) altering the amount of Ccl extract added; (c) monitoring changes over reaction time; and (d) at different reaction temperatures.

In this current investigation, the optimal experimental parameters for *C. creticum* extract-mediated biosynthesis of AgNPs were established to be: 1 mM silver nitrate concentration, reacted with Ccl-extract at a volume ratio of 5:1 ($AgNO_3$: Ccl-extract), at a reaction temperature of 80°C and an incubation period of 75 minutes. Notably, under these optimized conditions, spectroscopic analysis confirmed the disappearance of the slight

absorption hump observed near 350 nm, and a single, sharper, narrower, and nearly symmetrical SPR peak appeared (Figure.II.5). This spectral behavior indicates the predominance of monodisperse spherical NPs with a uniform size distribution[48]. These structural properties contribute to the improved stability and reproducibility of AgNPs, giving them multiple application advantages.

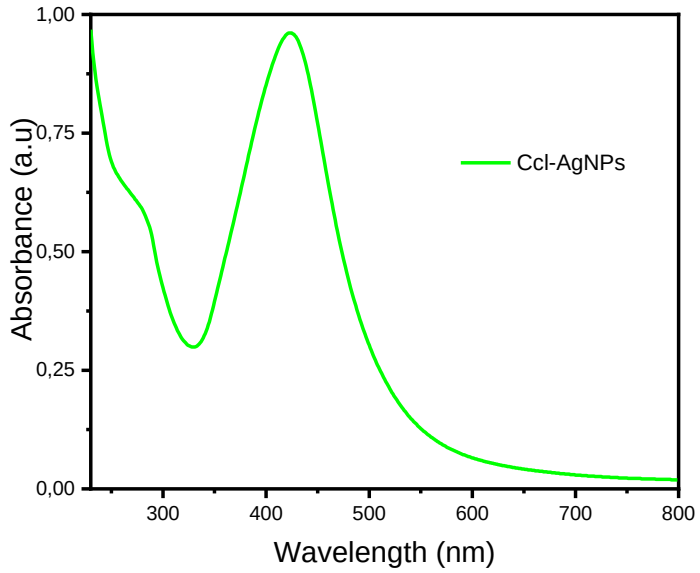


**FIGURE.II. 5.** UV-vis spectrum of the optimally produced Ccl-AgNPs.

### II.3.4. Stability of Ccl-AgNPs

The practical applicability of AgNPs is linked to the stability of colloidal behavior under environmental and physiological conditions containing intervening mediators such as ions and electrolytes. To assess this feature, Ccl-AgNPs were treated with a series of aqueous sodium chloride (NaCl) solutions at concentrations ranging from 0.0001 to 2 M, and their stability was monitored using UV-vis spectroscopy (Figure.II.6(a)). The SPR band of Ccl-AgNPs exhibited a gradual decrease in intensity with increasing electrolyte concentration. This plasmonic attenuation can be attributed to the aggregation of NPs, resulting from the electrical double-layer (EDL) compression phenomenon in electrolyte-rich environments, and the subsequent reduction of surface charge density and interparticle electrostatic repulsion diminishing[49]. Additionally, free $Cl^-$ ions in the solution interact directly with the Ccl-AgNPs surface, facilitating charge neutralization, interparticle adhesion, and eventual coalescence[50,51]. Notably, Ccl-AgNPs maintained their stability up to 1 M NaCl concentration, after which there was a pronounced decrease in adsorption when the ionic strength increased up to 2 M. This stability is consistent with physiological considerations: the reported normal range for chloride

ion concentration in human blood is 96–108 mEq/L[52] . This suggests the high robustness and stability of Ccl-AgNPs under harsh biological and environmental conditions, supporting their potential for biomedical and ecological applications.

The presence of elements and intercalating salts in real matrices can significantly alter the pH, influencing the colloidal stability of AgNPs. To evaluate the pH-dependent behavior of Ccl-AgNPs, the pH of the colloidal solutions was adjusted within a range of 2–10 by stepwise additions of 1 M hydrochloric acid or sodium hydroxide solution. The synthesized Ccl-AgNPs had a mild acidic character, with a pH of around 5. However, spectroscopic observations (Figure.II.6(b)) revealed a marked decrease in SPR peak intensity with decreasing pH, accompanied by the formation of visible precipitates in highly acidic conditions at pH 2. This suggests aggregation of NPs due to their destabilization, which is associated with proton-induced surface charge neutralization and the degradation and removal of phytochemical coating agents[53]. Conversely, the alkaline environment enhanced the intensity of the SPR peak, indicating enhanced stability of the colloidal dispersion. This stability at higher pH values can be attributed to the action of hydroxide ions ($OH^-$) as additional coordinating ligands on the surface of Ccl-AgNPs, which strengthens the electrostatic repulsion between the particles[54].

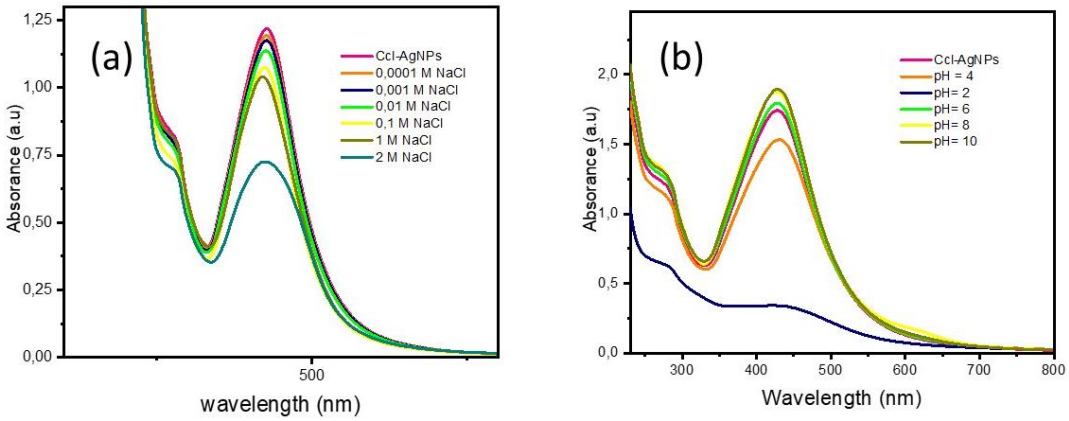


**FIGURE.II. 6.**UV-visible spectra of Ccl-AgNPs. a) in the presence of electrolyte concentration; and b) at various pH levels.

### II.3.5. Characterization of Ccl-AgNPs

#### *1. FTIR spectroscopy analyse*

FTIR spectra provide information on the synthesis mechanism, identifying the functional groups of secondary metabolites present in the extracts that play a key role in the reduction of metal ions and subsequent surface stabilization. The spectrum of Ccl-extract (Figure.II.7) revealed an abundance of phenolic chemicals that confer antioxidant and antimicrobial properties and enhance biocompatibility. The The vast absorption band observed

at 3334 $cm^{-1}$ is characteristic of O–H stretching vibrations in phenols, alcohols, carboxylic acid functions, and hydrogen-bonded water molecules. The distinct absorption peaks at 2925 and 2854 $cm^{-1}$ correspond to the asymmetric and symmetric stretching vibrations of the aliphatic methylene (–$CH_2$–) and methyl (–$CH_3$) groups, reflecting the existence of long-chain hydrocarbon backbones. The strong band at 1595 $cm^{-1}$, assigned to C=C stretching vibrations within aromatic rings, confirms the abundance of phenolic and protein structures. Furthermore, the band at 1401 $cm^{-1}$ likely originates from C–H deformation vibrations in alkanes and alkenes, or from C–C structure stretching within aromatic systems[55,56]. Additional characteristic peaks at 1261 and 1012 $cm^{-1}$ are associated with C–N stretching vibrations of aromatic and aliphatic amine groups, respectively[57,58]. These are likely derived from alkaloids or other nitrogen-containing metabolites such as proteins.

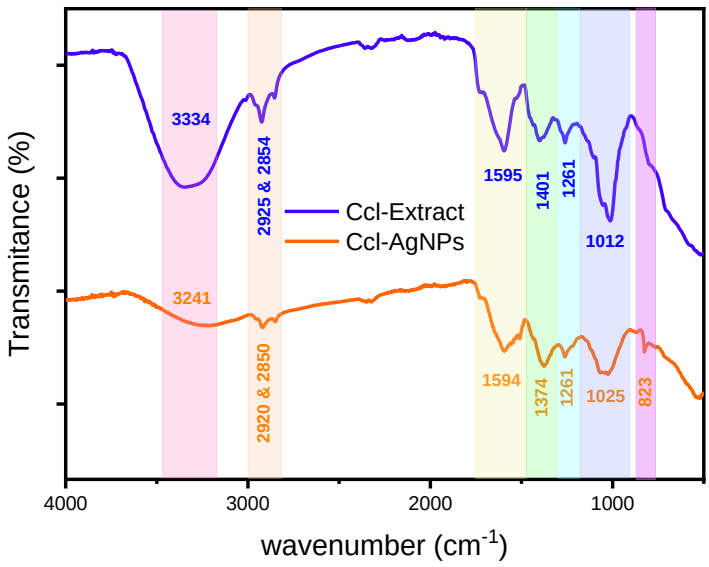


**FIGURE.II. 7.**FTIR spectra recorded for Ccl-extract and Ccl-AgNPs.

The FTIR spectrum of Ccl-AgNPs in Figure.II.7 exhibits a high resemblance to that of the crude Ccl-extract, with some noticeable changes in both the position and intensity of the characteristic absorption bands. These spectral shifts arise from the coordination and interaction of silver ($Ag^+$) ions with specific functional groups of the phytochemicals, which not only catalyze the reduction process but also provide spatial and electrostatic stability to the emerging NPs, preventing agglomeration. In the case of Ccl-AgNPs, the hydroxyl (–OH) stretching vibration and C–H stretching peaks shifted to lower wavenumbers and appeared with reduced intensity at 3241, 2920, and 2850 $cm^{-1}$, respectively. This attenuation compared to the Ccl-extract spectrum is due to the reduced availability of these functional moieties, resulting from their consumption during NPs formation[59]. Prior reports have confirmed the pivotal role of

hydroxyl groups in the biosynthesis of metallic-NPs: $Ag^+$ ions are reduced to metallic silver ($Ag^0$) by electron donation resulting from hydrogen bond breakage and oxidation of OH groups to carbonyl derivatives (R–C=O)[60,61].

There was also a significant shift in the characteristic bands at 1401 and 1012 $cm^{-1}$ that appeared in the spectrum of Ccl-AgNPs at 1374 and 1025 $cm^{-1}$, respectively, indicating the participation of aliphatic side chains and aromatics of heteroatom-rich groups of flavonoids and proteins in the reduction and stabilization processes. Additionally, the appearance of a weak new band at 821 $cm^{-1}$ is related to the C–H out-of-plane bending vibrations of the aromatic rings of the polyphenolic components. Overall, FTIR findings confirm the contribution of multiple classes of phytometabolites from the *C. criticum* leaf extract, including alcohols, phenols, flavonoids, alkaloids, and proteins, to the reduction, nucleation, and stabilization of AgNPs. The strong chelating capacity of the hydroxyl groups of polyphenols enables them to serve as primary reducers of silver ions. Meanwhile, the carbonyl group binds to and surrounds metals with high efficiency[62]. Proteins and amino acids then bind to the AgNPs via free amino groups ($–NH_2$) to form a natural coating layer that provides steric barriers and long-lasting colloidal stability[63].

***2. XRD examination***

The XRD pattern (Figure.II.8) demonstrates the crystalline nature of the biosynthesized Ccl-AgNPs, revealing the characteristic Bragg reflections typical of metallic silver. Five prominent diffraction peaks appeared at 2θ values of 38.15°, 44.10°, 64.39°, 77.30°, and 81.57°, which could be assigned to the (111), (200), (220), (311), and (222) crystal planes, respectively, consistent with the standard diffraction data for face-centered cubic (fcc) silver (ICSD file number 98-005-3761). Among these reflections, the (111) plane had the highest intensity, indicating a preferential direction of crystal growth in the NPs that occurred mainly along the (111) direction. This preferential orientation and dominance during nanoparticle formation is related to the thermodynamic stability of the (111) face, which typically possesses the lowest surface energy among the low-index planes of ccf metals[64,65].Furthermore, the Debye-Scherrer equation (Equation (1)) was used to calculate the average crystallite size of Ccl-AgNPs:

$$D = K\lambda/\beta \cos\theta \qquad (1)$$

where K is the Scherrer constant, λ is the wavelength of the X-ray source employed (commonly Cu Kα radiation, λ = 1.5406 Å), β corresponds to the full width at half maximum (FWHM) of the diffraction peak, θ denotes the Bragg angle, and D represents the mean

crystallite size. Based on this calculation for the most intense (111) reflection, the average crystallite size of the synthesized AgNPs was determined to be approximately 24.3 nm.

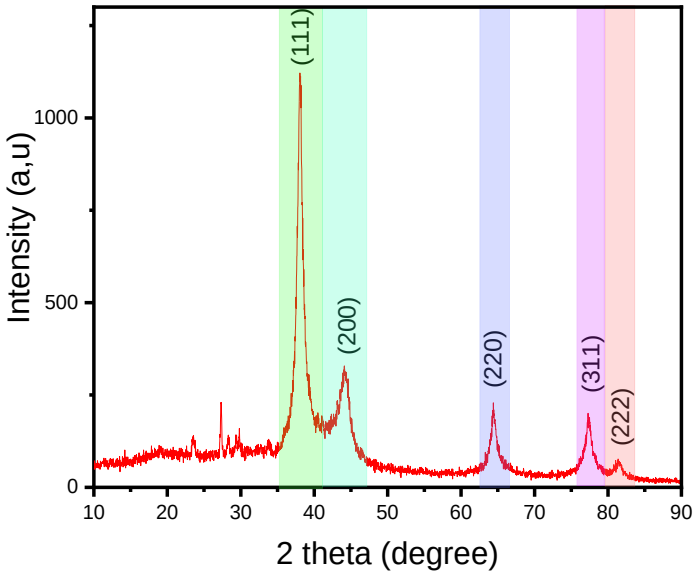


**FIGURE.II. 8.**XRD diffractogram of the bioginic Ccl-AgNPs.

***3. morphological and spectral analyses (SEM-EDX)***

Figure.II.9 (a) and (b) display scanning electron micrographs of green-synthesized Ccl-AgNPs recorded at two different magnifications. The low-magnification image (4 µm) provides an overview of the Ccl-AgNPs morphology, showing clusters of NPs. This clustering, which typically occurs in biosynthesized nanostructures, is likely related to interactions between the concentrated AgNPs and residual phytochemical biomolecules[66]. The organic molecules promote the affinity of the particles thanks to hydrogen bonds, electrostatic interactions, and van der Waals forces. In contrast, the higher-magnification micrograph (Figure.II.9(b)) reveals bright white spots corresponding to the silver nanoparticles. The brightness arises from the high electron density of metallic silver, which enhances the contrast of backscattered electrons in the SEM imaging[67]. The observed spots confirm a predominantly spherical shape of the particles, which is consistent with the UV-vis spectroscopy findings described earlier. Furthermore, some localized agglomerations appear, possibly due to solvent evaporation during synthesis and drying, or mechanical stress and compression caused by centrifugation and subsequent powdered processing[68].

Moreover, a dimensional quantitative assessment of the NPs' size distribution was performed using ImageJ software applied to ESEM micrographs[69,70]. As illustrated in Fig. 5(c),

the particle size histogram of Ccl-AgNPs exhibits sizes ranging from 15 to 60 nm, with an average particle diameter of approximately 32 nm. This estimated mean value closely matches the crystal size determined by XRD. The latter was calculated through the Scherrer equation, which correlates the broadening of the (111) diffraction peak with the dimensions of coherently diffracting crystalline domains[71,72]. Unlike XRD, which provides crystal size, SEM provides a direct visualization of the morphology and dimensions of whole particles. Since an individual nanoparticle may consist of a single crystal or several crystals clustered together, minor discrepancies between SEM and XRD-derived measurements are to be expected.

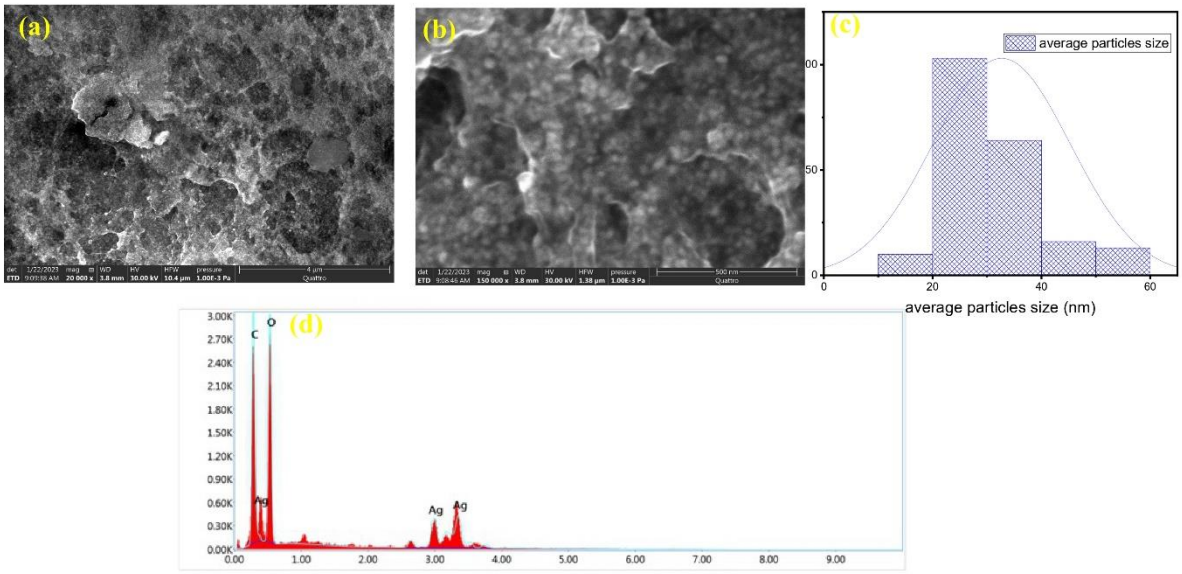


**FIGURE.II. 9.**(a, b) SEM images of Ccl-AgNPs captured at varying magnifications; (c) histogram illustrating the particle size distribution; and (d) EDS elemental composition profile of Ccl-AgNPs.

EDS analysis allows the verification of the crystalline properties and elemental composition of AgNPs. Characteristically, EDS is a widely employed technique for determining the elemental makeup of metallic NMs, providing distinctive spectral peaks that represent fingerprints of specific elements. In the case of nanosilver, it is well established that spherical AgNPs exhibit distinct optical peaks in the 2.7–3.4 keV range arising from the excitation of SPR[73,74]. The EDX-ray spectroscopy spectrum (Figure.II.9(d)) revealed prominent silver peaks located near 3 keV, validating the successful biological synthesis of crystalline AgNPs. Alongside the silver signals, prominent carbon and oxygen peaks were observed in the EDS spectrum, which are attributed to organic molecules from secondary metabolites derived from the Ccl-extract. In addition, quantitative analysis (Table.II.4) indicated that the relative weight percentages of silver, carbon, and oxygen were 24.68%, 30.48%, and 44.85%, respectively.

This compositional pattern strongly supports the formation of hybrid organic-metallic nanoparticles, wherein metallic silver cores are encapsulated by a surrounding layer of phytochemicals, enhancing colloidal stability and imparting additional bioactive properties and biocompatibility[75].

**TABLE.II.4.**Elemental profile of Ccl-AgNPs

| Element | Weight % | Atomic % | Error % | Net Int. | R | A | F |
|---|---|---|---|---|---|---|---|
| C K | 30.48 | 45.56 | 8.01 | 269.87 | 0.8871 | 0.4730 | 1.0000 |
| O K | 44.85 | 50.33 | 9.65 | 312.83 | 0.9012 | 0.3131 | 1.0000 |
| Ag L | 24.68 | 4.11 | 4.85 | 74.89 | 0.9524 | 0.9663 | 1.0040 |

***4. Thermogravimetric analysis***

Thermogravimetric analysis (TGA) was employed to evaluate the thermal behavior, degradation pattern, and surface chemistry of bioproduced AgNPs across different temperature conditions, as well as to confirm the presence of organic capping agents derived from plant metabolites on their surfaces. The thermogram of Ccl-AgNPs exhibited a multi-step decomposition pattern extending from ambient temperature to 1000°C, reflecting three consecutive weight-loss processes caused by moisture content, volatile compounds, weakly chemical bond cleavage, and degradation of the surface-associated organic matter[76]. The initial mass loss at temperatures below 133°C is estimated to be 4.24%, which is mainly due to the evolution of moisture from physically adsorbed water molecules and the evaporation of low-boiling volatiles on the surface of Ccl-AgNPs. A second significant weight loss of 29.56% was recorded between 133 and 350 °C, attributed to the thermal decomposition of plant-derived secondary metabolites acting as surface-coating agents. At temperatures exceeding 350 °C, a predominant weight loss of 31.92% was achieved, linked to the breakdown of more heat-resistant organic species, including oxyaromatic compounds[77]. The persistence of the remaining organic matter at elevated temperatures suggests strong interactions between the biomolecules layer and the NPs surface. Furthermore, the TGA profile not only provides evidence of the thermal and physicochemical stability of the NPs but also enables the measurement of the organic-to-inorganic ratio, which is a crucial factor for assessing the yield and purity of the NMs[78]. At the maximum temperature of 1000 °C, a constant residue of 34.28% remained, corresponding to pure metallic silver, confirming the metallic crystalline Ag core of the nanoparticles beneath the organic phytochemical layer.

Interestingly, the DSC profile of Ccl-AgNPs presented in Figure 1 exhibits a strong convergence with the TGA-DTA data, where two distinct thermal events were recorded: an

exothermic transition near 338°C and a distinct endothermic peak at approximately 944°C. The exothermic peak is consistent with the second stage of weight loss in the TGA curve and can likely be attributed to the decomposition of phytochemical-derived surfactants, as well as the possibility of a partial crystalline phase transformation within the Ag matrix[79,80]. Conversely, the endothermic phase transition is characteristic of the melting process of metallic silver, reflecting the intrinsic high thermal stability and crystallinity of Ccl-AgNPs.

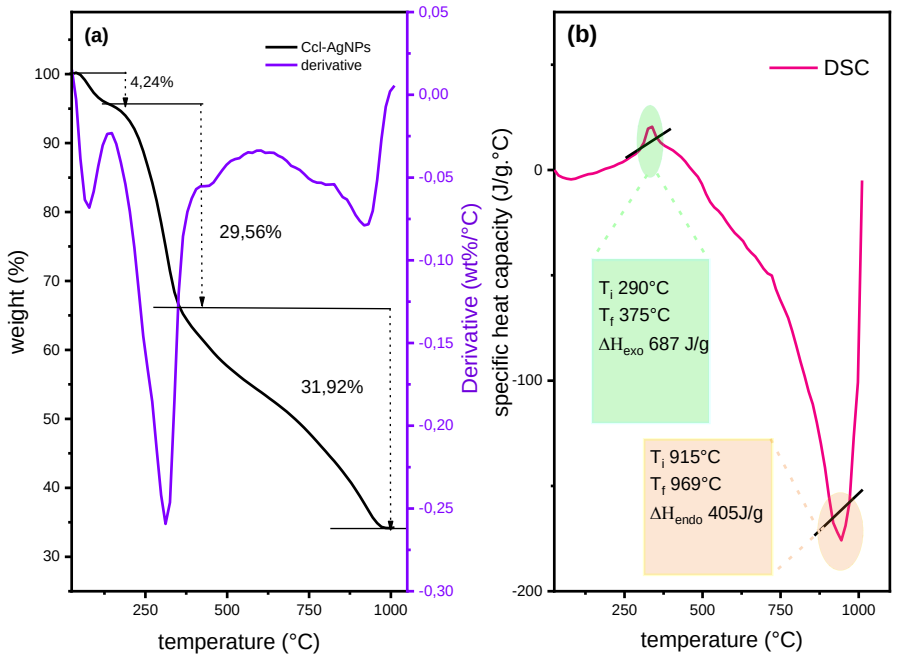


**FIGURE.II. 10**.(a)TGA–DTA plot of Ccl-AgNPs; and (b) corresponding DSC curve.

## II.4. Conclusion

In conclusion, these experimental findings confirmed the potential of *C. criticum* leaf extract as a simultaneous reducing and capping agent in a sustainable, green, and safer nanotechnological route for the bioproduction of silver nanoparticles. The aqueous extraction of secondary metabolites from the leaves was valorized using single-factor experiments on key extraction parameters such as temperature and feed-to-distilled water ratio to determine the optimal conditions for achieving the highest yield of total phenolic and flavonoid content. To further optimize nanoparticle formation, a "one-factor-at-a-time" strategy was employed to regulate and control synthesis parameters, aiming to maximize nanoparticle yield, stability, and dispersion. The progress of the reduction reaction and NPs growth was closely monitored through UV-vis spectroscopy. The optical properties, crystal and morphological structure, and thermal and chemical stability of the optimized Ccl-AgNPs were characterized: FTIR data

revealed the involvement of phytochemicals in both ion reduction and surface passivation; TGA and EDS analyses confirmed the formation of a robust organic layer surrounding the AgNPs; the XRD pattern indicated an fcc crystal structure for the silver; and DSC profile supported the crystalline nature of the Ccl-AgNPs. Meanwhile, SEM assessment revealed the morphology of AgNPs consisting of dispersed clusters of spherical particles with an average size of 32 nm. Taken together, these results underscore the integrated and advanced properties of Ccl-AgNPs, highlighting their potential applications in diverse fields, particularly in pharmaceuticals, environmental remediation, and food safety monitoring. The next chapter will discuss and evaluate these application areas in more detail.

## References


1. Dresler S, Szymczak G, Wójcik M. Comparison of some secondary metabolite content in the seventeen species of the Boraginaceae family. *Pharmaceutical Biology*. 2017;55(1):691-695. doi:10.1080/13880209.2016.1265986

2. Menghini L, Ferrante C, Zengin G, Mahomoodally MF, Leporini L, Locatelli M, Cacciagrano F, Recinella L, Chiavaroli A, Leone S, Brunetti L, Orlando G. Multiple pharmacological approaches on hydroalcoholic extracts from different parts of *Cynoglossum creticum* Mill. (Boraginaceae). *Plant Biosystems - An International Journal Dealing with all Aspects of Plant Biology*. 2019;153(5):633-639. doi:10.1080/11263504.2018.1527790

3. Methacanon P, Krongsin J, Gamonpilas C. Pomelo (Citrus maxima) pectin: Effects of extraction parameters and its properties. *Food Hydrocolloids*. 2014;35:383-391. doi:10.1016/j.foodhyd.2013.06.018

4. Herrera-Marín P, Fernández L, Pilaquinga F. F, Debut A, Rodríguez A, Espinoza-Montero P. Green synthesis of silver nanoparticles using aqueous extract of the leaves of fine aroma cocoa Theobroma cacao linneu (Malvaceae): Optimization by electrochemical techniques. *Electrochimica Acta*. 2023;447:142122. doi:10.1016/j.electacta.2023.142122

5. Singleton VL, Orthofer R, Lamuela-Raventós RM. [14] Analysis of total phenols and other oxidation substrates and antioxidants by means of folin-ciocalteu reagent. In: *Methods in Enzymology*. Vol 299. Elsevier; 1999:152-178. doi:10.1016/S0076-6879(99)99017-1

6. Turkoglu A, Duru ME, Mercan N, Kivrak I, Gezer K. Antioxidant and antimicrobial activities of Laetiporus sulphureus (Bull.) Murrill. *Food Chemistry*. 2007;101(1):267-273. doi:10.1016/j.foodchem.2006.01.025

7. Hamedi S, Shojaosadati SA. Rapid and green synthesis of silver nanoparticles using Diospyros lotus extract: Evaluation of their biological and catalytic activities. *Polyhedron*. 2019;171:172-180. doi:10.1016/j.poly.2019.07.010

8. Kushwah M, Bhadauria S, Singh KP, Gaur MS. Antibacterial and Antioxidant Activity of Biosynthesized Silver Nanoparticles Produced by *Aegle marmelos* Fruit Peel Extract. *Analytical Chemistry Letters*. 2019;9(3):329-344. doi:10.1080/22297928.2019.1626279

9. Roeder E, Liu K, Mtterlein R. Quantitative photometrische Bestimmung der Pyrrolizidinalkaloide in Symphity Radix. *Fresenius J Anal Chem*. 1992;343(8):621-624. doi:10.1007/BF00324124

10. Elangovan K, Elumalai D, Anupriya S, Shenbhagaraman R, Kaleena PK, Murugesan K. Phyto mediated biogenic synthesis of silver nanoparticles using leaf extract of Andrographis echioides and its bio-efficacy on anticancer and antibacterial activities. *Journal of Photochemistry and Photobiology B: Biology*. 2015;151:118-124. doi:10.1016/j.jphotobiol.2015.05.015

11. Verma. PHYTOCHEMICAL AND PHARMACOLOGICAL EVALUATION OF SELECTED PLANTS. *American Journal of Biochemistry and Biotechnology*. 2013;9(3):291-299. doi:10.3844/ajbbsp.2013.291.299

12. A.M L, R A, M.S I, M.Y K, A K, M N. Phytochemical Analysis and Thin Layer Chromatography Profiling of Crude Extracts from Senna Occidentalis(Leaves). Cao X, ed. *JBBS*. 2019;2(1):12-21. doi:10.14302/issn.2576-6694.jbbs-19-2791

13. Yadav R, Agarwala M. Phytochemical analysis of some medicinal plants. *Journal of Phytology*. Published online 2011.

14. Mokrani A, Madani K. Effect of solvent, time and temperature on the extraction of phenolic compounds and antioxidant capacity of peach (Prunus persica L.) fruit. *Separation and Purification Technology*. 2016;162:68-76. doi:10.1016/j.seppur.2016.01.043

15. Anokwuru CP, Anyasor GN, Ajibaye O, Fakoya O, Okebugwu P. Effect of extraction solvents on phenolic, flavonoid and antioxidant activities of three nigerian medicinal plants. *Nature and Science*. 2011;9(7):53-61.

16. Alara OR, Abdurahman NH, Olalere OA. Ethanolic extraction of flavonoids, phenolics and antioxidants from Vernonia amygdalina leaf using two-level factorial design. *Journal of King Saud University - Science*. 2020;32(1):7-16. doi:10.1016/j.jksus.2017.08.001

17. Kadir DH. Statistical evaluation of main extraction parameters in twenty plant extracts for obtaining their optimum total phenolic content and its relation to antioxidant and antibacterial activities. *Food Science & Nutrition*. 2021;9(7):3491-3499. doi:10.1002/fsn3.2288

18. Maghsoudlou Y, Asghari Ghajari M, Tavasoli S. Effects of heat treatment on the phenolic compounds and antioxidant capacity of quince fruit and its tisane's sensory properties. *J Food Sci Technol*. 2019;56(5):2365-2372. doi:10.1007/s13197-019-03644-6

19. Predescu NC, Papuc C, Nicorescu V, Gajaila I, Goran GV, Petcu CD, Stefan G. The influence of solid-to-solvent ratio and extraction method on total phenolic content, flavonoid content and antioxidant properties of some ethanolic plant extracts. *Rev Chim*. 2016;67(10):1922-1927.

20. Hamdan S, Daood HG, Toth-Markus M, Illés V. Extraction of cardamom oil by supercritical carbon dioxide and sub-critical propane. *The Journal of Supercritical Fluids*. 2008;44(1):25-30. doi:10.1016/j.supflu.2007.08.009

21. Belwal T, Dhyani P, Bhatt ID, Rawal RS, Pande V. Optimization extraction conditions for improving phenolic content and antioxidant activity in Berberis asiatica fruits using response surface methodology (RSM). *Food Chemistry*. 2016;207:115-124. doi:10.1016/j.foodchem.2016.03.081

22. Stamatopoulos K, Chatzilazarou A, Katsoyannos E. Optimization of Multistage Extraction of Olive Leaves for Recovery of Phenolic Compounds at Moderated Temperatures and Short Extraction Times. *Foods*. 2013;3(1):66-81. doi:10.3390/foods3010066

23. Chew SY, Teoh SY, Sim YY, Nyam KL. Optimization of ultrasonic extraction condition for maximal antioxidant, antimicrobial, and antityrosinase activity from Hibiscus cannabinus

L. leaves by using the single factor experiment. *Journal of Applied Research on Medicinal and Aromatic Plants*. 2021;25:100321. doi:10.1016/j.jarmap.2021.100321

24. Azahar NF, Gani SSA, Mohd Mokhtar NF. Optimization of phenolics and flavonoids extraction conditions of Curcuma Zedoaria leaves using response surface methodology. *Chemistry Central Journal*. 2017;11(1):96. doi:10.1186/s13065-017-0324-y

25. Dymek A, Widelski J, Wojtanowski KK, Vivcharenko V, Przekora A, Mroczek T. Fractionation of Lycopodiaceae Alkaloids and Evaluation of Their Anticholinesterase and Cytotoxic Activities. *Molecules*. 2021;26(21):6379. doi:10.3390/molecules26216379

26. Tempone AG, Pieper P, Borborema SET, Thevenard F, Lago JHG, Croft SL, Anderson EA. Marine alkaloids as bioactive agents against protozoal neglected tropical diseases and malaria. *Nat Prod Rep*. 2021;38(12):2214-2235. doi:10.1039/D0NP00078G

27. Maher P. The Potential of Flavonoids for the Treatment of Neurodegenerative Diseases. *IJMS*. 2019;20(12):3056. doi:10.3390/ijms20123056

28. Farha AK, Yang QQ, Kim G, Li HB, Zhu F, Liu HY, Gan RY, Corke H. Tannins as an alternative to antibiotics. *Food Bioscience*. 2020;38:100751. doi:10.1016/j.fbio.2020.100751

29. Min BS, Miyashiro H, Hattori M. Inhibitory effects of quinones on RNase H activity associated with HIV-1 reverse transcriptase. *Phytother Res*. 2002;16(S1):57-62. doi:10.1002/ptr.808

30. Mohamad Ishak NS, Numaguchi T, Ikemoto K. Antiviral Effects of Pyrroloquinoline Quinone through Redox Catalysis To Prevent Coronavirus Infection. *ACS Omega*. 2023;8(47):44839-44849. doi:10.1021/acsomega.3c06040

31. Osbourn A, Goss RJM, Field RA. The saponins – polar isoprenoids with important and diverse biological activities. *Nat Prod Rep*. 2011;28(7):1261. doi:10.1039/c1np00015b

32. Mroczek T, Widelski J, Glowniak K. Optimization of extraction of pyrrolizidine alkaloids from plant material. *Chemia analityczna*. 2006;51(4):567.

33. Al-Subaie SF, Alowaifeer AM, Mohamed ME. Pyrrolizidine Alkaloid Extraction and Analysis: Recent Updates. *Foods*. 2022;11(23):3873. doi:10.3390/foods11233873

34. Ovais M, Khalil AT, Islam NU, Ahmad I, Ayaz M, Saravanan M, Shinwari ZK, Mukherjee S. Role of plant phytochemicals and microbial enzymes in biosynthesis of metallic nanoparticles. *Appl Microbiol Biotechnol*. 2018;102(16):6799-6814. doi:10.1007/s00253-018-9146-7

35. Noguez C. Surface Plasmons on Metal Nanoparticles: The Influence of Shape and Physical Environment. *J Phys Chem C*. 2007;111(10):3806-3819. doi:10.1021/jp066539m

36. Arul V, Sethuraman MG. Facile green synthesis of fluorescent N-doped carbon dots from Actinidia deliciosa and their catalytic activity and cytotoxicity applications. *Optical Materials*. 2018;78:181-190. doi:10.1016/j.optmat.2018.02.029

37. Ali S, Rahim M, Fazil P, Ahmad MS, Ullah A, Shah MR, Rukh G, Ateeq M, Khattak R, Khan MS, Abu Ali OA, Saleh DI. Synthesis and Photonics Applications of Afzelechin Conjugated Silver Nanoparticles. *Coatings*. 2021;11(11):1295. doi:10.3390/coatings11111295

38. Mahmoud MA, Chamanzar M, Adibi A, El-Sayed MA. Effect of the Dielectric Constant of the Surrounding Medium and the Substrate on the Surface Plasmon Resonance Spectrum and Sensitivity Factors of Highly Symmetric Systems: Silver Nanocubes. *J Am Chem Soc*. 2012;134(14):6434-6442. doi:10.1021/ja300901e

39. Ahn EY, Jin H, Park Y. Assessing the antioxidant, cytotoxic, apoptotic and wound healing properties of silver nanoparticles green-synthesized by plant extracts. *Materials Science and Engineering: C*. 2019;101:204-216. doi:10.1016/j.msec.2019.03.095

40. Wan H, Liu Z, He Q, Wei D, Mahmud S, Liu H. Bioreduction (AuIII to Au0) and stabilization of gold nanocatalyst using Kappa carrageenan for degradation of azo dyes. *International Journal of Biological Macromolecules*. 2021;176:282-290. doi:10.1016/j.ijbiomac.2021.02.085

41. Xiong Y, Wan H, Islam M, Wang W, Xie L, Lü S, Kabir SMF, Liu H, Mahmud S. Hyaluronate macromolecules assist bioreduction (Au III to Au 0 ) and stabilization of catalytically active gold nanoparticles for azo contaminated wastewater treatment. *Environmental Technology & Innovation*. 2021;24:102053. doi:10.1016/j.eti.2021.102053

42. Mie G. Beiträge zur Optik trüber Medien, speziell kolloidaler Metallösungen. *Annalen der Physik*. 1908;330(3):377-445. doi:10.1002/andp.19083300302

43. Shukla S, Masih A, Aryan, Mehata MS. Catalytic activity of silver nanoparticles synthesized using Crinum asiaticum (Sudarshan) leaf extract. *Materials Today: Proceedings*. 2022;56:3714-3720. doi:10.1016/j.matpr.2021.12.468

44. Mountrichas G, Pispas S, Kamitsos EI. Effect of Temperature on the Direct Synthesis of Gold Nanoparticles Mediated by Poly(dimethylaminoethyl methacrylate) Homopolymer. *J Phys Chem C*. 2014;118(39):22754-22759. doi:10.1021/jp505725v

45. Siddiqui MR, Khan M, Khan, Adil, Tahir, Tremel W, Khathlan, Warthan. Green synthesis of silver nanoparticles mediated by Pulicaria glutinosa extract. *IJN*. Published online April 2013:1507. doi:10.2147/IJN.S43309

46. Van Westen T, Groot RD. Effect of Temperature Cycling on Ostwald Ripening. *Crystal Growth & Design*. 2018;18(9):4952-4962. doi:10.1021/acs.cgd.8b00267

47. Gómez-Graña S, Perez-Ameneiro M, Vecino X, Pastoriza-Santos I, Perez-Juste J, Cruz J, Moldes A. Biogenic Synthesis of Metal Nanoparticles Using a Biosurfactant Extracted from Corn and Their Antimicrobial Properties. *Nanomaterials*. 2017;7(6):139. doi:10.3390/nano7060139

48. Raza M, Kanwal Z, Rauf A, Sabri A, Riaz S, Naseem S. Size- and Shape-Dependent Antibacterial Studies of Silver Nanoparticles Synthesized by Wet Chemical Routes. *Nanomaterials*. 2016;6(4):74. doi:10.3390/nano6040074

49. Zhang Y, Chen Y, Westerhoff P, Hristovski K, Crittenden JC. Stability of commercial metal oxide nanoparticles in water. *Water Research*. 2008;42(8-9):2204-2212. doi:10.1016/j.watres.2007.11.036

50. Islam NU, Amin R, Shahid M, Amin M. Gummy gold and silver nanoparticles of apricot (Prunus armeniaca) confer high stability and biological activity. *Arabian Journal of Chemistry*. 2019;12(8):3977-3992. doi:10.1016/j.arabjc.2016.02.017

51. Wang X, Yuan L, Deng H, Zhang Z. Structural characterization and stability study of green synthesized starch stabilized silver nanoparticles loaded with isoorientin. *Food Chemistry*. 2021;338:127807. doi:10.1016/j.foodchem.2020.127807

52. Rein JL, Coca SG. "I don't get no respect": the role of chloride in acute kidney injury. *American Journal of Physiology-Renal Physiology*. 2019;316(3):F587-F605. doi:10.1152/ajprenal.00130.2018

53. Basu S, Ghosh SK, Kundu S, Panigrahi S, Praharaj S, Pande S, Jana S, Pal T. Biomolecule induced nanoparticle aggregation: Effect of particle size on interparticle coupling. *Journal of Colloid and Interface Science*. 2007;313(2):724-734. doi:10.1016/j.jcis.2007.04.069

54. Yaqoob S, Rahim S, Bhayo AM, Shah MR, Hameed A, Malik MI. A Novel and Efficient Colorimetric Assay for Quantitative Determination of Amlodipine in Environmental, Biological and Pharmaceutical Samples. *ChemistrySelect*. 2019;4(34):10046-10053. doi:10.1002/slct.201902334

55. Alamier WM, Hasan N, Syed IS, Bakry AM, Ismail KS, Gedda G, Girma WM. Silver Nanoparticles' Biogenic Synthesis Using Caralluma subulata Aqueous Extract and Application for Dye Degradation and Antimicrobials Activities. *Catalysts*. 2023;13(9):1290. doi:10.3390/catal13091290

56. Uzunuigbe EO, Kappo AP, Mlowe S, Revaprasadu N. Bioinspired Synthesis of Acacia senegal Leaf Extract Functionalized Silver Nanoparticles and Its Antimicrobial Evaluation. Acierno D, ed. *Journal of Nanomaterials*. 2020;2020:1-8. doi:10.1155/2020/6474913

57. El-Naggar NEA, Hussein MH, El-Sawah AA. Bio-fabrication of silver nanoparticles by phycocyanin, characterization, in vitro anticancer activity against breast cancer cell line and in vivo cytotxicity. *Sci Rep*. 2017;7(1):10844. doi:10.1038/s41598-017-11121-3

58. Alahdal FAM, Qashqoosh MTA, Kadaf Manea Y, Salem MAS, Hasan Khan R, Naqvi S. Ultrafast fluorescent detection of hexavalent chromium ions, catalytic efficacy and antioxidant activity of green synthesized silver nanoparticles using leaf extract of P. austroarabica. *Environmental Nanotechnology, Monitoring & Management*. 2022;17:100665. doi:10.1016/j.enmm.2022.100665

59. Singh I, Gupta S, Gautam HK, Dhawan G, Kumar P. Antimicrobial, radical scavenging, and dye degradation potential of nontoxic biogenic silver nanoparticles using Cassia fistula pods. *Chem Pap*. 2021;75(3):979-991. doi:10.1007/s11696-020-01355-3

60. Takcı DK, Ozdenefe MS, Genc S. Green synthesis of silver nanoparticles with an antibacterial activity using Salvia officinalis aqueous extract. *Journal of Crystal Growth*. 2023;614:127239. doi:10.1016/j.jcrysgro.2023.127239

61. Olajire AA, Mohammed AA. Bio-directed synthesis of gold nanoparticles using Ananas comosus aqueous leaf extract and their photocatalytic activity for LDPE degradation. *Advanced Powder Technology*. 2021;32(2):600-610. doi:10.1016/j.apt.2021.01.009

62. Mosaviniya M, Kikhavani T, Tanzifi M, Tavakkoli Yaraki M, Tajbakhsh P, Lajevardi A. Facile green synthesis of silver nanoparticles using Crocus Haussknechtii Bois bulb extract: Catalytic activity and antibacterial properties. *Colloid and Interface Science Communications*. 2019;33:100211. doi:10.1016/j.colcom.2019.100211

63. Udayasoorian C, Kumar KV, Jayabalakrishnan M. Extracellular synthesis of silver nanoparticles using leaf extract of Cassia auriculata. *Dig J Nanomater Biostruct*. 2011;6(1):279-283.

64. Yu BD, Scheffler M. Anisotropy of Growth of the Close-Packed Surfaces of Silver. *Phys Rev Lett*. 1996;77(6):1095-1098. doi:10.1103/PhysRevLett.77.1095

65. Alam MdA, Sadia SI, Shishir MdKH, Bishwas RK, Ahmed S, Al-Reza SMd, Jahan SA. Crystallinity integration and crystal growth behavior study of preferred oriented (111) cubic silver nanocrystal. *Inorganic Chemistry Communications*. 2025;173:113834. doi:10.1016/j.inoche.2024.113834

66. Ssekatawa K, Byarugaba DK, Kato CD, Wampande EM, Ejobi F, Nakavuma JL, Maaza M, Sackey J, Nxumalo E, Kirabira JB. Green Strategy–Based Synthesis of Silver Nanoparticles for Antibacterial Applications. *Front Nanotechnol*. 2021;3:697303. doi:10.3389/fnano.2021.697303

67. Pietrodangelo A, Pareti S, Perrino C. Improved identification of transition metals in airborne aerosols by SEM–EDX combined backscattered and secondary electron microanalysis. *Environ Sci Pollut Res*. 2014;21(6):4023-4031. doi:10.1007/s11356-013-2261-1

68. Srećković NZ, Nedić ZP, Liberti D, Monti DM, Mihailović NR, Katanić Stanković JS, Dimitrijević S, Mihailović VB. Application potential of biogenically synthesized silver nanoparticles using *Lythrum salicaria* L. extracts as pharmaceuticals and catalysts for organic pollutant degradation. *RSC Adv*. 2021;11(56):35585-35599. doi:10.1039/D1RA05570D

69. Salawu EY, Elvis AO, Ajayi OO, Ongbali SO, Afolalu SA. Particle size distribution analysis of carburized HT250 gray cast iron using ImageJ. *Materials Today: Proceedings*. Published online August 2023:S2214785323046011. doi:10.1016/j.matpr.2023.08.321

70. Mazzoli A, Favoni O. Particle size, size distribution and morphological evaluation of airborne dust particles of diverse woods by Scanning Electron Microscopy and image processing program. *Powder Technology*. 2012;225:65-71. doi:10.1016/j.powtec.2012.03.033

71. Vorokh AS. Scherrer formula: estimation of error in determining small nanoparticle size. *Nanosystems: Phys Chem Math*. Published online June 24, 2018:364-369. doi:10.17586/2220-8054-2018-9-3-364-369

72. Ahmad HS, Ateeb M, Noreen S, Farooq MI, Baig MMFA, Nazar MS, Akhtar MF, Ahmad K, Ayub AR, Shoukat H, Hadi F, Madni A. Biomimetic synthesis and characterization of

silver nanoparticles from Dipterygium glaucum extract and its anti-cancerous activities. *Journal of Molecular Structure*. 2023;1282:135196. doi:10.1016/j.molstruc.2023.135196

73. Muthukrishnan S, Bhakya S, Senthil Kumar T, Rao MV. Biosynthesis, characterization and antibacterial effect of plant-mediated silver nanoparticles using Ceropegia thwaitesii – An endemic species. *Industrial Crops and Products*. 2015;63:119-124. doi:10.1016/j.indcrop.2014.10.022

74. Jebril S, Khanfir Ben Jenana R, Dridi C. Green synthesis of silver nanoparticles using Melia azedarach leaf extract and their antifungal activities: In vitro and in vivo. *Materials Chemistry and Physics*. 2020;248:122898. doi:10.1016/j.matchemphys.2020.122898

75. Pai M, Ahmed E, Batakurki S, Kumar SG, Kusanur R. Green synthesis of Palladium magnetic nanoparticles decorated on carbon nanospheres using Chenopodium and their application as heterogenous catalyst in the Suzuki-Miyaura coupling reaction. *Applied Surface Science Advances*. 2023;16:100427. doi:10.1016/j.apsadv.2023.100427

76. George IE, Cherian T, Ragavendran C, Mohanraju R, Dailah HG, Hassani R, Alhazmi HA, Khalid A, Mohan S. One-pot green synthesis of silver nanoparticles using brittle star Ophiocoma scolopendrina: Assessing biological potentialities of antibacterial, antioxidant, anti-diabetic and catalytic degradation of organic dyes. *Heliyon*. 2023;9(3):e14538. doi:10.1016/j.heliyon.2023.e14538

77. Gharari Z, Hanachi P, Sadeghinia H, Walker TR. Eco-Friendly Green Synthesis and Characterization of Silver Nanoparticles by Scutellaria multicaulis Leaf Extract and Its Biological Activities. *Pharmaceuticals*. 2023;16(7):992. doi:10.3390/ph16070992

78. López-Miranda JL, Esparza R, González-Reyna MA, España-Sánchez BL, Hernandez-Martinez AR, Silva R, Estévez M. Sargassum Influx on the Mexican Coast: A Source for Synthesizing Silver Nanoparticles with Catalytic and Antibacterial Properties. *Applied Sciences*. 2021;11(10):4638. doi:10.3390/app11104638

79. Nakkala JR, Mata R, Bhagat E, Sadras SR. Green synthesis of silver and gold nanoparticles from Gymnema sylvestre leaf extract: study of antioxidant and anticancer activities. *J Nanopart Res*. 2015;17(3):151. doi:10.1007/s11051-015-2957-x

80. González-Henríquez CM, Pizarro GDC, Sarabia-Vallejos MA, Terraza CA, López-Cabaña ZE. In situ-preparation and characterization of silver-HEMA/PEGDA hydrogel matrix nanocomposites: Silver inclusion studies into hydrogel matrix. *Arabian Journal of Chemistry*. 2019;12(7):1413-1423. doi:10.1016/j.arabjc.2014.11.012

# *Chapter III*

## *Assessment the performance of Ccl-AgNPs in biopharmaceutcal and analytcal applicatons*

## III.1. Introduction

Silver nanoparticles, particularly those synthesized via plant-mediated routes, have demonstrated tremendous potential applications across diverse scientific and technological domains. These include energy-related systems such as energy harvesting and storage, environmental applications including water purification and pollutant sensing, food and nutrition fields like smart packaging, as well as therapeutic and biomedical applications ranging from gene and drug delivery to bioimaging, bone cement reinforcement, and tissue regeneration[1–4]. In this experimental section, the pharmaceutical applications of Ccl-AgNPs will be explored. Their antioxidant capabilities will be systematically investigated using five complementary in vitro assays; DPPH, ABTS, reducing power, hydroxyl radical scavenging, and phenanthroline assays in order to clarify their free radical scavenging mechanisms of action. The antimicrobial efficacy of Ccl-AgNPs will be further examined through standardized microdilution tests. Moreover, their functionality as an LSPR-based chemosensor for neomycin sulfate detection will be investigated, focusing on the detection mechanism, molecular interactions, sensitivity, selectivity, and practical applicability in real environmental, biological, and veterinary samples.

## III.2. Materials and Procedures

### III.2. 1.Reactive, Bacteria and medications

All chemicals and reagents employed in this study were of analytical research grade to ensure accuracy and reliability of the experimental results. Unless otherwise stated, materials were sourced from Sigma-Aldrich, Fluka Chemie, and Huntsman Corporation. The compounds used included: o-phenanthroline (≥99%), 2,2-diphenyl-1-picrylhydrazyl (DPPH, elemental analysis, ≥90%), butylated hydroxytoluene (BHT, FCC & FG, ≥99%), 2,2′-azino-bis(3-ethylbenzothiazoline-6-sulfonic acid) (ABTS, ≥98%, HPLC grade), ascorbic acid (99%), ferric chloride (puriss. p.a., reag. Ph. Eur., ≥99%), sodium hydroxide (≥97.0%), sodium carbonate (ACS anhydrous, ≥99.5%), calcium chloride (anhydrous, ≥97%), sodium citrate tribasic dihydrate (≥99%, FG), ethylenediaminetetraacetic acid (EDTA, ≥98.0%), urea (ACS reagent, 99.0–100.5%), trichloroacetic acid (TCA, ACS, ≥99.5%), α-tocopherol (≥96%, HPLC grade), potassium persulfate (ACS reagent, ≥99.0%), butylated hydroxyanisole (BHA, ≥98.5%), magnesium nitrate hexahydrate (BioXtra, ≥98%), magnesium sulfate heptahydrate

(ReagentPlus, ≥99.0%), sodium chloride (ACS, ≥99.0%), potassium ferricyanide (99%), citric acid (99.5%, FCC, FG), salicylic acid (ACS reagent grade, ≥99.0%), fructose (≥99%, HPLC), maltose monohydrate (≥95%), lactose (Ph. Eur.), potassium permanganate (ACS reagent, ≥99.0%), and iron(II) sulfate heptahydrate (99%).

Microbial studies were conducted using four standard ATCC bacterial strains were kindly provided by the Pharmaceutical Microbiology Laboratory, Ege University ; Staphylococcus aureus (ATCC 29213), Enterococcus faecalis (ATCC 29212), Pseudomonas aeruginosa (ATCC 27853), and Escherichia coli (ATCC 25922). In addition, a selection of pharmaceutical compounds were incorporated in the sensor tests, provided by BOC Sciences and İlsan İlaç ve Hammaddeleri Sanayi Ticaret A.Ş. (Turkey). These included atenolol, caffeine, capecitabine, dextromethorphan hydrobromide, diclofenac sodium, neomycin sulfate, Nipagin M, paracetamol, propantheline bromide, salbutamol sulfate, sodium valproate, and theophylline.

### III.2.2. Investigating of the Antioxidant Potential of Ccl-AgNPs

#### *1. DPPH Radical Neutralization Test*

The activity of Ccl-extract and Ccl-AgNPs was determined using the (DPPH) radical scavenging assay, as originally described by Blois[5], with slight modifications. In a 96-well microplate, varying concentrations of redispersed Ccl-AgNPs or Ccl-extract (dissolved in distilled water) were mixed with the methanolic DPPH (0.1 mM) solution at a fixed volumetric ratio of 1:4 (sample: DPPH). The reaction mixtures were incubated in the dark at room temperature for 30 minutes to prevent photodegradation of the radical. Following incubation, the decrease in absorbance was recorded at 517 nm. Standard antioxidants, including ascorbic acid, α-tocopherol, BHA, and BHT, were assayed in parallel as positive controls for comparison. The radical scavenging capacity was calculated as a percentage reduction in absorbance relative to a DPPH-only control. The results were expressed as the half-maximal inhibitory concentration ($IC_{50}$), defined as the concentration of Ccl-AgNPs or Ccl-extract (µg/mL) required to quench 50% of the DPPH radicals.

#### *2. ABTS Radical Cation Decolorization Assay*

The ability of Ccl-AgNPs and Ccl-extract in antiradical and decolorize the radical cations ($ABTS^{\bullet+}$) was assessed according to the method described by Re et al.[6], with minor modifications. The $ABTS^{\bullet+}$ working solution was generated by mixing 7 mM ABTS in distilled water with 2.45 mM potassium persulfate, followed by incubation of the mixture in the dark at room temperature for 16 hours to allow complete radical formation. Prior to use, the resulting solution was diluted to an absorbance of 0.700 ± 0.02 at 734 nm. For the assay, 40 µL of

different concentrations of CCl nanoparticles or CCl extract were added separately to 160 µL of the above-prepared cationic solution. The mixtures were incubated in the dark for 10 minutes at room temperature to minimize light-induced degradation. Subsequently, the decrease in absorbance was measured at 734 nm. The scavenging activity was expressed as the concentration required to reduce the $ABTS^{\bullet+}$ absorbance by 50% ($IC_{50}$). Synthetic antioxidants, including BHT and BHA, were included as positive controls for comparison of antioxidant capacity.

***3. Reducing power capacity evaluation***

The reductive potential of Ccl-extrat and its derivative AgNPs was assessed following the procedure of Oyaizu[7], with slight adjustments. Briefly, 10 µL of Ccl-AgNPs at different concentrations were combined with 40 µL of phosphate buffer (200 mM, pH 6.6) and 50 µL of potassium ferricyanide solution (10 g/L). The reaction mixture was incubated at 50 °C for 20 minutes to facilitate the reduction process. After incubation, 50 µL of trichloroacetic acid solution (10%, w/v) was added to terminate the reaction, followed by the sequential addition of 40 µL of distilled water and 10 µL of ferric chloride solution (1.0 g/L). The resulting mixture was thoroughly mixed, and absorbance was recorded at 700 nm. The reducing activity was quantified as the effective concentration corresponding to an absorbance value of 0.50 ($A_{0.5}$), calculated through linear regression analysis of the calibration curve. Standard antioxidants, including catechin, BHT, ascorbic acid, α-tocopherol, and , were assayed in parallel for comparative evaluation.

***4. Phenanthroline-based reducing capacity assay***

The reducing potential of the biogical perapated NMs was further assessed using the 1,10-phenanthroline method as described by Szydłowska-Czerniak et al.[8] with minor changes. In this method, 10 µL of the test Ccl-extract or Ccl-NPs at different concentrations was combined with 50 µL of ferric chloride solution (0.2%, w/v) and 30 µL of 1,10-phenanthroline solution (0.5%, w/v). The reaction volume was adjusted to 200 µL with methanol. The prepared mixtures were incubated at 30 °C for 20 minutes in the dark to prevent light-induced interference, before measuring the absorbance at 510 nm. The reducing capacity of the samples was quantified as the concentration corresponding to an absorbance of 0.50 ($A_{0.5}$, µg/mL). Well-established antioxidant compounds, namely catechin, BHA, ascorbic acid, and BHT, were employed as reference standards for comparative analysis.

***5. Salicylic acid–based hydroxyl radical scavenging assay***

The hydroxyl radical scavenging activity of the extracts and Ccl-AgNPs were determined using the salicylic acid method originally described by N. Smirnoff and Q.J.

Cumbes[9], with modifications to fit a 96-well microplate format. Briefly, 40 µL of the different samples dilitions was added to a reaction mixture consisting of 24 µL of $FeSO_4$ solution (8 mM), 20 µL of hydrogen peroxide solution (20 mM), and 80 µL of salicylic acid solution (3 mM). The mixtures were incubated at 37 °C for 30 min to allow the Fenton reaction to generate hydroxyl radicals, followed by measuring the absorbance of the reaction the hydroxyl salicylate complex products were measured at 510 nm. the finding was expressed as the half-maximal inhibitory concentration ($IC_{50}$), defined as the concentration of extract or Ccl-AgNPs (µg/mL) required to inhibit 50% of hydroxyl radical formation.

### III.2.3. Antibacterial Efficacy of Biosynthesized Ccl-AgNPs

Antimicrobial efficacy of the greener Ccl-AgNPs was assessed through assuming the minimum inhibition concentration (MIC). This was carried out using the broth microdilution approach, adapted in part from Clinical and Laboratory Standards Institute (CLSI) protocols[10]. Four well-characterized reference bacterial strains were selected as model organisms: E. faecalis ATCC 29212, S. aureus ATCC 29213, E. coli ATCC 25922, and P. aeruginosa ATCC 27853. Prior to the assay conducting, bacterial strains were revived and subcultured in Mueller-Hinton broth (MHB) and incubated at 37 °C for 18 h to obtain cultures in the exponential growth phase. The resulting suspensions were then standardized to match the turbidity of a 0.5 McFarland standard using sterile physiological saline as the diluent. These suspensions were subsequently diluted 1:100 in MHB to yield a final inoculum density of ~5 × 10^5 CFU/mL, suitable for microdilution testing.

MIC assays were carried out in sterile, flat-bottom 96-well microtiter plates preloaded with 50 µL of MHB. To initiate the dilution series, 50 µL of the redispersed Ccl-AgNP suspension was dispensed to the first well of each row. Serial two-fold dilutions were subsequently performed along the plate, producing in final nanoparticle concentrations ranging from 15.62 to 1000 µg/ml. Each well then received 50 µl of the prepared bacterial suspension. The inoculated microplates were incubated at 37 °C for 24 h under static conditions. Following incubation period, bacterial growth was assessed by visual inspection of turbidity in each well. The MIC was recorded as the fewest concentration of Ccl-AgNPs that fully inhibited visible growth of the test organism. To provide a comparative baseline, the antimicrobial activity of the Ccl-extract alone was also assessed under identical conditions.

### III.2.4. The potential suitability of Ccl-AgNPs as colorimetric drug sensors.

In order to explore the analytical suitability of Ccl-stabilized silver nanoparticles (Ccl-AgNPs) as nanoscale probes for chemosensing, their interaction with neomycin sulfate (NEO)

and a panel of clinically relevant pharmaceutical compounds was investigated, encompassing β-blockers (atenolol), central nervous system stimulants (caffeine), antineoplastic agents (capecitabine), antitussives (dextromethorphan hydrobromide), nonsteroidal anti-inflammatory drugs (diclofenac sodium), preservatives (methylparaben, known as Nipagin M), analgesics (paracetamol), anticholinergics (propantheline bromide), bronchodilators (salbutamol sulfate and theophylline), and anticonvulsants (sodium valproate). The colloidal suspensions of Ccl-AgNPs were combined with aqueous solutions (1.0 mM) of each pharmaceutical compound. Mixing was carried out in clean test tubes at a fixed volumetric ratio of 1:1 (v/v) under ambient laboratory conditions for several minutes. The preliminary detection of drug-AgNPs interactions with nanoparticles was assessed; visually through observing immediate colorimetric alterations in the colloidal suspensions, and spectroscopically by monitoring the corresponding shifts or intensity variations SPR band of Ccl-AgNPs.

***1. Characterization***

To further understand and gain deeper insight into the mechanism of NEO detection and to elucidate the interactions between this antibiotic and Ccl-AgNPs, the NEO-Ccl-AgNPs complex were isolated and characterized. Specifically, Ccl-AgNPs treated with NEO were subjected to centrifugation at 2,000 rpm for 5 min. The precipitated agglomerats subsequently collected and air-dried under ambient conditions without further purification to preserve their chemical integrity. The dried pellet complexes were analyzed using FTIR (ATR-QATRTM-S spectrometer , Shimadzu, Japan), ESEM-EDS (Quattro S-ESEM instrument, Thermo Fisher Scientific), and XRD ( D8 Advance ECO diffractometer, Bruker AXS).

***2. Processing of environmental and biological test mediums***

The feasibility of the Ccl-AgNP-based colorimetric assay for NEO detection was assessed across different matrices. Tap water were taken from Ege University (Izmir), anddirectly employed, without any additional pretreatment, to prepare neomycin sulfate solutions at concentrations of 10, 30, and 50 µM. Subsequently, these solutions were combined with Ccl-AgNP suspensions at a 1:1 (v/v) ratio, and the variations in absorption intensity and surface plasmon resonance band were recorded.

In parallel, rabbit blood samples were collected obtained from healthy animals housed at the Department of Biopharmaceutics and Pharmacokinetics, Ege University. Plasma was isolated by blood centrifugation at 4,000 rpm for 20 min at 25 °C. For sensing analysis, the plasma was diluted 1:100 with distilled water and subsequently fortified with NEO to obtain final concentrations of 10, 30, and 50 µM. Each spiked plasma sample was then combined with an equal volume of Ccl-AgNP colloidal, after which the optical responses were recorded by

UV–vis spectroscopy. The percentage recovery of NEO was determined using the standard recovery equation.

$$Recovery = (\text{founded NEO concentration}/added\ NEO\ concentration) \times 100 \quad (1)$$

***3. Examination of veterinary medicine preparation***

To validate the applicability of the proposed Ccl-AgNP probe in practical settings, its sensing response was examined using a real veterinary pharmaceutical product. For this purpose, Neoxyvit-AL, a commercially available powder formulation containing 30 mg/g of neomycin sulfate, was selected. A series of NEO concentrations were prepared by dissolving accurately weighed amounts of the drug in distilled water. The solutions were afterwards treated with colloidal Ccl-AgNP under the same experimental conditions as those used for standard reference samples. The optical behavior of the mixtures was characterized photospectroscopy.

## III.3. Results

### III.3.1. Antioxidant Capacity and Efficacy of Ccl-AgNPs

The importance of flavonoids and phenolic compounds, as major classes of plant-derived secondary metabolites, lies in the fact that their concentration and chemical profile directly govern the reaction pathway and kinetics of silver ion reduction. They also have a crucial influence on the morphology of the resulting NPs, determining parameters such as average size, surface charge, and electrostatic stability within the colloidal system[11]. Experimental quantification revealed that Ccl-AgNPs exhibited high levels of bioactive compounds, with a total phenolic content (TPC) of 246.15 ± 6.73 µg GAE/mg Ccl-AgNPs and a total flavonoid content (TFC) of 143.61 ± 3.5 µg QE/mg Ccl-AgNPs. This high phytochemical load strongly supports the formation of smaller and more homogeneous AgNPs, limiting the overgrowth of particles by stabilizing the emerging Ag nuclei[1]. Notably, these values were markedly higher than those measured in the crude Ccl-extract, which contained 181.55 µg GAE/mg (TPC) and 109.58 µg QE/mg (TFC). This enrichment suggests preferential adsorption and incorporation of phenolic and flavonoid moieties onto the NPs surface during the synthesis process. Similar results have been documented in previous reports observing this phenomenon, which may be attributed to the higher bulk density of the AgNPs compared to the aqueous extract[12].

To ensure a reliable evaluation of the antioxidant efficacy of Ccl-AgNPs, five complementary assays were employed, namely DPPH, ABTS, reducing power, phenanthroline,

and hydroxyl radical scavenging tests. The use of multiple approaches was essential given the phytochemically complex nature of Ccl-AgNPs, which contain diverse classes of bioactive compounds acting through different antioxidant pathways. This multi-assay framework provides a more comprehensive understanding of the antioxidant mechanisms attributed to both the AgNPs core and its phytochemical shell. The results, expressed as $IC_{50}$ and $A_{0.5}$ values, are summarized in Table.III.1.

The DPPH radical scavenging experiment clearly revealed that Ccl-AgNPs possessed a considerable antioxidant effect, recording an $IC_{50}$ value of 20.62 ± 0.13 µg/mL. This effect was notably stronger than that of that of its counterpart Ccl-extract ($IC_{50}$: 30.99 ± 0.16 µg/mL), suggesting that the incorporation of metallic Ag nuclei enhanced the free radical-quenching efficiency of the extract. Despite this, the activity was still inferior when compared with standard antioxidants. Specifically, synthetic stabilizers BHA ($IC_{50}$: 6.14 ± 0.41 µg/mL) and BHT ($IC_{50}$: 12.99 ± 0.41 µg/mL), as well as natural antioxidants α-tocopherol ($IC_{50}$: 13.02 ± 5.17 µg/mL) and ascorbic acid ($IC_{50}$: 14.47 ± 0.61 µg/mL), displayed superior efficacy. A comparable pattern was observed in the $ABTS^+$ radical assay: Ccl-AgNPs showed a moderate blue-green chromophore decolorization capacity with an $IC_{50}$ of 39.25 ± 3.51 µg/mL, which was substantially less effective than the potent activity BHT and BHA.

Hydroxyl radicals ($^{\bullet}OH$) are recognized as one of the most damaging reactive oxygen species, represent a major contributor to oxidative stress and can readily induce structural damage to vital biomolecules, particularly DNA. For this reason, assessing the effectiveness of antioxidants compounds to neutralize $^{\bullet}OH$ is considered essential. The hydroxyl radical scavenging assay employing salicylic acid as a probe is commonly employed for this purpose. In this assay, hydroxyl radicals generated through the Fenton reaction hydroxylate salicylic acid, yielding dihydroxybenzoic acid (DHA), which can be quantitatively measured[13]. In this system, Ccl-AgNPs exhibited pronounced inhibitory effects on DHA formation, achieving an $IC_{50}$ value of 135.66±0.26 µg/mL, significantly outperforming the Ccl-extract ($IC_{50}$: 306.80±8.40 µg/mL). This improvement is likely related to the distinctive photocatalytic surface activity and electron transfer ability of the AgNPs, which facilitate more efficient interaction with reactive species[14]. Remarkably, scavenging ability of Ccl-AgNPs also exceeded that of standard reference ascorbic acid and Catechin ($IC_{50}$: 326.65±3.22 and 376.39±4.40 µg/mL, respectively).

To further assess the redox potential and electron-donating ability of Ccl-AgNPs, two complementary tests were employed: the ferric reductive power and the 1,10-phenanthroline reduction assay. Both methods rely on the transfer of electrons to ferric ions ($Fe^{3+}$), thereby

converting them to their reduced ferrous state ($Fe^{2+}$)[15,16]. In the ferric reducing power test, this transformation is monitored by a visible color shift, as the characteristic yellow hue of $Fe^{3+}$ diminishes as it is reduced to $Fe^{2+}$, which produces a distinctive blue-green coloration. Similarly, in the 1,10-phenanthroline method, the orange-colored tris-complex $[Fe(phen)_3]^{3+}$ undergoes reduction to the more thermodynamically stable chelated $[Fe(phen)_3]^{2+}$ complex, characterized by an intense orange-red . The iron(III) reduction power of Ccl-AgNPs was quantified with an $A_{0.5}$ value of 123.66 ± 2.48 µg/mL, which is weaker than that of the leaves extract itself ($A_{0.5}$ = 83.48±3.26 µg/mL), suggesting that some of the intrinsic reducing constituents of Ccl-extract are more potent than the NPs-bound form. However, the capacity of the positive samples was stronger; α-Tocopherol (34.93±0.38 µg/mL), catechin (28.98±1.17 µg/mL), ascorbic acid (10.41±1.40 µg/mL), and BHA (8.41±0.67 µg/mL). In the phenanthroline assay, Ccl-AgNPs displayed significant activity, with an $A_{0.5}$ concentration of 26.17±3.08 µg/mL, though still weaker than the Ccl-extract (10,28±0,49 µg/mL). By contrast, classical antioxidant standards ascorbic acid, catechin, butylated, BHT, and BHA demonstrated far superior $Fe^{3+}$ reducing in presence of 1,10-phenanthroline efficiencies (Table. III. 1).

Ccl-AgNPs demonstrated significant antioxidant potential, which can be attributed primarily to the redox-active phytochemicals, particularly phenolic compounds, that remain bound to their surface. These biomolecules, known for their ability to donate electrons and hydrogen atoms, act synergistically with the $Ag^0$-core, which itself function as a catalytic center. This combined mechanism enables the colloidal Ccl-AgNPs hybrid to effectively neutralize reactive free radicals and to chelate transition metals, thereby contributing to redox homeostasis and reducing oxidative stress in biological or chemical systems[17–19] . As emphasized by P. Dauthal and M. Mukhopadhyay[20] , the superior antioxidant properties of bioginic-NPs are closely linked to surface phenomena: the extensive NPs interface provides abundant active sites for the adsorption of natural antioxidant phytoconstituents agents, while the nanoscale dimensions ensure a high surface-to-volume ratio that maximizes molecular interactions with free radicals.

**TABLE.III. 1.** Antioxidant performance of Ccl-AgNPs, Ccl-extract, and tested reference standards.

| samples | DPPH assay | ABTS assay | (˙OH) scavenging assay | Reducing power assay | Phenanthroline assay |
|---|---|---|---|---|---|
| | IC50 (µg/mL) | IC50 (µg/mL) | IC50 (µg/mL) | A0.50 (µg/mL) | A0.50 (µg/mL) |
| Ccl-AgNPS | 20,62±0.13 | 39.25±3.51 | 135.66±0.26 | 123.66±2.48 | 26,17±6.22 |
| Ccl-extract | 30.99 ± 0.16 | NT | 306.80±8.40 | 83.48±3.26 | 10,28±0,49 |
| BHA | 6.14±0.41 | 1.29±0.30 | NT | 8.41±0.67 | 0,93±0,07 |
| BHT | 12.99±0.41 | 1.81±0.10 | NT | NT | 2,24±0,17 |
| α-Tocopherol | 13.02±5,17 | NT | NT | 34.93±2.38 | NT |
| Ascorbic acid | 14.47±0.61 | NT | 326.65±3.22 | 10.41±1.40 | 5,86±0,14 |
| Catechin | NT | NT | 376.39±4.40 | 28.98±1.17 | 4,84±0,04 |

All $IC_{50}$ and $A_{0.50}$ values are reported as mean ± SD based on triplicate independent measurements; NT indicates that the compound was not tested.

### III.3.2. Antibacterial Potential of Ccl-AgNPs and Their Mechanism

Research on the biomedical applications of AgNPs has reinforced the long-established use of bulk silver in combating bacterial infections and has further highlighted the novel enhanced potential of its nanoscale in addressing the pressing challenge of multidrug-resistant (MDR) pathogens[21,22]. Green biosynthesis could be a sustainable alternative process that contributes to reducing the potential toxic and cytotoxicity, bio-existent, ecological persistence effects of AgNPs. In the present envestigation, the antibacterial efficacy of Ccl-AgNPs and *C. creticum* leaves extract was evaluated against four American Type Culture Collection bacterial strains through the standardized microdilution assay. The results, summarized in Table.III.2, demonstrated that the Ccl-AgNPs exhibited the strongest inhibitory activity against the Gram-negative bacterium P. aeruginosa, achieving a MIC of 31.25 µg/ml. For the remaining tested strains E. faecalis, E. coli, and S. aureus, inhibition was achieved at the lowest concentration of62.5 µg/ml, indicating a consistent antibacterial effect, albeit somewhat low.

In contrast, the crude C. creticum leaf extract alone did not display any inhibitory activity for all four strains at the tested concentrations, suggesting the absence of inherent antibacterial compounds or cytotoxic agents, and highlighting the non-toxic nature of the plant extract employed in AgNPs synthesis. These findings collectively underscore the role of green-synthesized silver nanoparticles as promising antimicrobial agents, with a particular emphasis on their pronounced activity against Gram-negative pathogens; the Pseudomonas aeruginosa emerging as the most susceptible organism among the strains tested. These observation aligns with earlier reports demonstrating that green-synthesized AgNPs, particularly those mediated

by plant extracts, tend to exhibit superior antibacterial activity against Gram-negative bacteria compared to Gram-positive counterparts[2,23,24] .

Despite extensive investigations, the precise antibacterial mechanisms of silver nanoparticles (AgNPs) remain only partially understood[25]. Current evidence suggests that AgNPs exert their effects through multiple, interconnected pathways based on physicochemical interactions at both the cell surface and within the cell. One of the primary mechanisms involves the electrostatic interaction between positively charged Ag+ ions released from AgNPs and negatively charged functional groups such as phosphates and thiols present in bacterial cell walls and membranes. This interaction disrupts membrane integrity, increases permeability, and ultimately leads to structural deformation and eventual rupture[26,27] . The differing susceptibilities of Gram-positive and Gram-negative bacteria are largely explained by their cell wall architectures: the thick and multilayered peptidoglycan matrix of Gram-positive bacteria limits silver ion access, whereas the thinner peptidoglycan layer and lipopolysaccharide-rich outer membrane envelope of Gram-negative bacteria facilitate greater AgNPs attachment and penetration[28,29].

In addition to surface-level interactions, the nanoscale size and spherical or semi-spherical morphology of AgNPs provide a high surface area, enhancing their ability to interact with microbial cells and penetrate the intracellular environment[30] . Once internalized, AgNPs and thier Ag+ ions can catalyze the generation of reactive oxygen species (ROS), including free radicals, which induce oxidative stress and compromise essential biomolecular functions. Simultaneously, AgNPs interfere with cellular respiration, promote adenosine triphosphate (ATP) depletion, and impair key genetic processes by preventing DNA replication and inhibiting cell division and proliferation[31–34].

**TABLE.III.2.** Results of mcrodilution assays for Ccl-AgNPs and Ccl-NPs against ATCC bacterial.

| Simples concentration (µg/mL) | Bacterial growth | | | | | | | |
|---|---|---|---|---|---|---|---|---|
| | E. faecalis ATCC 29212 | | S. aureus ATCC 29213 | | E. coli ATCC 25922 | | P. aeruginosa ATCC 27853 | |
| | Ccl-AgNPs | Ccl-extract | Ccl-AgNPs | Ccl-extract | Ccl-AgNPs | Ccl-extract | Ccl-AgNPs | Ccl-extract |
| 15.625 | + | + | + | + | + | + | + | + |
| 31.25 | + | + | + | + | + | + | - | + |
| 62.5 | - | + | - | + | - | + | - | + |
| 125 | - | + | - | + | - | + | - | + |
| 250 | - | + | - | + | - | + | - | + |
| 500 | - | + | - | + | - | + | - | + |
| 1000 | - | + | - | + | - | + | - | + |
| MIN | 62.5 | >1000 | 62.5 | >1000 | 62.5 | >1000 | 31.25 | >1000 |

### III.3.3. Application of Ccl-AgNPs as a Colorimetric Sensing Probe

The applicability of Ccl-AgNPs as a potential as a selective plasmonic sensing probe for pharmaceutical detection examined. For this purpose, the colloidal Ccl-AgNPs suspension was individually exposed to a constant concentration of different pharmaceutical compounds, and the corresponding alterations in the UV–visible absorption spectra were recorded before and after drug addition. As presented in Figure.III.1(a), with the sole exception of neomycin sulfate (NEO), the localized SPR band of Ccl-AgNPs remained essentially unaffected by most analytes, indicating negligible NPs interaction with tested drugs. In contrast, the exposure to NEO produced a pronounced decrease in absorbance intensity, accompanied by a distinct red shift of the maximum absorption wavelength from 424 nm to 451 nm. Such spectral changes were also visually evident: the characteristic brown color of the Ccl-AgNPs suspension rapidly darkened within minutes following NEO addition, ultimately leading to the formation of a brown precipitate, consistent with nanoparticle agglomeration (Figure.III.1(b)). Based on these preliminary observations, the Ccl-AgNPs can be regarded as a promising colorimetric and plasmonic nanosensor for the detection of neomycin.

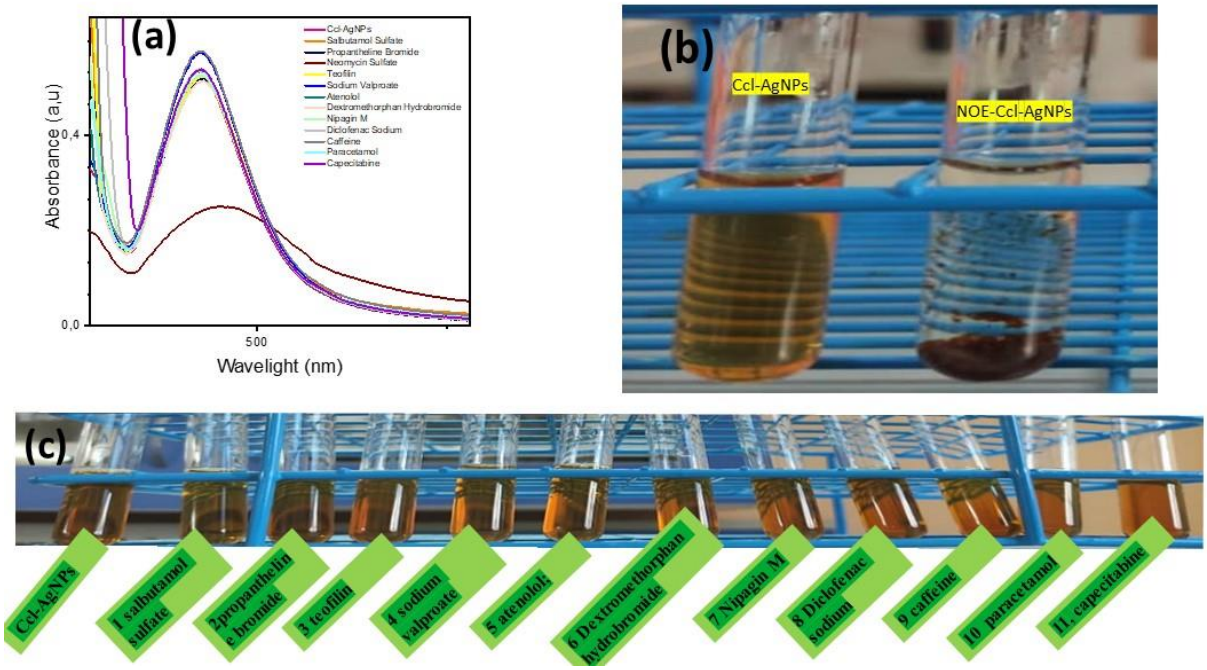


**FIGURE.III. 1.**(a) UV–vis spectra of Ccl-AgNPs after exposure to different pharmaceutical solutions; (b) visible color change of the colloidal Ccl-AgNPs in the presence of neomycin sulfate; and (c) appearance of the colloidal solutions upon interaction with the other tested drugs.

#### *1.Mechanism of NEO detection through Ccl-AgNPs Colorimetric Response*

To further clarify the agglomeration behavior of Ccl-AgNPs in the presence of NEO and to better understand the nature of their interaction, a combination of SEM-EDS, FTIR, and

XRD analyses was employed. The SEM micrographs of NEO-Ccl-AgNPs (Figure.III.2(a, b)) revealed a marked reduction in interparticle spacing, with NPs appearing in clustered and agglomerated forms rather than as well-dispersed pristine Ccl-AgNPs colloids. Such structural agglomeration is consistent with the optical response observed in UV–vis spectroscopy, namely, the reduction in surface SPR intensity and the bathochromic shift of the absorption maximum. These findings corroborate the principle of plasmonic colorimetric sensing via nanoparticle agglomeration, whereby analyte-induced destabilization of colloidal systems[35,36].

Furthermore, the EDS spectrum of the NEO–Ccl-AgNPs complex (Figure.III.2(c)) displayed additional nitrogen and sulfur signals that were not detected in the pristine Ccl-AgNPs profile. The emergence of these elements' peaks, originating from the neomycin molecules, provides direct evidence of their attachment onto the nanoparticle surface[37]. This observation strongly suggests the establishment of specific chemical interactions and possible coordination bonds between the functional groups of neomycin and Ccl-AgNPs.

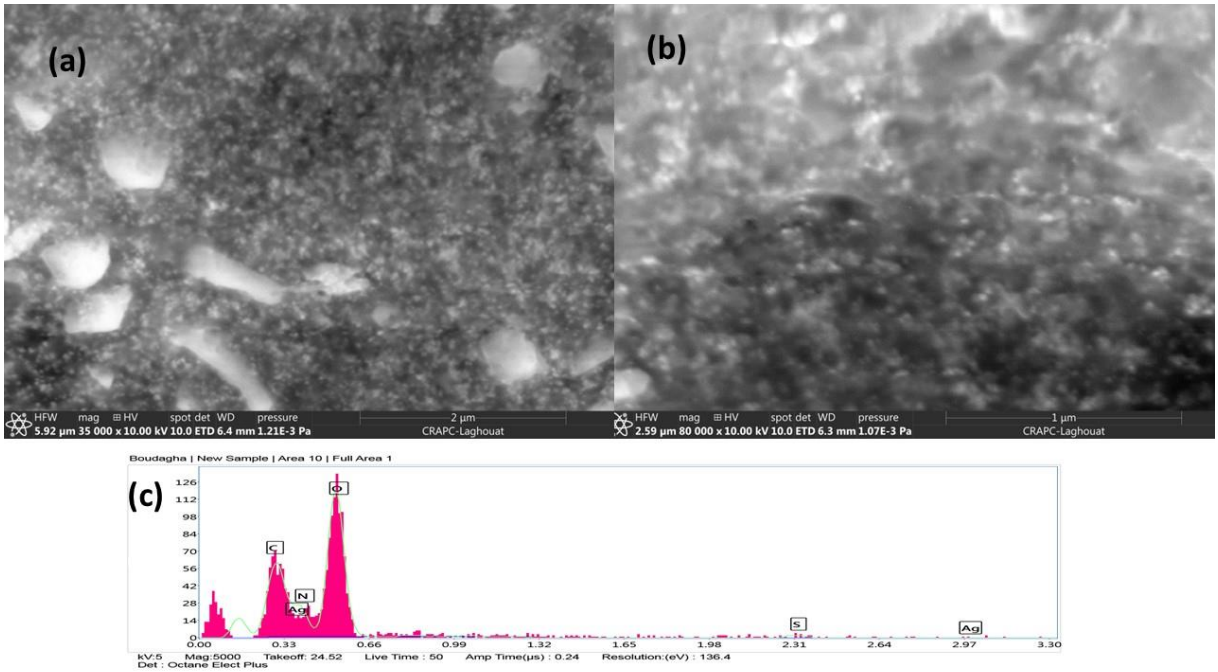


**FIGURE.III. 2.**(a,b) SEM images of NEO-Ccl-AgNPs complxe; and (c) corresponding EDS spectrum.

FT-IR spectra of neomycin sulfate, C. cretum-AgNPs, and their potential conjugate complex (NEO-Ccl-AgNPs) were obtained and are displayed in Figure.III.3. The spectrum of NEO is marked by a broad, prominent, and diffuse absorption band spanning 3600–2400 $cm^{-1}$, which is characteristic of overlapping vibrational modes from multiple functional groups. Specifically, the region between 3600 and 3100 $cm^{-1}$ corresponds to the stretching vibrations of amino (–NH) and hydroxyl (–OH) groups, reflecting the high density of polar functionalities of the polyhydroxylated and aminoglycosidic nature of neomycin[38,39]. The bands observed

between 3000 and 2800 $cm^{-1}$ are assigned to aliphatic C–H stretching vibrations, characteristic of the glycosidic backbone. In the fingerprint region of aminoglycoside antibiotics, the absorption peaks at 1618 and 1521 $cm^{-1}$ are indicative of N–H bending vibrations associated with cycloaliphatic amines[40]. Moreover, a sharp and strong absorption at 1018 $cm^{-1}$ is ascribed to carbon-nitrogen (C–N) stretching vibrations, and a band observed at 606 $cm^{-1}$ is linked to the bending vibrations of the sulfur dioxide ($SO_2$), generated by the counter-ion present in NEO sulfate[41,42].

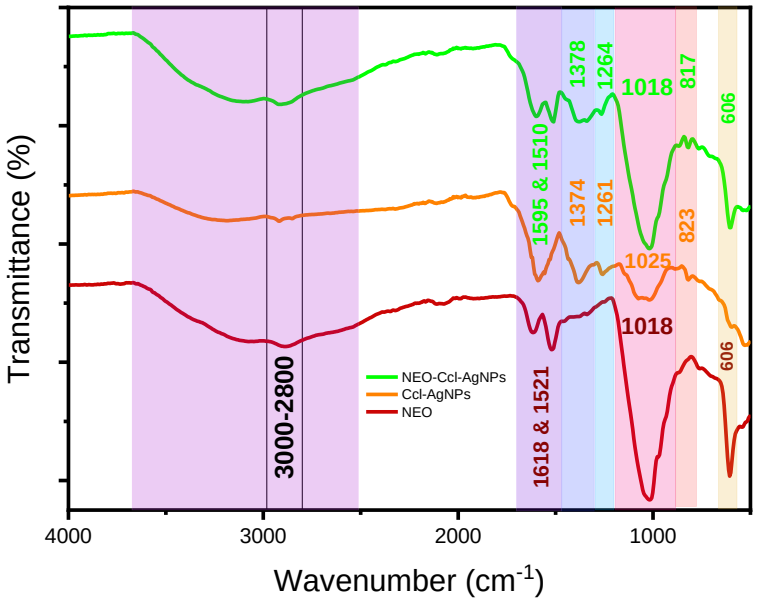


**FIGURE.III. 3.**Comparative FT-IR spectra of neomycin sulfate (NEO), Ccl-AgNPs, and their complex NEO-Ccl-AgNPs.

The FTIR spectrum of the NEO-Ccl-AgNPs complex revealed overlapping features from both NEO and Ccl-AgNPs, accompanied by distinct spectral modifications. Noteworthy, the characteristic aromatic C=C stretching band derived from the Ccl-extract in the Ccl-AgNPs spectrum was absent in the NEO-Ccl-AgNPs spectrum, indicating possible participation of aromatic moieties in the conjugation reaction or their masking by new interactions. Meanwhile, the N–H bending vibrations of neomycin, initially detected at 1618 and 1521 $cm^{-1}$, shifted to lower wavenumbers (1595 and 1510 $cm^{-1}$). Such downshifts are typically associated with changes in the electronic environment of amine groups, suggesting the involvement of nitrogen functionalities and aromatic residues in the binding process[43]. The region between 2800 and 3000 $cm^{-1}$ also exhibited noticeable variations relative to the spectrum of Ccl-AgNPs, consistent with changes in the stretching modes of aliphatic $CH_3$ and $CH_2$ groups, possibly due to altered molecular orientations after complexation[44,45]. Furthermore, the O–H stretching range

also became wider after the interaction of Ccl-Ag nanoparticles with NEO, a phenomenon typically associated with enhanced hydrogen bonding due to strong intermolecular interactions between the hydroxyl and amine groups of neomycin and the surface phenolic -OH groups of Ccl-AgNPs[46,47]. These spectral variations strongly support the agglomeration of Ccl-AgNPs arises from synergistic interactions, including hydrogen bonds, electrostatic attractions, and π–π stacking potential, which lead to the agglomeration of the hybrid nanostructure through the crosslinking associations between the polyphenols, proteins Ccl-extract , and NEO functional groups.

The X-ray diffraction pattern of NEO-Ccl-AgNPs (Figure.III.4) provided further evidence for the sensitization mechanism through agglomeration of AgNPs. The diffraction peaks observed at 2θ = 38.18°, 44.35°, 64.23°, 77.49°, and 81.55° correspond to the (111), (200), (220), (311), and (222) planes of face-centered cubic (fcc) silver (ICSD file No. 98-060-4629). Importantly, these reflections are identical to those observed in the CCl-AgNPs. The persistence of these peaks without significant shift after treatment with NEO suggests that its presence does not disrupt the intrinsic crystal lattice of Ccl-AgNPs, as well as the absence of strong covalent, ionic, or stoichiometric bonding interactions that could otherwise alter the crystalline framework[48,49]. The calculated crystallite size of NEO-Ccl-AgNPs was 24.87 nm, nearly identical to that of Ccl-AgNPs (24.3 nm), which supports the conclusion that the particles preserved their crystalline nature and did not undergo fusion, but rather assembled into larger agglomerated structures. Additionally, a broad hump between 0° and 25° was detected, which is characteristic of amorphous organic compounds, along with a distinct minor peak at 20.19° attributed to amorphous neomycin[50,51]. The appearance of this signal provides direct evidence for the successful surface conjugation of NEO onto Ccl-AgNPs.

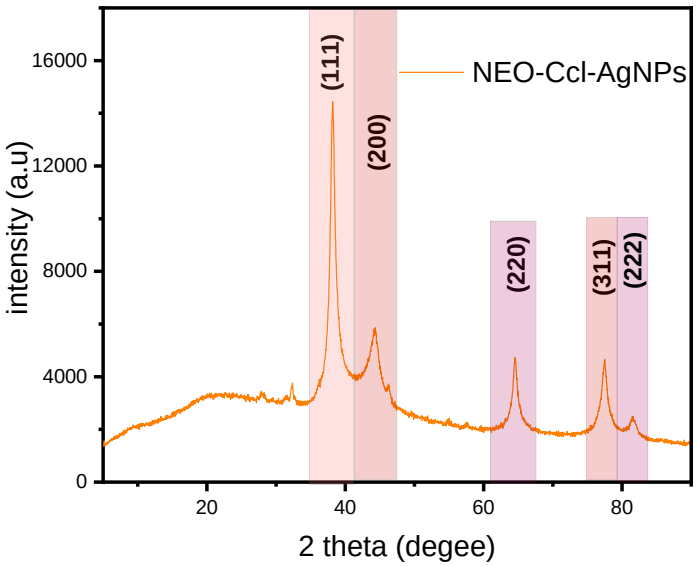


**FIGURE.III. 4**. X-ray diffraction pattern of the NEO-Ccl-AgNPs.

The interaction stoichiometry between Ccl-AgNPs and neomycin (NEO) was further evaluated using the Job plot method of continuous variation[52]. In this approach, the absorbance at 424 nm as a function of the molar fraction of NEO (1mM), while keeping the total molar concentration of the two components constant. The Job plot curve (Figure.III.5) displayed a distinct maximum value at a molar fraction of 0.5, corresponding to the convergence point, which represents maximum complex formation. This finding confirms that the most stable association occurs at an equimolar ratio, indicating a 1:1 binding relationship between Ccl-AgNPs and NEO.

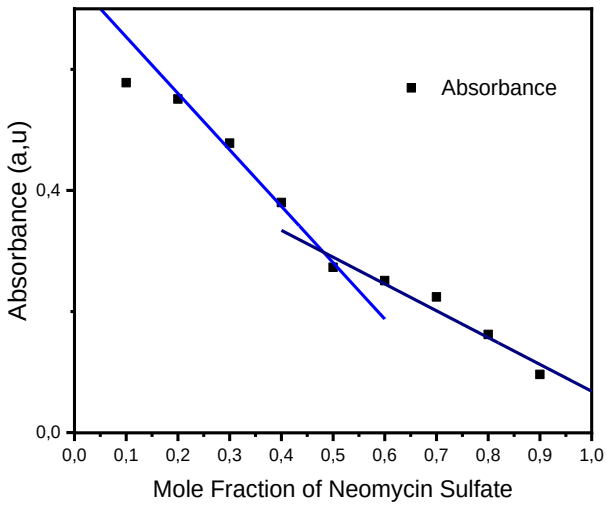


**FIGURE.III.5.**Continuous variation (Job) plot illustrating the stoichiometric interaction between Ccl-AgNPs and NEO.

### *2. Analytical quantification of Neomycin sulfate*

The sensitivity of Ccl-AgNPs toward neomycin (NEO) was quantitatively examined by performing a titration experiment in which different concentrations of NEO (0.01–200 µM) treated with Ccl-AgNPs solutions and monitoring the corresponding alterations in SPR absorption band intensity. As illustrated in Figure.III.6(a,b), the calibration plot of the absorbance at 424 nm versus NEO concentration exhibited outstanding linearity within the dynamic range of 0.5–50 µM, with a regression coefficient of $R^2 = 0.998$, demonstrating the high accuracy and reliability of the sensor response. The analytical sensitivity of Ccl-AgNPs system was further assessed the determination of the limit of detection (LOD), calculated using the standard formula LOD = 3.3 × (standard deviation of intercept/slope)[53]. Based on this approach, the LOD of for NEO was found to be 1.81 µM, indicating the potential application of Ccl-AgNP as a highly sensitive nanoplatform for quantitative detection of neomycin at low micromolar levels.

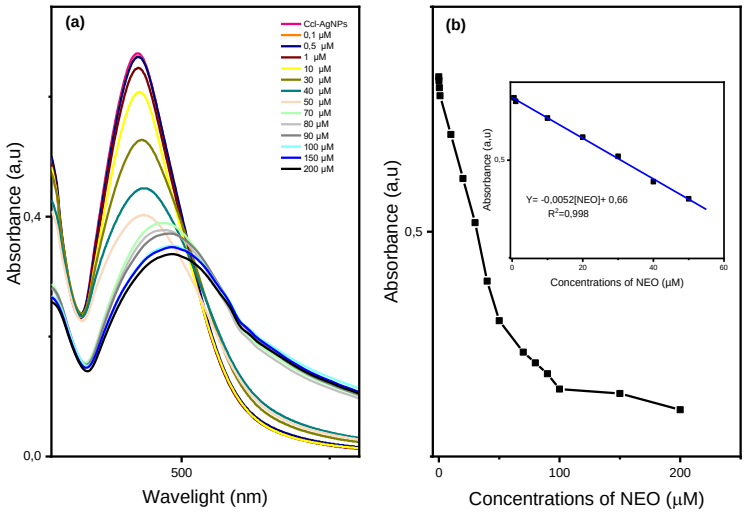


**FIGURE.III. 6.** (a) UV–vis spectra illustrating the spectral response of Ccl-AgNPs upon interaction with different concentrations of NEO; and (b) calibration plot of absorbance at 424 nm as a function of NEO concentration.

### *3. Assessment of interference tolerance*

The selectivity of a sensing probe is a decisive factor for its practical application, as it determines the ability to discriminate the target analyte in the presence of coexisting species and potential interfering agents[54,55]. To assess this property, an interference study was carried out to investigate the selectivity of Ccl-AgNPs toward NEO in the presence of common organic and inorganic constituents typically found in environmental and biological matrices. The tested interferents included major ions abundant in potable water and blood ($Na^+$, $Ca^{2+}$, $K^+$, $NH_4^+$,

$Mg^{2+}$, $Cl^{-}$, $CO_3^{2-}$, and $SO_4^{2-}$)[56,57] as well as representative biomolecules in the blood matrix (fructose, lactose, maltose), metabolites from plasma (ascorbic acid and urea), and anticoagulants widely used in clinical samples and animal blood products (trisodium citrate and ethylenediaminetetraacetic acid-EDTA)[58,59]. For the assay, each interferent (1 mM) was combined with an equimolar concentration of NEO (1 mM) and Ccl-AgNPs in a 1:1:1 volume ratio. As shown in Figure.III.7, the introduction of these coexisting species did not result in noticeable alteration variation in the absorption intensity of the NEO–Ccl-AgNPs complex. This outcome clearly demonstrates the excellent selectivity and anti-interference capability of the colorimetric Ccl-AgNPs sensor, highlighting its potential for reliable detection of neomycin in complex biological and environmental samples.

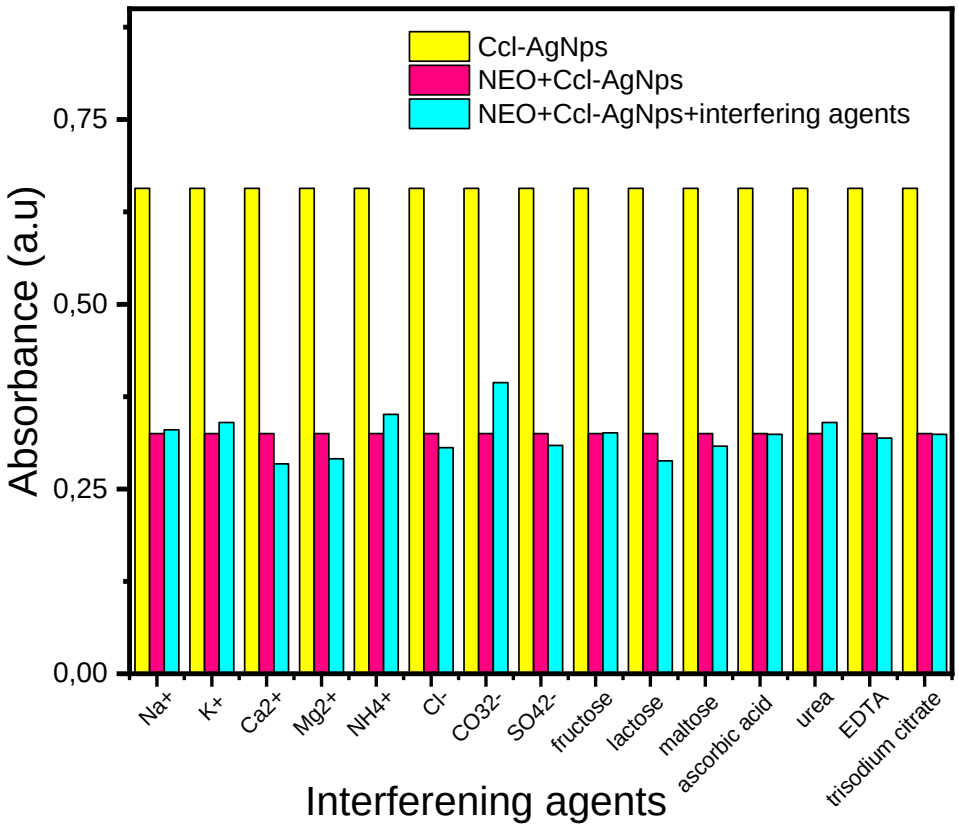


**FIGURE.III. 7.** Effect of various coexisting organic and inorganic interferents on the selective response of Ccl-AgNPs toward NEO.

***4. Detection of NEO in real matrixes***

The practical performance of the Ccl-AgNPs-based colorimetric sensing system for NEO detection was further evaluated using real sample, namely tap water, rabbit blood plasma, and commercial veterinary pharmaceutical. In order to minimize matrix effects, plasma samples were diluted with distilled water prior to analysis, whereas tap water was analyzed directly without pretreatment[60]. Each matrix was spiked with defined concentrations of NEO and subsequently subjected to the established Ccl-AgNPs colorimetric protocol. As illustrated in

the UV–vis spectra (Figure.III.8), exposure of Ccl-AgNPs to spiked plasma and water samples resulted in a marked decrease in absorption intensity along with a distinct red shift of the SPR band, consistent with NEO-induced nanoparticle agglomerations.

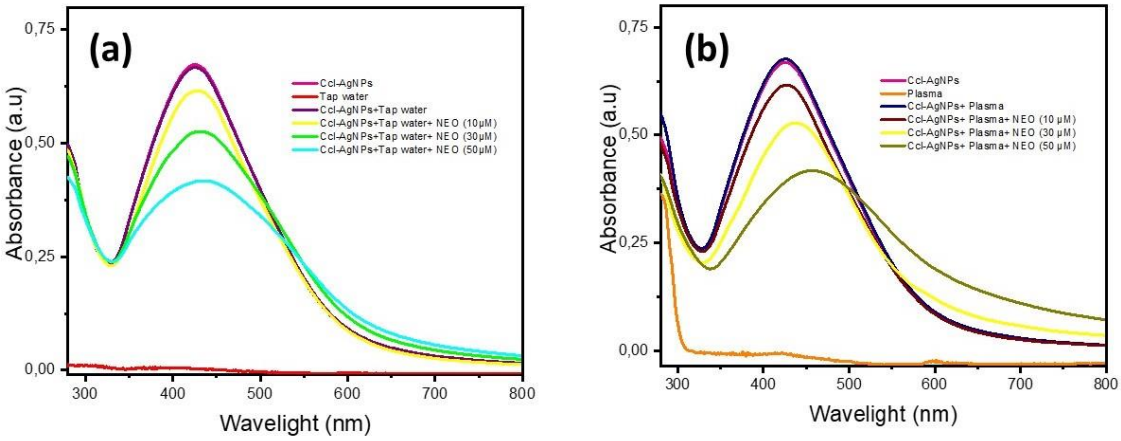


**FIGURE.III. 8.**NEO recognition in a real medium. (a); Drinking water samples; and (b) animal blood plasma fractions.

The quantitative of neomycin (NEO) by Ccl-AgNPs-based sensing platform, was further validated in real matrices, including biological fluids, environmental water samples, and veterinary pharmaceutical preparations, through recovery experiments (Table.III.3). The percentage recoveries obtained ranged from 93.2–104.0% in rabbit plasma samples, 92.62–97.3% in tap water, and 94.55–105.76% in veterinary drug preparations. These recovery values fall within the generally accepted limits of analytical precision, underscoring the robustness of the proposed assay in complex matrices. In the case of plasma, satisfactory recovery rates reflect the ability of method to withstand the complexity of biological fluids, where proteins, amino acids, and metabolites typically interfere with analyte detection[61]. Similarly, for tap water samples, this sensor method demonstrated robustness against concurrent ions and inorganic components, while accurate recovery from veterinary preparations confirms its potential application in routine pharmaceutical quality control[62,63].

**TABLE.III.3.** Quantitative recovery assessment of NEO in real-world matrixes.

| Sample | Concentration of the added NEO (µM) | Calculated Concentration (µM) | Recovery% |
|---|---|---|---|
| Public water supply | 10 | 9.73 | 97.3 |
| | 30 | 27.78 | 92.62 |
| | 50 | 48.17 | 96.34 |
| Biological plasma | 10 | 9.326 | 93.27 |
| | 30 | 28.20 | 94.01 |
| | 50 | 52.01 | 104.03 |
| Animal medicinal product | 10 | 10.57 | 105.76 |
| | 30 | 28.36 | 94.55 |
| | 50 | 50.86 | 101.73 |

## III.4. Conclusion

In summary, C. creticum leaf-extract-mediated silver nanoparticles (Ccl-AgNPs) have emerged as versatile nanomaterials with significant applications in the pharmaceutical sciences, specifically in biopharmaceutical and analytical contexts. Their multifunctionality has been demonstrated through antioxidant tests, where Ccl-AgNPs demonstrating potent free radical scavenging, transition metal ion reduction, and exceptional efficiency in quenching hydroxyl radicals and their reactive derivatives. In addition, Ccl-AgNPs exhibited noteworthy antimicrobial efficacy, particularly against pathogenic Gram-negative bacterial strains, supporting their relevance as alternative antibacterial agents.

Analytically, the potential of Ccl-AgNPs as a SPR-based colorimetric sensing platform was explored for the selective detection of neomycin sulfate. The system demonstrated high sensitivity and selectivity, achieving a LOD of 1.81 μM, while also displaying commendable stability and resistance to interference from complex biological and environmental matrices. Finally, the incorporation of Ccl-AgNPs with synergistic phyto-biocompatible and nanometallic properties is expected to improve the biopharmaceutical functionality of nano-conjugated polymers such as polyaniline nanotubes.

## References

1. Ahn EY, Jin H, Park Y. Assessing the antioxidant, cytotoxic, apoptotic and wound healing properties of silver nanoparticles green-synthesized by plant extracts. *Materials Science and Engineering: C*. 2019;101:204-216. doi:10.1016/j.msec.2019.03.095

2. Srećković NZ, Nedić ZP, Liberti D, Monti DM, Mihailović NR, Katanić Stanković JS, Dimitrijević S, Mihailović VB. Application potential of biogenically synthesized silver nanoparticles using *Lythrum salicaria* L. extracts as pharmaceuticals and catalysts for organic pollutant degradation. *RSC Adv*. 2021;11(56):35585-35599. doi:10.1039/D1RA05570D

3. Ahmed B, Bilal Tahir M, Sagir M, Hassan M. Bio-inspired sustainable synthesis of silver nanoparticles as next generation of nanoproduct in antimicrobial and catalytic applications. *Materials Science and Engineering: B*. 2024;301:117165. doi:10.1016/j.mseb.2023.117165

4. Biswas S, Dutta B, Bhattacharya S. Consequence of silver nanoparticles embedment on the carrier mobility and space charge limited conduction in doped polyaniline. *Applied Surface Science*. 2014;292:420-431. doi:10.1016/j.apsusc.2013.11.154

5. Blois MS. Antioxidant Determinations by the Use of a Stable Free Radical. *Nature*. 1958;181(4617):1199-1200. doi:10.1038/1811199a0

6. Re R, Pellegrini N, Proteggente A, Pannala A, Yang M, Rice-Evans C. Antioxidant activity applying an improved ABTS radical cation decolorization assay. *Free Radical Biology and Medicine*. 1999;26(9-10):1231-1237. doi:10.1016/S0891-5849(98)00315-3

7. Oyaizu M. Studies on products of browning reaction. Antioxidative activities of products of browning reaction prepared from glucosamine. *JpnJNutrDiet*. 1986;44(6):307-315. doi:10.5264/eiyogakuzashi.44.307

8. Szydlowskaczerniak A, Dianoczki C, Recseg K, Karlovits G, Szlyk E. Determination of antioxidant capacities of vegetable oils by ferric-ion spectrophotometric methods. *Talanta*. 2008;76(4):899-905. doi:10.1016/j.talanta.2008.04.055

9. Smirnoff N, Cumbes QJ. Hydroxyl radical scavenging activity of compatible solutes. *Phytochemistry*. 1989;28(4):1057-1060. doi:10.1016/0031-9422(89)80182-7

10. Mohammed MJ, Marston CK, Popovic T, Weyant RS, Tenover FC. Antimicrobial Susceptibility Testing of *Bacillus anthracis* : Comparison of Results Obtained by Using the National Committee for Clinical Laboratory Standards Broth Microdilution Reference and Etest Agar Gradient Diffusion Methods. *J Clin Microbiol*. 2002;40(6):1902-1907. doi:10.1128/JCM.40.6.1902-1907.2002

11. Pradeep M, Kruszka D, Kachlicki P, Mondal D, Franklin G. Uncovering the Phytochemical Basis and the Mechanism of Plant Extract-Mediated Eco-Friendly Synthesis of Silver Nanoparticles Using Ultra-Performance Liquid Chromatography Coupled with a Photodiode Array and High-Resolution Mass Spectrometry. *ACS Sustainable Chem Eng*. 2022;10(1):562-571. doi:10.1021/acssuschemeng.1c06960

12. Bhattacharjee S, Ghosh C, Sen A, Lala M. Characterization of Firmiana colorata (Roxb.) R. Br. leaf extract and its silver nanoparticles reveal their antioxidative, anti-microbial, and anti-inflammatory properties. *Int Nano Lett*. 2023;13(3-4):235-247. doi:10.1007/s40089-023-00392-6

13. Yang X, Zhang D, Song L min, Xu Q, Li H, Xu H. Chemical Profile and Antioxidant Activity of the Oil from Peony Seeds ( *Paeonia suffruticosa* Andr.). Tundis R, ed. *Oxidative Medicine and Cellular Longevity*. 2017;2017(1):9164905. doi:10.1155/2017/9164905

14. Guo MY, Ng AMC, Liu F, Djurišić AB, Chan WK. Photocatalytic activity of metal oxides—The role of holes and OH radicals. *Applied Catalysis B: Environmental*. 2011;107(1-2):150-157. doi:10.1016/j.apcatb.2011.07.008

15. Mashentseva AA, Dehaen W, Seitembetov TS, Seitembetova AJ. COMPARISON OF THE ANTIOXIDANT ACTIVITY OF THE DIFFERENT BETULA PENDULA ROTH. EXTRACTS FROM NORTHERN KAZAKHSTAN. Published online 2011.

16. Segneanu AE, Vlase G, Vlase T, Sicoe CA, Ciocalteu MV, Herea DD, Ghirlea OF, Grozescu I, Nanescu V. Wild-Grown Romanian Helleborus purpurascens Approach to Novel Chitosan Phyto-Nanocarriers—Metabolite Profile and Antioxidant Properties. *Plants*. 2023;12(19):3479. doi:10.3390/plants12193479

17. Suganthy N, Sri Ramkumar V, Pugazhendhi A, Benelli G, Archunan G. Biogenic synthesis of gold nanoparticles from Terminalia arjuna bark extract: assessment of safety aspects and neuroprotective potential via antioxidant, anticholinesterase, and antiamyloidogenic effects. *Environ Sci Pollut Res*. 2018;25(11):10418-10433. doi:10.1007/s11356-017-9789-4

18. Bedlovičová Z, Strapáč I, Baláž M, Salayová A. A Brief Overview on Antioxidant Activity Determination of Silver Nanoparticles. *Molecules*. 2020;25(14):3191. doi:10.3390/molecules25143191

19. Khorrami S, Zarrabi A, Khaleghi M, Danaei M, Mozafari M. Selective cytotoxicity of green synthesized silver nanoparticles against the MCF-7 tumor cell line and their enhanced antioxidant and antimicrobial properties. *IJN*. 2018;Volume 13:8013-8024. doi:10.2147/IJN.S189295

20. Dauthal P, Mukhopadhyay M. In-vitro free radical scavenging activity of biosynthesized gold and silver nanoparticles using Prunus armeniaca (apricot) fruit extract. *J Nanopart Res*. 2013;15(1):1366. doi:10.1007/s11051-012-1366-7

21. Medici S, Peana M, Nurchi VM, Zoroddu MA. Medical Uses of Silver: History, Myths, and Scientific Evidence. *J Med Chem*. 2019;62(13):5923-5943. doi:10.1021/acs.jmedchem.8b01439

22. Raza M, Kanwal Z, Rauf A, Sabri A, Riaz S, Naseem S. Size- and Shape-Dependent Antibacterial Studies of Silver Nanoparticles Synthesized by Wet Chemical Routes. *Nanomaterials*. 2016;6(4):74. doi:10.3390/nano6040074

23. Takcı DK, Ozdenefe MS, Genc S. Green synthesis of silver nanoparticles with an antibacterial activity using Salvia officinalis aqueous extract. *Journal of Crystal Growth*. 2023;614:127239. doi:10.1016/j.jcrysgro.2023.127239

24. Mosaviniya M, Kikhavani T, Tanzifi M, Tavakkoli Yaraki M, Tajbakhsh P, Lajevardi A. Facile green synthesis of silver nanoparticles using Crocus Haussknechtii Bois bulb extract: Catalytic activity and antibacterial properties. *Colloid and Interface Science Communications*. 2019;33:100211. doi:10.1016/j.colcom.2019.100211

25. Singh C, Anand SK, Upadhyay R, Pandey N, Kumar P, Singh D, Tiwari P, Saini R, Tiwari KN, Mishra SK, Tilak R. Green synthesis of silver nanoparticles by root extract of Premna integrifolia L. and evaluation of its cytotoxic and antibacterial activity. *Materials Chemistry and Physics*. 2023;297:127413. doi:10.1016/j.matchemphys.2023.127413

26. Gharari Z, Hanachi P, Sadeghinia H, Walker TR. Eco-Friendly Green Synthesis and Characterization of Silver Nanoparticles by Scutellaria multicaulis Leaf Extract and Its Biological Activities. *Pharmaceuticals*. 2023;16(7):992. doi:10.3390/ph16070992

27. Li HF, Pan ZC, Chen JM, Zeng LX, Xie HJ, Liang ZQ, Wang Y, Zeng NK. Green synthesis of silver nanoparticles using Phlebopus portentosus polysaccharide and their antioxidant, antidiabetic, anticancer, and antimicrobial activities. *International Journal of Biological Macromolecules*. 2024;254:127579. doi:10.1016/j.ijbiomac.2023.127579

28. López-Miranda JL, Esparza R, González-Reyna MA, España-Sánchez BL, Hernandez-Martinez AR, Silva R, Estévez M. Sargassum Influx on the Mexican Coast: A Source for Synthesizing Silver Nanoparticles with Catalytic and Antibacterial Properties. *Applied Sciences*. 2021;11(10):4638. doi:10.3390/app11104638

29. Vishwanath R, Negi B. Conventional and green methods of synthesis of silver nanoparticles and their antimicrobial properties. *Current Research in Green and Sustainable Chemistry*. 2021;4:100205. doi:10.1016/j.crgsc.2021.100205

30. Wasilewska A, Klekotka U, Zambrzycka M, Zambrowski G, Święcicka I, Kalska-Szostko B. Physico-chemical properties and antimicrobial activity of silver nanoparticles fabricated by green synthesis. *Food Chemistry*. 2023;400:133960. doi:10.1016/j.foodchem.2022.133960

31. George IE, Cherian T, Ragavendran C, Mohanraju R, Dailah HG, Hassani R, Alhazmi HA, Khalid A, Mohan S. One-pot green synthesis of silver nanoparticles using brittle star Ophiocoma scolopendrina: Assessing biological potentialities of antibacterial, antioxidant, anti-diabetic and catalytic degradation of organic dyes. *Heliyon*. 2023;9(3):e14538. doi:10.1016/j.heliyon.2023.e14538

32. Abbaszadegan A, Ghahramani Y, Gholami A, Hemmateenejad B, Dorostkar S, Nabavizadeh M, Sharghi H. The Effect of Charge at the Surface of Silver Nanoparticles on Antimicrobial Activity against Gram-Positive and Gram-Negative Bacteria: A Preliminary Study. Hazan R, ed. *Journal of Nanomaterials*. 2015;2015(1):720654. doi:10.1155/2015/720654

33. Hashemitabar G, Aflakian F, Sabzevar AH. Assessment of antibacterial, antioxidant, and anticancer effects of biosynthesized silver nanoparticles using Teucrium polium extract. *Journal of Molecular Structure*. 2023;1291:136076. doi:10.1016/j.molstruc.2023.136076

34. Ren Loi H, Abbasiliasi S, Bothi Raja P, Shamzi Mohamed M, Tan WN, Suan Ng H, Chi-Wei Lan J, Shun Tan J. Biosynthesis of silver nanoparticles using nitrate reductase produced by Lactobacillus plantarum CAM 4: Characterization and in vitro evaluation of

its antimicrobial efficiency. *Journal of Molecular Liquids*. 2023;376:121476. doi:10.1016/j.molliq.2023.121476

35. Can K, Can Z, Üzer A, Apak R. Visual colorimetric sensor for nitroguanidine detection based on hydrogen bonding−induced aggregation of uric acid−functionalized gold nanoparticles. *Talanta*. 2023;260:124585. doi:10.1016/j.talanta.2023.124585

36. Aijaz A, Raja DA, Khan FA, Barek J, Malik MI. A Silver Nanoparticles-Based Selective and Sensitive Colorimetric Assay for Ciprofloxacin in Biological, Environmental, and Commercial Samples. *Chemosensors*. 2023;11(2):91. doi:10.3390/chemosensors11020091

37. Syed RU, Moni SS, Nawaz M, Bin Break MK, Khalifa NE, Abdelwahab SI, Alharbi RM, Alfaisal RH, Al Basher BN, Alhaidan EM. Formulation and Evaluation of Amikacin Sulfate Loaded Dextran Nanoparticles against Human Pathogenic Bacteria. *Pharmaceutics*. 2023;15(4):1082. doi:10.3390/pharmaceutics15041082

38. Serbezeanu D, Iftime MM, Ailiesei GL, Ipate AM, Bargan A, Vlad-Bubulac T, Rîmbu CM. Evaluation of Poly(vinyl alcohol)–Xanthan Gum Hydrogels Loaded with Neomycin Sulfate as Systems for Drug Delivery. *Gels*. 2023;9(8):655. doi:10.3390/gels9080655

39. Rapacz-Kmita A, Stodolak-Zych E, Ziabka M, Rozycka A, Dudek M. Instrumental characterization of the smectite clay–gentamicin hybrids. *Bull Mater Sci*. 2015;38(4):1069-1078. doi:10.1007/s12034-015-0943-7

40. Nabipour H, Soltani B, Ahmadi Nasab N. Gentamicin Loaded Zn2(bdc)2(dabco) Frameworks as Efficient Materials for Drug Delivery and Antibacterial Activity. *J Inorg Organomet Polym*. 2018;28(3):1206-1213. doi:10.1007/s10904-018-0781-3

41. Rahmati M, Babapoor E, Dezfulian M. Amikacin-loaded niosome nanoparticles improve amikacin activity against antibiotic-resistant Klebsiella pneumoniae strains. *World J Microbiol Biotechnol*. 2022;38(12):230. doi:10.1007/s11274-022-03405-2

42. Batul R, Bhave M, J. Mahon P, Yu A. Polydopamine Nanosphere with In-Situ Loaded Gentamicin and Its Antimicrobial Activity. *Molecules*. 2020;25(9):2090. doi:10.3390/molecules25092090

43. Raja DA, Shah MR, Malik MI. Polyethyleneimine stabilized silver nanoparticles as an efficient and selective colorimetric assay for promethazine. *Analytica Chimica Acta*. 2022;1223:340216. doi:10.1016/j.aca.2022.340216

44. Raja DA, Musharraf SG, Shah MR, Jabbar A, Bhanger MI, Malik MI. Poly(propylene glycol) stabilized gold nanoparticles: An efficient colorimetric assay for ceftriaxone. *Journal of Industrial and Engineering Chemistry*. 2020;87:180-186. doi:10.1016/j.jiec.2020.03.041

45. Castro-Campos FG, Esquivel-Fajardo EA, Morales-Sánchez E, Rodríguez-García ME, Barron-Garcia OY, Ramirez-Gutierrez CF, Loarca-Piña G, Gaytán-Martínez M. Resistant Starch Type 5 Formation by High Amylopectin Starch–Lipid Interaction. *Foods*. 2024;13(23):3888. doi:10.3390/foods13233888

46. Rohit JV, Kailasa SK. Simple and selective detection of pendimethalin herbicide in water and food samples based on the aggregation of ractopamine-dithiocarbamate

functionalized gold nanoparticles. *Sensors and Actuators B: Chemical*. 2017;245:541-550. doi:10.1016/j.snb.2017.02.007

47. Ul Ain N, Aslam Z, Yousuf M, Waseem WA, Bano S, Anis I, Ahmed F, Faizi S, Malik MI, Shah MR. Green synthesis of methyl gallate conjugated silver nanoparticles: a colorimetric probe for gentamicin. *New J Chem*. 2019;43(4):1972-1979. doi:10.1039/C8NJ04565H

48. Alam MdT, Rauf MohdA, Siddiqui GA, Owais M, Naeem A. Green synthesis of silver nanoparticles, its characterization, and chaperone-like activity in the aggregation inhibition of α-chymotrypsinogen A. *International Journal of Biological Macromolecules*. 2018;120:2381-2389. doi:10.1016/j.ijbiomac.2018.09.006

49. Kyaw ST, Maung MM, Aung MKT. X-ray diffraction characterization for optimal crystallite aggregates of phyto-synthesized silver nanoparticles (agnps) by Ocimum sanctum l. Leaf extract. *Journal of Chemistry*. 2018;2:7-15.

50. Nugrahani I, Min SS. Hydrate transformation of sodium sulfacetamide and neomycin sulphate. *Int J Pharm Pharm Sci*. 2015;7(10):409-415.

51. Motahari S, Alamdari A, Malayeri MR. Crystallization of neomycin nanoparticles in the presence of polyvinyl pyrrolidone (PVP). *Nanoscale Adv*. 2025;7(8):2272-2289. doi:10.1039/D4NA01031K

52. Long BM, Pfeffer FM. On the use of 'shortcuts' in the method of continuous variation (Job's method). *Supramolecular Chemistry*. 2015;27(1-2):136-140. doi:10.1080/10610278.2014.909044

53. Sarkar M, Khandavilli S, Panchagnula R. Development and validation of RP-HPLC and ultraviolet spectrophotometric methods of analysis for the quantitative estimation of antiretroviral drugs in pharmaceutical dosage forms. *Journal of Chromatography B*. 2006;830(2):349-354. doi:10.1016/j.jchromb.2005.11.014

54. Cui Y, Jiang J. Analysis on Anti-Interference Performance of Sensor in Explosive Electromagnetic Environment. *IEEE Sensors J*. 2024;24(3):2895-2904. doi:10.1109/JSEN.2023.3341957

55. Chen G, Li J, Zhu H, Wang Y, Ji H, Meng F. Optical fiber gas sensor with multi-parameter sensing and environmental anti-interference performance. *Journal of Industrial Information Integration*. 2024;38:100565. doi:10.1016/j.jii.2024.100565

56. Li X, Zhang Y, Wu T, Sun X, Yang T, Wang L, Li X, Wang J, Wang Y, Yu H. Major ions in drinking and surface waters from five cities in arid and semi-arid areas, NW China: spatial occurrence, water chemistry, and potential anthropogenic inputs. *Environ Sci Pollut Res*. 2020;27(5):5456-5468. doi:10.1007/s11356-019-07149-9

57. Rein JL, Coca SG. "I don't get no respect": the role of chloride in acute kidney injury. *American Journal of Physiology-Renal Physiology*. 2019;316(3):F587-F605. doi:10.1152/ajprenal.00130.2018

58. Csurka T, Pásztor-Huszár K, Tóth A, Pintér R, Friedrich LF. Investigation of the effect of trisodium-citrate on blood coagulation by viscometric approach. *Progress*. 2021;16(S2):19-26. doi:10.1556/446.2020.20003

59. Wright A. Characterizing the Presence of EDTA in Blood Samples. *VCU Forensic Science Directed Research Projects*. Published online 2021. doi:10.25772/D18M-7B40

60. Naqvi S, Anwer H, Ahmed SW, Siddiqui A, Shah MR, Khaliq S, Ahmed A, Ali SA. Synthesis and characterization of maltol capped silver nanoparticles and their potential application as an antimicrobial agent and colorimetric sensor for cysteine. *Spectrochimica Acta Part A: Molecular and Biomolecular Spectroscopy*. 2020;229:118002. doi:10.1016/j.saa.2019.118002

61. Hughes NC, Bajaj N, Fan J, Wong EY. Assessing the Matrix Effects of Hemolyzed Samples in Bioanalysis. *Bioanalysis*. 2009;1(6):1057-1066. doi:10.4155/bio.09.91

62. Kanoun O, Lazarević-Pašti T, Pašti I, Nasraoui S, Talbi M, Brahem A, Adiraju A, Sheremet E, Rodriguez RD, Ben Ali M, Al-Hamry A. A Review of Nanocomposite-Modified Electrochemical Sensors for Water Quality Monitoring. *Sensors*. 2021;21(12):4131. doi:10.3390/s21124131

63. Dispas A, Sacré PY, Ziemons E, Hubert P. Emerging analytical techniques for pharmaceutical quality control: Where are we in 2022? *Journal of Pharmaceutical and Biomedical Analysis*. 2022;221:115071. doi:10.1016/j.jpba.2022.115071

# *General Conclusion*

Contemplating and observing nature have always been the primary driving force of human civilization, intellectual and technological progress from the earliest times to our era and even into the future. From the philosophical inquiries of antiquity to the empirical rigor of modern science, nature has been both the subject and the inspiration of human curiosity. Aristotle's assertion that "nature does nothing in vain" encapsulates an early recognition of the inherent order in natural phenomena, while Charles Darwin's reflection that "there is grandeur in this view of life, with its several powers, having been originally breathed into a few forms or into one" epitomizes the evolutionary perspective that unites all living systems through common origins.

In the contemporary era, this enduring dialogue with the natural world continues to shape scientific innovation, particularly in fields such as biotechnology, green chemistry, and nanotechnology. The convergence and integration of the principles, methodologies, and analytical tools derived from these three modern scientific domains have given rise to a dynamic and interdisciplinary research area known as green bio-nanotechnology. In this context, the present thesis is devoted to the development of novel nanomaterials with enhanced physicochemical and biological properties, targeting applications in biopharmaceutical, and environmental remediation domains. To achieve this objective, a renewable plant biomass with unexplored potential for nanotechnology was exploited: *Cynoglossum creticum*. This species, recognized as one of the most noxious and toxic weeds, is characterized by its rapid growth, high adaptability, and ecological distribution across northern Algeria, particularly in roadside areas and marginal habitats.

In the first two experimental parts of this thesis, aqueous extracts of *C. criticum* leaves were employed as a biogenic medium for the synthesis of silver nanoparticles (Ccl-AgNPs), thereby eliminating the need for toxic chemical reducing agents and aligning with the principles of green chemistry. The resultant Ccl-AgNPs were subjected to comprehensive physicochemical characterization through a suite of spectroscopic, microscopic, thermogravimetric techniques (UV–vis, FTIR, XRD, SEM, EDS, TGA and DSC). Furthermore, the biopharmaceutical and analytical potential of Ccl-AgNPs were assessed with regard to their potential antimicrobial, antioxidant, and biosensing applications. The main findings and implications are summarized in the following paragraphs.

An extraction ratio of 0.1% (w/v) C. *creticum* leaf powder to solvent ratio at 70°C for 60 min identified as optimal for maximizing the recovery phenolic compound while maintaining structural stability. These conditions also minimized the co-extraction of undesirable pyrrolizidine alkaloids (PAs), thereby enhancing extract safety. The one variable at a time approach aided by UV-vis spectroscopy, determined the optimal experimental parameters for the synthesis of stable, monodisperse Ccl-AgNPs with a near-uniform size distribution, as follows: a 1 mM $AgNO_3$ solution reacted with the Ccl-extract at a 5:1 volume ratio ($AgNO_3$: CCl), at 80 °C for 75 min.

FTIR analysis revealed the active participation of phytochemicals in the synthesis process through sequential reduction, stabilization, and surface passivation mechanisms. EDS and TGA data further substantiated their stabilizing role, indicating a solid organic coating enveloping the $Ag^0$ metallic core. XRD patterns highlighted the crystalline structure of the Ccl-AgNPs, representing the fcc silver structure, with an average crystal size of 24.3 nm. SEM micrographs depicted predominantly spherical nanoparticles, arranged as dispersed clusters, with an average particle size of approximately 32 nm.

Furthermore, Ccl-AgNPs exhibited versatile functional properties with significant potential in pharmaceutical applications. They exhibited pronounced antioxidant activity, effectively reducing transition metal ions and neutralizing free radicals, particularly hydroxyl species and their derivatives. Antibacterial evaluations revealed significant inhibitory effect against all four tested strains, with Pseudomonas aeruginosa being the most susceptibility (MIC = 31.25 µg/mL). From an analytical standpoint, Ccl-AgNPs served as an efficient SPR-based colorimetric platform for the selective detection of neomycin sulfate, achieving a detection limit of 1.81 µM. The probe was further validated for accurate neomycin sulfate quantification in in environmental samples, biological fluids, and veterinary formulations, yielding recovery rates between 92.62% and 105.76%.

The lest experimental part of the thesis focused on assessing the capability of the Ccl-extract to promote the deposition of AgNPs onto polyaniline nanotubes (PANI-NTs). The nanotubes were synthesized through an environmentally benign soft template-based self-assembly process. The resulting Ag/PANIx nanocomposites containing different masses of PANI (50, 100, 150, 200, and 250 mg) were subsequently subjected to comprehensive physicochemical characterization. Their biological relevance was further explored through the evaluation of antioxidant and antibacterial activities. The subsequent paragraphs present and discuss the principal findings.

XRD patterns confirmed the successful synthesis of a semi-crystalline emeraldine salt phase of polyaniline nanotubes, while also verifing the successful incorporation and growth of AgNPs within the PANI framework, exhibiting average crystallite sizes between 18.1 and 23.9 nm. FTIR spectra provided insight into the polymerization process of PANI, revealing para-conjugation during aniline polymerization leading to a linear polymer backbone. The presence of hydrogen bonding further supported the self-assembly mechanism responsible for nanotube formation. SEM analysis elucidated the organized nanostructure of PANI, characterized by interconnected nanotubes with smooth surfaces. SEM images of Ag/PANIx NCs also confirmed the successful formation of spherical AgNPs anchored to the PANI surface and embedded within its internal pores, developing a rougher structure.

BET and BJH analyses confirmed that the incorporation of AgNPs into the PANI matrix led to a notable enhancement in specific surface area, as the AgNPs effectively altered the porous architecture and promoted the formation of additional microporous regions along the PANI-NT. TGA analysis further indicated improved thermal stability of the Ag/PANIx nanocomposites resulted from strong interfacial interactions between the silver nanoparticles and the PANI chains. Moreover, the embedding of AgNPs within the PANI nanotubes resulted in an increased fluorescence quantum yield and intensified photoluminescence.

Additionally, PANI nanofibers demonstrated moderate to satisfactory biological activity. Antioxidant assays indicated that emeraldine salt form PANI nanotubes operate through complementary pathways involving proton and electron transfer toward free radicals and transition metal ions, respectively. The deposition of AgNPs on PANI-NT further enhanced the antioxidant performance, resulting from synergistic interactions and improved specific surface area. Broth microdilution analysis revealed that the antibacterial effect of PANI-NT was microorganism species-dependent, with greater inhibition observed against P. aeruginosa and E. faecalis. Ag/PANIx NCs preserved the inhibitory behavior of pure PANI yet displayed improved antibacterial efficacy, likely due to combined mechanisms involving electrostatic adhesion and the release of $Ag^{+}$ ions and ultrafine AgNPs.

The synthesis potential of Cynoglossum creticum extract, a toxic weed detrimental to livestock, combined with the pharmaceutical and biosensing functionalities of Ccl-AgNPs , along with the established synergistic activity of Ag/PANI nanohybrid, enables the development of a straightforward and efficient nanotechnological strategy for environmental and health applications. This synthetic approach is a ripe candidate for evaluation within the framework

of the circular bioeconomy, transforming a species that constitutes a neglected biomass into a valuable nanotechnology resource.